EXCHANGE INTERACTIONS AND RELAXATION IN PARAMAGNETS

by

J. R. Beswick B.A.

Being a thesis

submitted to the University of Keele

for the Degree of Doctor of Philosophy

Department of Physics,
University of Keele,
Keele, Staffordshire.

December, 1972.

ACKNOWLEDGMENTS

My thanks are due to the following:

Professor D. J. E. Ingram for the provision of research facilities in his department.

Dr. D. E. Dugdale for his advice, guidance and the preparation of many of the crystals investigated in this thesis.

Dr. B. Henderson for his general supervision and encouragement.

My wife, Jane, for her care, patience and fortitude, not only in typing this thesis.

My colleagues for the many rewarding hours spent in their company.

All other members of the Physics Department for their help and co-operation.

The Science Research Council for a maintenance grant and the Department of Employment and my wife for additional support.

ABSTRACT

This thesis presents some investigations into a variety of paramagnetic systems. Electron paramagnetic resonance is often used to investigate the behaviour of paramagnetic ions present as substitutional impurities in diamagnetic host crystals. Measurements have been carried out at liquid helium temperatures on single crystals of aluminium acetylacetonate doped to 2% with ruthenium^{3+} ions. The spectrum at nitrogen temperatures has been reported by Jarrett (1957) who found two ruthenium sites. The behaviour of each site can be described by

$$H_s = \underline{S}.\underline{g}.\underline{H}$$

Jarrett found $g_z = 2.82$, $g_x = 1.28$, $g_y = 1.74$ at $77^{\circ}K$. At $4.2^{\circ}K$ we find that six strong resonances are observed which correspond to six ruthenium sites, equivalent in pairs along the crystallographic [b] direction and in the (b) plane. The g values of these equivalent pairs are

	g_z	g_x	g_y
	2.60	0.75	1.83
	2.55	0.96	1.91
	2.56	1.00	1.905
error	±0.01	±0.015	±0.01

This behaviour is interpreted in terms of a phase change in the crystal, occurring between nitrogen and helium temperatures. At certain orientations hyperfine splittings were observed. No detailed investigation of this was possible but the hyperfine interaction appeared to be isotropic with $|A| \simeq 15 \times 10^{-4}$ cm^{-1}.

We also report spin-lattice relaxation studies on substitutional copper ions in single crystals of calcium cadmium acetate hexahydrate. The relaxation was found to depend exponentially on temperature, namely

$$T_1 = A \exp (15/T)$$

The usual processes giving rise to such behaviour are discounted as being not applicable. Because the atomic weight of copper is approximately half that of cadmium, which it replaces, we believe that the copper ion is acting as a mass defect in the lattice. In this case we are able to explain the form of the relaxation behaviour and account, in part, for the different values of T_1 measured at each hyperfine component. Relaxation studies on the undoped calcium copper acatate hexahydrate suggest that a phonon bottleneck is present. This may possibly offer further evidence for our interpretation of the relaxation processes occurring at low copper concentrations.

We have also investigated a series of dimeric complexes in which paramagnetic pairs form a natural part of the crystal structure. After unsuccessful attempts to obtain useful crystals containing cobalt dimers attention was turned to some dimeric complexes of the form $Cs_3M_2Cl_9$, where M = Cr, V or Ti. The early crystal growths containing chromium dimers contained several impurity spectra which are described and discussed in the thesis. One such spectrum, which was only observable at very low temperatures ($< 3^{\circ}K$), was attributed to a single spin 3/2 chromium ion. Its behaviour could be described by an axial spin Hamiltonian of the form

$$H_s = g_z\beta H_z S_z + g_x\beta H_x S_x + D\left[S_z^2 - \tfrac{1}{3}S(S+1)\right]$$

where $g_z = 1.981$, $g_x = 1.988$, $|D| = 0.097\ cm^{-1}$.

In addition a broad resonance was seen at high temperatures which was no longer found at $4.2^{\circ}K$. At $4.2^{\circ}K$ a spin 1 system was present.

By modifying the crystal growth it was possible to produce crystals showing only the spin 1 system at helium temperatures. An axial spin Hamiltonian was sufficient to describe the angular variation of this spectrum at $4.2^{\circ}K$ with

$$g_z = 1.974 \qquad g_x = 2.001 \qquad D = +0.185\ cm^{-1}$$

This spectrum is held to arise from a pair state formed by exchange interactions between the two chromium ions in each dimer. The intensity of

the spectrum was measured as a function of temperature and, assuming an isotropic exchange interaction between the chromium ions of the form $J(\underline{S}_1 \cdot \underline{S}_2)$, we find

$$J = 17 \pm 1^{\circ}K$$

Large changes in the spectrum were observed. Below $8^{\circ}K$ the magnitude of the D term was very temperature dependent whereas, at higher temperatures, the spin 1 resonances merged into one line. The linewidth of this single resonance was markedly temperature dependent. We have been able to describe the behaviour of the single resonance by considering exchange interactions between neighbouring dimers. We find exchange interactions of ~ 0.65 cm^{-1} are sufficient to predict the observed behaviour of the linewidth. We have also measured the angular dependence of the linewidth at room temperature, at both X and Q band, and are able to account for the anisotropy which differs at each frequency.

Investigations into $Cs_3V_2Cl_9$ did not show paramagnetic behaviour, which is explained by the expected magnitude of the zero field splittings. $Cs_3Ti_2Cl_9$ showed a broad high field resonance below $60^{\circ}K$ which underwent large intensity changes. This is tentatively attributed to a spin 1 pair state with a zero field splitting of 4.75 cm^{-1}. The exchange energy probably lies in the range $150 - 250^{\circ}K$.

A series of crystals were investigated which it was hoped would contain the same anion as the cesium salts. In these crystals the cations were alkylammonium groups which reduce exchange interactions between dimers by increasing their spatial separation. Chromium dimers with a tetraethylammonium cation showed four resonances characteristic of a spin 2 centre which could be described by the spin Hamiltonian

$$H_s = g_z \beta H_z S_z + g_x \beta H_x S_x + D S_z^2 - \tfrac{1}{3} S(S+1)$$

with $g_z = 1.984$ $g_x = 1.980$ $|D| = 0.0434$ cm^{-1}

This sprectrum was attributed to a spin 2 pair state and, assuming isotropic

exchange within each dimer, the exchange parameter was measured as

$$J = 20 \pm 2^{\circ}K$$

This value for J is close to that measured in $Cs_3Cr_2Cl_9$ but D_2 is only about half the value we might expect to find in the cesium salt from a knowledge of the crystal structure. Transitions within the spin 1 and 3 manifolds are held to be broadened beyond resolution. Preliminary measurements were made on chromium dimers with a tetrapropylammonium cation which gave similar results.

CONTENTS

INTRODUCTION

Electron paramagnetic resonance (e.p.r.) forms a branch of high resolution spectroscopy employing microwave frequencies. It differs from simple spectroscopy in that the system under investigation is 'tuned', by the application of a magnetic field, to resonate at the detecting frequency as opposed to the more usual method of tuning the detecting system. This restricts the e.p.r. technique to systems that have energy levels which are able to respond to applied magnetic fields. Paramagnetic systems contain unpaired electrons with non-zero angular momentum and consequently they possess a magnetic moment. It is the interaction between the electronic magnetic moment and the applied magnetic field which allows the energy levels of paramagnets to be tuned to the resonance condition.

Since the electronic energy levels are also determined by the symmetry and strength of the surrounding crystal field, e.p.r. can tell much about the local atomic environment. Information can also be obtained about interactions between a paramagnetic ion and its neighbours. Quantum mechanical exchange interactions become important when the interactions between ions which are close to each other are considered. Such exchange interactions may considerably modify the observed spectrum. Aspects of this are found in Chapter VI which reports investigations into a series of dimeric complexes.

When two energy levels are at resonance the microwave field perturbs the spin populations from their equilibrium values. Mechanisms exist to bring the spins back to internal thermal equilibrium and to equilibrium with the remainder of the crystal. Such relaxation mechanisms are considered in Chapter II while Chapter V is a study of the spin-lattice relaxation behaviour of a substitutional copper ion.

Chapter I reviews the basic theory of e.p.r. while Chapter III discusses the experimental apparatus and the techniques employed in obtaining the results of this thesis. Chapter IV is an investigation into some substitutional ruthenium sites.

CHAPTER I

THE THEORY OF ELECTRON PARAMAGNETIC RESONANCE

1.1 Quantum Mechanical Description of Resonance

When an atomic electron has a resultant electronic angular momentum $\underline{J}$, arising either from pure spin or from an admixture of spin and orbital momentum, it will have an associated magnetic moment $\underline{\mu}$,

$$\underline{\mu} = \gamma \underline{J} \qquad (1.1)$$

where γ is the gyromagnetic ratio, a constant for any particular energy state. The interaction between an applied magnetic field $\underline{H}$ and the electron is

$$\mathcal{H} = - \underline{\mu} \cdot \underline{H} = - \gamma \underline{H} \cdot \underline{J} \qquad (1.2)$$

$\underline{J}$ being quantised in the applied field. Defining a dimensionless angular momentum operator $\underline{S}$ by $\underline{J} = \hbar \underline{S}$ we find S^2 takes $2S+1$ integer or half integer eigenvalues $S,(S-1),(S-2),\ldots\ldots,-S$. Any component of $\underline{S}$ such as $\underline{S}_z$ commutes with S^2 and has simultaneous eigenvalues with it. With an applied field of magnitude H_0 applied in the z direction the Hamiltonian is

$$\mathcal{H} = \gamma \hbar H_0 \underline{S}_z \qquad (1.3)$$

with eigenvalues corresponding to allowed electronic energies of

$$E = \gamma \hbar H_0 M_s \qquad (1.4)$$

where $M_s = S,(S-1),\ldots\ldots,-S$.

Transitions will be induced between such energy levels by a perturbing interaction when the perturbation operator has non-zero matrix elements between different states. To conserve energy for a direct transition of energy ΔE a time dependent interaction of angular frequency ω is required where

$$\hbar \omega = \Delta E \qquad (1.5)$$

These conditions are met by an oscillatory magnetic field $H_x \cos \omega t \underline{i}$

applied perpendicularly to H_0, then

$$\mathcal{H}_{pert} = \gamma \hbar H_x \cos \omega t \, \underline{S}_x \qquad (1.6)$$

The only non-zero matrix elements of $\underline{S}_x$ are between states with $\Delta M_s = \pm 1$. The allowed transitions given by this selection rule have energies

$$\Delta E = \gamma \hbar H_0 = g \beta H_0 \qquad (1.7)$$

β is the Bohr magneton and g the spectroscopic splitting factor. Effectively g represents the total angular momentum of the state.

The paramagnetic resonance technique is to induce transitions among the 2S+1 energy levels. At thermal equilibrium the energy level populations are determined by the Boltzmann distribution function,

$$N_i \propto \exp\left\{\frac{-E_i}{kT}\right\} \qquad (1.8)$$

For a two level system, with $E_2 > E_1$, the population difference is

$$\approx \frac{N_1 + N_2}{2} \cdot \frac{h\nu}{kT} \qquad h\nu \ll kT \qquad (1.9)$$

Then, at microwave frequencies ($\sim 10^{10}$ hz), where the probability of quantum absorption equals that for stimulated emission, a net absorption of energy from the r.f. field occurs because of the population imbalance. Such a magnetic system would soon become saturated were it not for the spin-lattice relaxation mechanisms discussed in Chapter II.

1.2 Crystal Field Theory

We now consider how the ground state energies of paramagnetic centres are derived. When a paramagnetic ion is introduced into a crystal lattice its magnetic properties are modified. The theoretical treatment of this, which has been reviewed elsewhere (e.g. Orton, 1968), is outlined below.

The first two terms of the free ion Hamiltonian are,

$$H = \sum_i^N \left[\frac{\nabla_i^2}{2m} - \frac{Ze^2}{r_i}\right] + \sum_{i>j}^N \frac{e^2}{r_{ij}} \qquad (1.10)$$

for an N electron ion. The first term represents the electron kinetic energies plus the coulomb interaction of the electrons with the stationary nucleus while the second expresses the inter-electron coulomb repulsions. The energy of these terms is $\sim 10^5 cm^{-1}$.

The wave equation associated with this Hamiltonian can only be solved approximately. The first term is just the sum of N hydrogen atom type problems which can be solved. The wavefunction of an electron in a spherical field differs only from a hydrogen wavefunction in its radial part, thus allowing the usual separation of variables. By requiring each electron to move independently in a spherically symmetric net potential V(r), taken as the electron-nuclear coulomb potential modified by a spherically symmetric potential due to the average effect of the repulsive coulomb forces with the other electrons, the problem is still theoretically solvable. The Schroedinger equation becomes

$$-\frac{h^2}{2m}\sum_i^N \nabla_i^2 \psi_T + \sum_i^N V_i(r_i)\psi_T = E_T \psi_T \qquad (1.11)$$

Since we now have non-interacting electrons, ψ_T may be written as the product of one electron wavefunctions giving N one particle Schroedinger equations such as

$$-\frac{h^2}{2m} \nabla_i^2 \psi(r_i, \theta_i, \phi_i) + V_i(r_i)\psi(r_i, \theta_i, \phi_i) = E_i \psi(r_i, \theta_i, \phi_i) \qquad (1.12)$$

Solutions are found by the Self Consistent Field method wherein initial estimates for ψ_i and V_i are substituted into the Schroedinger equations which are then solved numerically to give new forms of the ψ_i. The new ψ_i are used to determine new V_i and the process repeated until a self consistent solution is found. By filling these final eigenstates in such a way as to minimise the total energy with due regard to the exclusion principle it is possible to describe the ion's ground state. By specifying n and l values for each eigenstate the configuration is described.

The next step is to calculate the eigenstates of H between configurational states. Since the operators L ($= \sum l_i$) and S ($= \sum s_i$) commute

with H they have simultaneous eigenvalues with it. Consequently, by choosing linear combinations of one electron wavefunctions which are already angular momentum eigenfunctions as basis functions, the direct diagonalisation of the matrix is simplified. This treatment splits the configuration into terms, specified by the quantum numbers L, S, M_L, M_S. Hund's rules are then applied to obtain the ground term (that with maximum L consistent with maximum S).

A free ion treatment next considers the magnetic coupling between the spin and orbital angular momenta, typically $\sim 10^2 cm^{-1}$, as a perturbation. However, the potential due to the static crystalline electric field V_c must be included in the calculations. The point of inclusion of V_c as a perturbation will depend on its magnitude relative to the terms in the free ion Hamiltonian. Three cases are generally recognised. The weak crystal field approximation occurs when V_c is less than the spin-orbit interaction while the strong crystal field approximation has V_c greater than the inter-electron coulomb repulsion term. Usually, for the third transition group, the medium field case holds where V_c is applied as a perturbation before spin-orbit coupling.

In crystal field theory the influence of neighbouring ions is assumed to occur entirely through the electric field they produce at the magnetic ion site while acting as point charges. V_c then satisfies Laplace's equation the solutions to which are generalised Legendre polynomials

$$V_c = \sum_n V_n^m = \sum_n \sum_{m=n}^{-n} \sum_i A_n^m r^n Y_n^m(\theta_i, \phi_i) \qquad (1.13)$$

where Y_n^m are the normalised harmonics

$$Y_n^m(\theta, \phi) = (-1)^m \left[\frac{1}{4\pi} \frac{(2n+1)(n-|m|)!}{(n+|m|!)} \right]^{\frac{1}{2}} p_n^m(\cos\theta) e^{im\phi}$$

In order to evaluate V_c the free ion electron wavefunctions are written as a sum of the same harmonics $Y_n^m(\theta, \phi)$. Symmetry restrictions reduce V_c to two terms for d electrons. Matrix elements are evaluated by the Operator Equivalents method of Stevens (1952), the diagonalised matrix giving the 'levels' produced by the crystal field. Usually the crystal field leaves an

orbitally non-degenerate ground state but, even if a field of high symmetry left orbital degeneracy, a theorem due to Jahn and Teller predicts a spontaneous local distortion to remove the degeneracy.

The remaining terms to be applied as perturbations to the orbital singlet ground state $|1\rangle$ are the spin-orbit coupling $\lambda \underline{L}.\underline{S}$ and a Zeeman term $\beta \underline{H}.(\underline{L} + 2\underline{S})$ of energy $\sim 1 cm^{-1}$. Abragam and Price (1951) developed a treatment for this perturbation step that allows experimental results to be presented in a few parameters. Quenching of the orbital magnetic moment follows since in a singlet orbital state the expectation value of the orbital magnetic moment is zero. This causes the stronger spin-orbit coupling to vanish in first order allowing the two remaining terms to be applied together. The energy shift to second order is

$$E = \langle 1, M_{S_1} | \lambda \underline{L}.\underline{S} + \beta \underline{H}(\underline{L} + 2\underline{S}) | 1, M_{S_1} \rangle + \sum \frac{|\langle 1, M_{S_1} | \lambda \underline{L}.\underline{S} + \beta \underline{H}(\underline{L} + 2\underline{S}) | n, M_{S_n} \rangle|^2}{(E_1 - E_n)} \qquad (1.14)$$

Writing $\underline{S} = \sum \underline{s}_i$ and $\underline{L} = \sum \underline{l}_i$ gives

$$E = 2\beta \underline{H}.\underline{S} - \sum \frac{(\lambda \underline{s}_i + \beta \underline{H}_i)(\lambda \underline{s}_j + \beta \underline{H}_j)\langle 1|\underline{l}_i|n\rangle\langle n|\underline{l}_j|1\rangle}{(E_n - E_1)}$$

$$= 2\beta \underline{H}.\underline{S} - \sum \mathcal{L}_{ij}(\beta^2 \underline{H}_i \underline{H}_j + 2\beta\lambda \underline{H}_i \underline{s}_j + \lambda^2 \underline{s}_i \underline{s}_j) \qquad (1.15)$$

where $\mathcal{L}_{ij} = \sum \frac{\langle 1|\underline{l}_i|n\rangle\langle n|\underline{l}_j|1\rangle}{(E_n - E_1)}$

The term in $\beta^2 \underline{H}_i \underline{H}_j$ represents temperature independent paramagnetism and is ignored as it shifts all levels equally.

Thus $H_s = \sum \left[2(\delta_{ij} - \lambda \mathcal{L}_{ij}) \beta \underline{H}_i \underline{s}_j - \lambda^2 \mathcal{L}_{ij} \underline{s}_i \underline{s}_j \right]$

which can be written in tensor notation as

$$H_s = \underline{H}.\underline{g}.\underline{S} + \underline{S}.\underline{D}.\underline{S} \qquad (1.16)$$

where $\underline{g}$ and $\underline{D}$ are real symmetric second rank tensors. A fictitious spin

appropriate to the observed transitions allows a spectrum to be described by this spin Hamiltonian. The fictitious spin is not necessarily equal to the true spin of the ion.

Interactions with nuclear spins introduce further terms of energy $\sim 10^{-2}cm^{-1}$. The magnetic interaction between electrons and nuclei has two contributions, a dipolar term and a Fermi contact interaction. A term $A\underline{I}.\underline{S}$ is introduced into the spin Hamiltonian to account for this where I is the nuclear spin. The 2I + 1 quantisation states of I in a magnetic field split each electronic fine structure transition into 2I + 1 hyperfine components.

1.3 Covalency

The ionic model alone is often insufficient to explain experimental results. It may be necessary to include covalency effects between the magnetic ion and its ligands. This problem is treated by the configuration interaction method or the molecular orbital method. The configuration interaction method adds to the original ionic configuration an admixture of a configuration in which an electron has been transferred from the metal ion to the ligand. The molecular orbital method takes for the wavefunction of each electron a linear combination of the atomic orbitals belonging to the magnetic ion and its neighbours. These processes are reviewed by Owen and Thornley (1966).

When paramagnetic ions occupy sites sufficiently close together for direct or indirect orbital overlap to occur spin-spin interactions modify the ground state. Direct orbital overlap between adjacent paramagnetic ions introduces problems of indistinguishability. Heisenberg showed that a coulomb interaction between such electrons leads to an exchange effect which couples their spins. This ferromagnetic exchange coupling can be represented by the term

$$H_{ex} = J\,\underline{S}_i.\underline{S}_j \qquad (1.17)$$

where J is the exchange integral and takes a negative value for ferromagnetism.

A SUPEREXCHANGE MECHANISM IN MnO

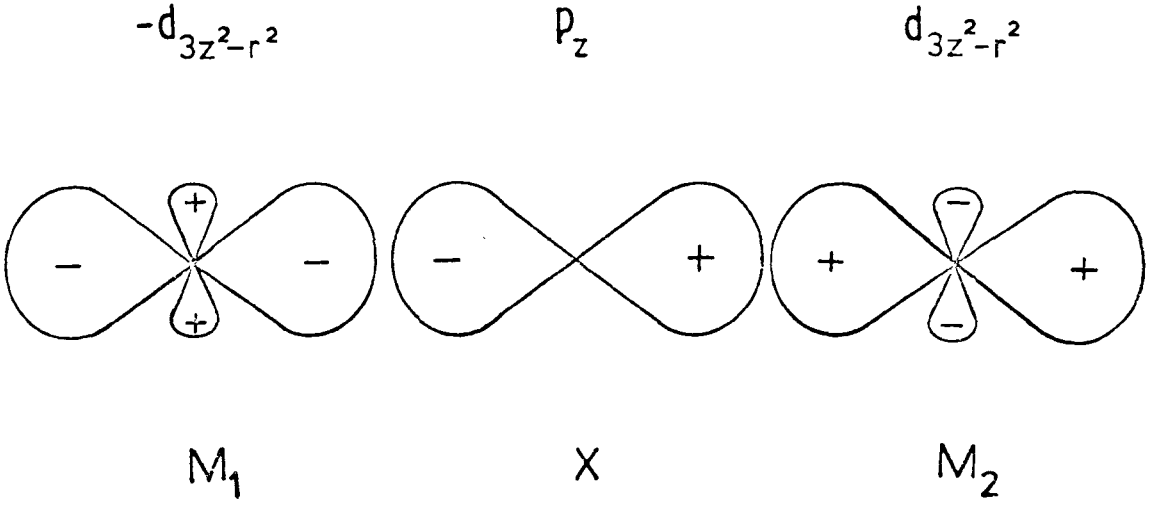

FIGURE 1.1

Higher order exchange terms also exist, $-j(\underline{S}_i.\underline{S}_j)^2$ etc., where typically $j/J \sim 1\%$.

Exchange interactions may also exist between paramagnetic ions separated by a diamagnetic ion. Such superexchange mechanisms involve spin transfer between all three ions. A classic case is the $Mn^{2+} - O^{2-} - Mn^{2+}$ structure of MnO. The configuration interaction approach adds to this a small admixture of the excited configuration $Mn^{+} - O^{2-} - Mn^{3+}$. The molecular orbital approach to this problem illustrates the physics of covalency. Consider the σ bonding process shown in figure 1.1. Small admixtures of the $2p_\sigma$ orbit on the O^{2-} ion give antibonding and bonding magnetic orbits.

$$\Phi_A = N_A(d - Ap) , \qquad \Phi_B = N_B(p + Bd) \tag{1.18}$$

where A and B are small admixture coefficients and N_A and N_B are normalising constants close to unity. The one electron Hamiltonian h, with terms in kinetic energy and the interactions with the metal and ligand nuclei and electrons, has a matrix element between p and d, $\langle p|h|d\rangle = a_{dp}$. To second order this gives an energy shift between Φ_A and Φ_B of

$$\Delta E = E(\Phi_A) - E(\Phi_B) = B^2(E_d - E_p) \tag{1.19}$$

where E_d and E_p are the energies of d and p respectively. Since there are two electrons in Φ_B there is a net energy stabilisation of ΔE. It is assumed that the two bonding electrons are paired giving no paramagnetic contributions so the distribution of unpaired spin is described by Φ_A. This gives a fraction $f \sim A^2$ of unpaired spin in the ligand p orbit. The fraction of unpaired spin on the metal ion is then $(1 - f)$ which means a fractional reduction k of approximately $(1 - f)$ in the total orbital moment of the metal ion. Experimental aspects of this will be encountered later.

To return to the example of MnO the magnetic molecular orbitals can be written as,

$$\Psi_1 = -d_1 + Ap_\sigma \qquad \Psi_2 = d_2 + Ap_\sigma \tag{1.20}$$

where the normalising constants are taken as unity. Using the notation (Mn(1), Mn(2)) the two unpaired electrons can be arranged as

$$(\uparrow,\downarrow) \quad (\uparrow,\uparrow) \quad (\uparrow\downarrow,\ )$$

The last arrangement gives the excited state ($Mn^{+} - O^{2-} - Mn^{3+}$) of energy U, the spins being antiparallel by Pauli's principle. The one electron Hamiltonian mixes this excited state into the antiparallel spins ground state depressing it relative to the parallel spins ground state by $4b^2/U$ where $b = \langle \Psi_1 | h | \Psi_2 \rangle$. This is equivalent to an antiferromagnetic interaction between the two spins of

$$J_e \, \underline{s}_1 \cdot \underline{s}_2 = (4b^2/U) \, \underline{s}_1 \cdot \underline{s}_2 \qquad (1.21)$$

In terms of the total spins the interaction is written

$$H_{ex} = J \, \underline{S}_1 \cdot \underline{S}_2 = \frac{b^2}{S^2 U} \, \underline{s}_1 \cdot \underline{s}_2 \qquad S = S_1, S_2 \qquad (1.22)$$

J is positive when representing an antiferromagnetic interaction.

Thus both ferromagnetic and antiferromagnetic interactions can be represented by a term of the form $J \, \underline{S}_1 \cdot \underline{S}_2$. If this term is much greater than any others in the spin Hamiltonian it forms states of total spin S (= $S_1 + S_2$, $S_1 + S_2 - 1, \ldots\ldots, 0$) with energies following a Landé interval rule. The $2S + 1$ substates of each total spin state are split by the remaining terms in H_s. When spin-orbit coupling is included the local symmetry imposed on the orbital angular momentum by the crystal field is transmitted to the spin giving rise to anisotropic exchange interactions. The anisotropy is represented by additional D_E and E_E terms in the spin Hamiltonian where D_E is of order $(g - 2)^2 . J$. The magnetic dipole-dipole interaction contributes a further term $D_d = -(g^2 \beta^2 / r_{ij}^3)$. The total spin Hamiltonian for an exchange coupled pair of ions i and j is then

$$H_s = H_i + H_j + J \, \underline{S}_i \cdot \underline{S}_j + (D_E + D_d)(3S_z^i S_z^j - \underline{S}_i \cdot \underline{S}_j) + E_e(S_x^i S_x^j - S_y^i S_y^j) \qquad (1.23)$$

where H_i is the spin Hamiltonian for the ith single ion.

CHAPTER II

PARAMAGNETIC RELAXATION MECHANISMS

In this Chapter various relaxation mechanisms are considered. They can be divided into three groups; spin-spin, spin-lattice and concentration dependent processes. They are taken in that order.

2.1 Spin-Spin Relaxation

In a crystal the many mutual interactions between paramagnetic ions, including exchange and dipole-dipole interactions, can broaden the Zeeman levels and give the spin system an internal energy. For spins with the same resonant frequency the precessing components of one magnetic dipole will set up an oscillatory field at another with just the right frequency to induce magnetic resonance transitions and vice versa. This causes a finite spin lifetime in a given quantum state which can be represented by a spin-spin relaxation time T_2. When disturbed, the spins re-establish internal thermal equilibrium in a time of order T_2.

Mutual spin flips occurring in an overlap region between two homogeneously broadened lines provide a mechanism whereby spins resonant with the microwave field can rapidly transfer absorbed energy to non-resonant spins. In crystals containing two different species of ions, or with ions of spin $> \frac{1}{2}$, the energy differences between pairs of Zeeman levels may be approximately equal or harmonically related. Co-operative processes can then occur involving simultaneous transitions almost conserving Zeeman energy, the imbalance being supplied from the internal energy of the spin system. Such cross relaxation processes were proposed by Bloembergen et al.(1959) and have been identified experimentally (e.g. Mims and McGee 1960).

Small spin-spin interactions will induce Zeeman transitions but under e.p.r. conditions this process is too weak to be of importance. It is necessary to consider interactions between the spin system and the lattice to

provide stronger relaxation mechanisms for relaxing Zeeman energies.

2.2 Spin-Lattice Relaxation

2.2.1 Rate Equations

Transition probabilities are derived from theoretical considerations and then related to experimental relaxation times by rate equations. If n_i is the population of state $|i>$ and P_{ij} the transition probability from $|i>$ to $|j>$ then, for the simple case of a two level system,

$$\dot{n}_1 = - n_1 P_{12} + n_2 P_{21} = - \dot{n}_2 \qquad (2.1)$$

Putting $n = n_1 - n_2$ and $N = n_1 + n_2$

$$\dot{n} = N(P_{21} - P_{12}) - n(P_{21} + P_{12}) \qquad (2.2)$$

If this transition is saturated with a pulse of microwave power at $t = 0$ $n_1 = n_2$ and the solution is

$$n = n_o \left\{ 1 - \exp\left\{ \frac{-t}{T_1} \right\} \right\} , \quad \text{where } \frac{1}{T_1} = P_{12} + P_{21} \qquad (2.3)$$

T_1 is the spin-lattice relaxation time. The spin system will regain its thermal equilibrium population distribution in an exponential manner characterised by the time constant T_1. More generally

$$\dot{n}_i = - n_i \sum P_{ij} + \sum n_j P_{ji} \qquad (2.4)$$

which has a general solution

$$n_i = n_{i_o} + \sum A_{ki} \exp\left\{ \frac{-t}{T_k} \right\} \qquad (2.5)$$

k takes a maximum value of 2S for a system of spin S. Only terms with large values of A_{ki} are observed experimentally.

2.2.2 The spin-lattice relaxation mechanism

Lattice vibrations modulate the crystalline electric field acting

on the magnetic ion. This causes modulation of the electron's orbital motion which the spin senses via spin-orbit coupling. This process was first formally developed by Van Vleck (1940) and later elaborated by Mattuck and Strandberg (1960) for iron group ions and Orbach (1961) for rare earth group ions.

A Debye model of the lattice is assumed and its Hamiltonian obtained by associating an harmonic oscillator with each vibrational mode at its frequency. Nearest neighbours to the paramagnetic ion, together with the ion itself, are considered to form a cluster. Vibrations of the cluster are represented in normal displacements of the neighbours which can be written as linear combinations of ordinary displacements. The ordinary displacements are expressed in terms of the phonon spectrum.

The crystal field potential at the magnetic ion is expanded in power series to second order in the normal displacements. The Hamiltonian for the complete system of ion and lattice can be arranged into three groups, terms in lattice co-ordinates only H_L, terms in paramagnetic electron co-ordinates only H_s and terms in mixed co-ordinates H_{INT}. The group in electron co-ordinates is precisely the one giving rise to the usual spin Hamiltonian. Thus

$$H = H_s + H_L + H_{INT} \qquad (2.6)$$

H_{INT} is considered to induce energy conserving quanta exchanges between the electron and the lattice, so matrix elements of H_{INT} are required between simultaneous eigenstates of H_s and H_L.

2.2.3 The direct process

Under the energy conservation condition

$$E_a - E_b = \hbar\omega_p \qquad (2.7)$$

the transition probability to first order is of the form

$$P_{ab} = \text{Constant} \cdot \omega_p^2 \cdot T \cdot |\langle a|H_p|b\rangle|^2 \qquad (2.8)$$

where H_p is that part of H_{INT} in electron co-ordinates. The transition

probability shows a linear dependence on temperature which arises from a high temperature approximation ($\hbar\omega_p \ll kT$) for the average number of phonons in each mode,

$$p(\omega_p) = \left[\exp\left(\frac{\hbar\omega_p}{kT}\right) - 1\right]^{-1} \approx \frac{kT}{\hbar\omega_p} \qquad (\hbar\omega_p \ll kT) \qquad (2.9)$$

When it is valid to write $\hbar\omega_p = g\beta H$ the transition probability shows a quadratic dependence on magnetic field.

It now becomes necessary to distinguish between Kramer's and non-Kramer's ions. Kramer's theorem tells that a system containing an odd number of electrons has at least two fold degeneracy in the absence of an external magnetic field. Although the transition probability for a non-Kramer's ion is given by equation 2.8, the matrix elements involved for a Kramer's ion are zero. To obtain a non-zero transition probability for a Kramer's ion the applied magnetic field must mix an excited doublet into the ground state doublet and then matrix elements between the mixed states are non-zero. This gives a transition probability dependent on the fourth power of H.

2.2.4 The Raman process

Second order calculations, using terms of $\mathcal{H}_{INT}$ quadratic in lattice operators or the linear terms taken to second order, give rise to the Raman relaxation process. Raman relaxation occurs by the simultaneous creation and destruction of two phonons whose energy difference equals the spin flip energy. Although the matrix elements for this process will be smaller than those involved in the direct process, this is offset by the fact that all phonons up to the Debye cut-off frequency can be involved, since only energy differences are important.

The probability of a transition between states $|a\rangle$ and $|b\rangle$ produced by the linear part of $\mathcal{H}_{INT}$ in second order is,

$$P_{ab} = \frac{2\pi}{\hbar}\sum_{i,j}\left|\sum_{t}\frac{\langle a,n_i|\,\mathcal{H}_{INT}\,|t,n_i-1\rangle\langle t,n_j|\,\mathcal{H}_{INT}\,|b,n_j+1\rangle}{-\Delta_t+\hbar\omega_i}\right|^2 (\rho_i)(\rho_j)$$

where $|t\rangle$ is an intermediate excited spin state at an energy Δ_t above a and (ρ_i) the density of phonon modes per unit frequency interval. The sum over i and j is restricted by the energy conservation condition that $\hbar(\omega_i-\omega_j)$ equals the spin flip energy.

For a non-Kramer's ion with only one level $|c\rangle$ close to $|a\rangle$ the transition probability can be evaluated by approximating the summation over i and j to an integration and evaluating the matrix elements of the lattice operators. Under the usual condition that $k\Theta_D < \Delta_c$ the main contribution to the ensuing integral comes from phonons of energy $\hbar\omega_i \sim kT$. An approximation for the integral then gives

$$1/T_1 \propto T^7 \qquad (2.10a)$$

For a Kramer's system a pair of time conjugate states are found in place of $|c\rangle$. The transition probability is now to be evaluated over both excited states, $|c\rangle$ and $|d\rangle$. It then becomes necessary to consider all of the possible transitions, $|a\rangle$ to $|b\rangle$ as well as $|b\rangle$ to $|a\rangle$, which are accounted for in a non-Kramer's derivation merely by doubling the integral. The spin parts of the matrix elements are of the form

$$\frac{\langle a|\mathcal{H}_{INT}|c\rangle\langle c|\mathcal{H}_{INT}|b\rangle}{-\Delta+\hbar\omega_i} + \frac{\langle a|\mathcal{H}_{INT}|c\rangle\langle c|\mathcal{H}_{INT}|b\rangle}{-\Delta-\hbar\omega_j}$$

$$+ \frac{\langle a|\mathcal{H}_{INT}|d\rangle\langle d|\mathcal{H}_{INT}|b\rangle}{-\Delta+\hbar\omega_i} + \frac{\langle a|\mathcal{H}_{INT}|d\rangle\langle d|\mathcal{H}_{INT}|b\rangle}{-\Delta-\hbar\omega_j}$$

Orbach (1961) has shown that, were it not for the differences in denominators, this would be zero as a consequence of the time reversal symmetry of Kramer's doublets. As it is, only a partial cancellation occurs and, when $|c\rangle$, $|d\rangle$ are higher in energy than $k\Theta_D$, one finds

$$1/T_1 \propto T^9 \qquad (2.10b)$$

Mixing of states by an applied magnetic field H can give a rate $\propto T^7H^2$.

2.2.5 The Orbach process

Orbach (1961) considered the situation when the first excited level $|c\rangle$ has an energy separation from the ground level less than the limiting Debye frequency ($\hbar\omega_D > \Delta_c$). When $\Delta_c = \hbar\omega_p$ the energy denominator of 2.9 vanishes and furthermore the integrals used to derive 2.9 diverge. To overcome this Orbach allowed the intermediate state a finite lifetime. However, this process is easiest to consider as a two step direct process with each step conserving energy.

Consider a doublet $|a\rangle$ and $|b\rangle$ where $E_b - E_a = \delta \ll kT$ relaxing through $|c\rangle$ where $E_c - E_b = \Delta < k\Theta_D$ then

$$\dot{n}_b = P_{cb}n_c - P_{bc}n_b$$
$$\dot{n}_a = P_{ca}n_c - P_{ac}n_a \qquad (2.11)$$

This has the solution

$$n_b - n_a = A'\exp\left\{\frac{-t}{T'}\right\} + A''\exp\left\{\frac{-t}{T''}\right\} + (n_b - n_a)_{\text{equilibrium}} \qquad (2.12)$$

$$(1/T','') = \tfrac{1}{2}\left(P_{cb} + P_{bc} + P_{ca} + P_{ac} \pm \left((P_{cb} + P_{bc} - P_{ca} - P_{ac})^2 + 4P_{ca}P_{cb}\right)^{\frac{1}{2}}\right)$$

To obtain the temperature dependence of this process the transition probabilities for direct transitions are taken as

$$P_{bc} = B_1 p(\Delta_c) \qquad P_{cb} = B_1(p(\Delta_c) + 1)$$
$$P_{ac} = B_2 p(\Delta_c + \delta) \qquad P_{ca} = B_2(p(\Delta_c + \delta) + 1) \qquad (2.13)$$

The temperature dependence of the direct process is determined by the matrix elements of the lattice operators which make the transition probability proportional to the number of phonons available, p, at the frequency required for the transition.

Generally $$p(\omega_p) = \left\{\exp\left\{\frac{\hbar\omega_p}{kT}\right\} - 1\right\}^{-1} \qquad (2.14)$$

Taking $p(\Delta + \delta) = p(\Delta)$ and substituting 2.13 and 2.14 into 2.12 will give

for the long experimentally observable relaxation time, taken arbitrarily as $1/T''$,

$$\frac{1}{T''} = \frac{B_1 B_2}{B_1 + B_2}\left\{2\exp\left\{\frac{-\Delta}{kT}\right\} + \left\{1 + \frac{4B_1B_2}{(B_1+B_2)^2}\right\}\exp\left\{\frac{-2\Delta}{kT}\right\} + \ldots\right\} \qquad (2.15)$$

When $B_1 = B_2$, to a good approximation,

$$\frac{1}{T''} = B \exp\left\{\frac{-\Delta}{kT}\right\} \qquad (2.16)$$

This process has been well verified experimentally (Scott and Jeffries 1962).

2.3 The Phonon Bottleneck

Experimentally spin-bath relaxation times are measured whereas calculated spin-lattice relaxation times are strictly spin-phonon relaxation times. At low temperatures an energy flow from spins to the lattice can cause the lattice temperature, for the phonons concerned, to exceed that of the bath. The lattice will then re-establish thermal equilibrium with the bath by new processes with their own relaxation times. Under certain circumstances the observed relaxation behaviour of the spin system can be dominated by such phonon relaxation times.

Energy can be transferred to the bath from the phonons responsible for relaxation in several ways. The rate determining process may involve the transfer of energy in space or frequency. The former process, the spatial bottleneck, has as a bath the liquid helium surrounding the crystal and gives relaxation times dependent on characteristic lengths of the crystal. The latter process, the spectral bottleneck, for which phonons with energy of order kT form the bath, gives various temperature dependencies. A review of phonon bottlenecks is given by Stoneham (1965).

This completes this survey of the relaxation mechanisms of isolated paramagnetic ions. The processes here reviewed account successfully for many experimental results. However, measurements on paramagnetic ions doped into diamagnetic hosts sometimes give relaxation times which depend on the

concentration of paramagnetic ions. Such concentration dependent relaxation processes cannot be interpreted in terms of theories developed for isolated ions.

2.4 Concentration Dependent Relaxation Processes

Several authors have suggested that concentration dependent relaxation processes occur by isolated ions cross relaxing to exchange coupled clusters of ions, (see 'Advances in Quantum Electronics' 1960 and 1961). Such clusters are expected to occur on statistical grounds. The density of clusters at low concentrations is related to the total paramagnetic concentration c by a simple power law, c^2 for pairs, c^3 for triads etc. When the cross relaxation rate is very fast the limiting process is the relaxation rate of the clusters.

Exchange coupled clusters are expected to relax faster than single ions (Harris and Yngvesson 1968) since,

1) Exchange splittings of the ground state are larger than the normal Zeeman splittings, giving clusters access to a more densely populated region of the phonon spectrum.

2) Exchange interactions depend very strongly upon the relative positions of the ions so modulation of inter-ion distances can couple spins strongly to the lattice.

3) Ground states which are not pure spin states are modified in second order by exchange interactions introducing small admixtures of excited states.

2.5 Reported Examples of Relaxation Involving Exchange

The first experimental confirmation of a relaxation mechanism involving exchange interactions was obtained by Gill (1962) working on chromium pairs in ruby. The relaxation of the $S = 3$, $M_s = 0$ to $S = 3$, $M_s = -1$ transition was explicable by a two phonon direct process via an intermediate lower state.

If the energy matrix for an exchange coupled pair of ions, each of

effective spin 3/2, is set up with respect to combinations of the uncoupled ion wavefunctions, a D term introduces off-diagonal elements connecting states with $\Delta S = \pm 2$, $\Delta M_s = 0$. An operator of the form $\underline{S}_1 \cdot \underline{S}_2$ then has matrix elements of order D/J connecting the same states. If modulation of J is to provide the relaxation mechanism, the probability of its producing a direct transition between $|i\rangle$ and $|j\rangle$ is proportional to,

$$|\langle i| \, dJ/dr \, (\underline{S}_1 \cdot \underline{S}_2) |j\rangle|^2 \approx (dJ/dr)^2 \, (D/J)^2 \qquad (2.17)$$

The mechanism should now be visualised as a two step process via the spin 1 manifold. Strictly a mixing of the spin states within each manifold is required in order to relax the Zeeman energy. By taking dJ/dr to be $13 cm^{-1} Å^{-1}$, a value that agrees well with estimates from other sources, Gill was able to fit the experimental data.

The relaxation of the single chromium ions was concentration dependent and was shown to be in order of magnitude agreement with cross relaxation to pairs.

A much more detailed and analytical paper has been presented by Harris and Yngvesson (1968). They measured the spin lattice relaxation of nearest neighbour exchange coupled pairs of Ir^{4+} ions in $(NH_4)_2PtCl_6$. This system has been extensively studied by the Clarendon group. The Ir^{4+} ion is octahedrally co-ordinated with an e.p.r. ground state of effective spin $\frac{1}{2}$. Isotropic exchange gives the usual singlet and triplet, the latter being split in zero field by anisotropic exchange terms. Paramagnetic transitions are observed within the triplet.

The authors consider possible relaxation mechanisms involving modulation of exchange interactions but none prove correct. For this system perturbations of the form $J' (\underline{S}_1 \cdot \underline{S}_2)$ give no off-diagonal elements between spin states. Modulation of the crystal field is treated by taking the normal modes of vibration of the pair complex as symmetric and antisymmetric combinations of the corresponding single ion modes. Symmetric combinations give rise to matrix elements directly between the triplet states causing direct relaxation

THE ENERGY LEVELS FOR SOME CLUSTERS OF S=½ IONS

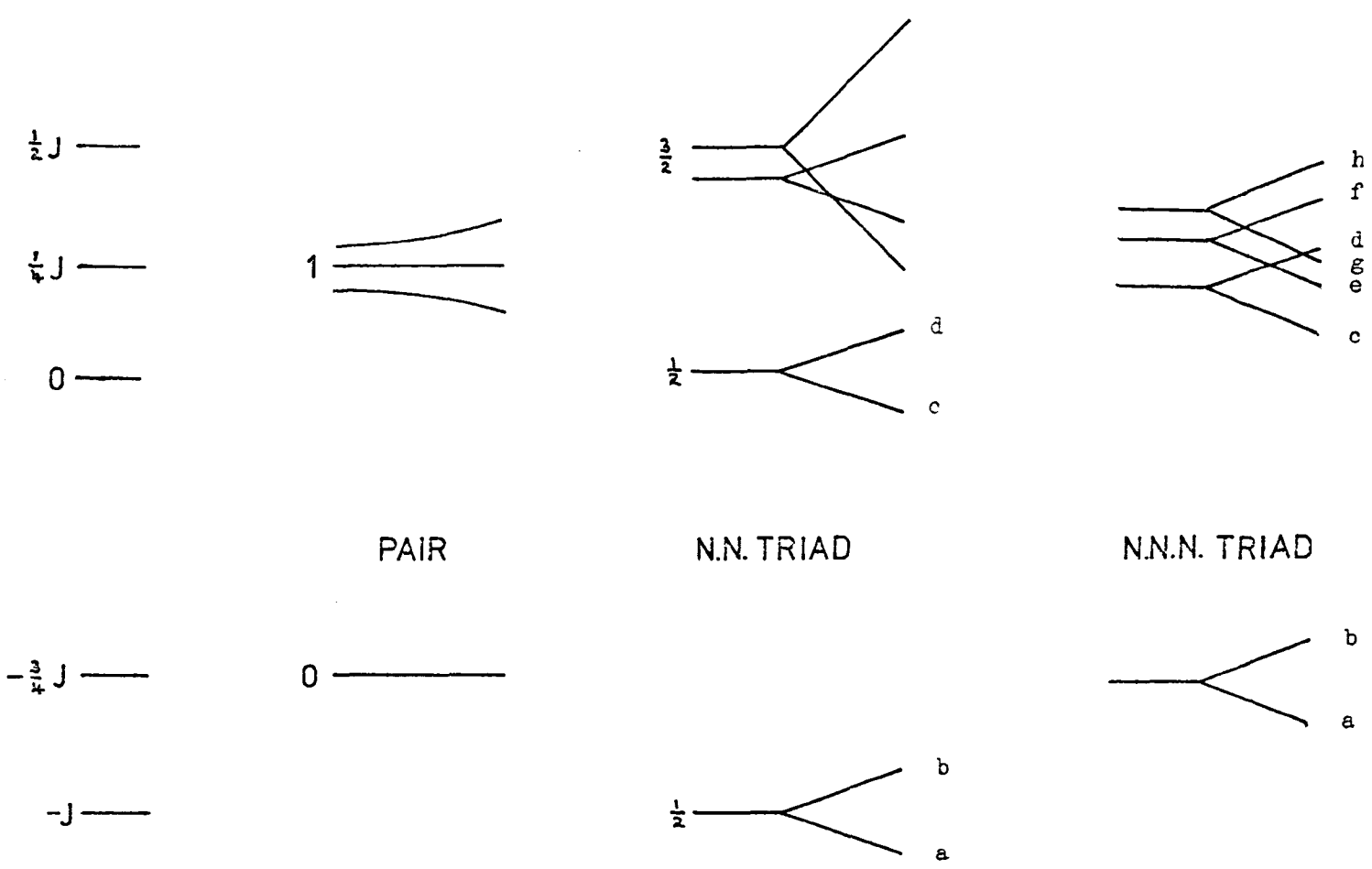

FIGURE 2.1

processes. The antisymmetric combinations lead to relaxation between the singlet and the triplet and hence to two phonon direct processes. It was decided that the latter process was, in the main, responsible for the experimental results.

The relaxation of isolated Ir^{4+} ions could be expressed as a sum of terms due to direct, Raman and concentration dependent processes. The concentration dependent term was of the form

$$\frac{1}{T_{1c}} = \text{constant}.c^2 \exp\left(\frac{-\Delta}{kT}\right) \qquad (2.18)$$

for concentrations of less than 3%. The energy Δ was very similar to the nearest neighbour exchange energy. Cross relaxation to the pair system previously described was discounted since the pairs relaxed too slowly and, furthermore, there was no coincidence of transitions to allow effective cross relaxation.

A likely form for the cluster appeared to be a nearest neighbour triad with the Hamiltonian

$$\mathcal{H} = J_1(\underline{S}_i.\underline{S}_j + \underline{S}_j.\underline{S}_k) \qquad (2.19)$$

The Zeeman splittings of the two doublets shown in figure 2.1 equal that for the single ion making cross relaxation between the two systems easy. Modulation of the two interactions gives two perturbation terms, one symmetric and one antisymmetric in $\underline{S}_i$ and $\underline{S}_k$. The antisymmetric term couples $|a\rangle$ to $|c\rangle$ and $|b\rangle$ to $|d\rangle$. However, in order to relax the Zeeman energy by exchange energy transitions, two phonon direct processes have to be invoked requiring, for example, $|c\rangle$ to be coupled to $|b\rangle$. This will only occur when states are mixed by anisotropic exchange which greatly reduces the efficiency of this process and also leads to the wrong temperature dependence.

A third possibility is a triad consisting of a nearest neighbour pair, one member of which has a next nearest neighbour, giving the Hamiltonian

$$\mathcal{H} = J_1(\underline{S}_i.\underline{S}_j) + J_2(\underline{S}_j.\underline{S}_k) \qquad (2.20)$$

Cross relaxation can occur between the doublet ground state and the single ions,

The states are similar to pair states but $J_2(\underline{S}_j.\underline{S}_k)$ produces a small perturbation on the energy levels ($J_2 \approx 0.06 J_1$). The antisymmetric perturbation term from the exchange Hamiltonian couples $|a\rangle$ and $|b\rangle$ to $|c\rangle$ and $|d\rangle$ (figure 2.1) giving fast relaxation between them. The term in J_2 introduces admixtures between the ground and excited states coupling $|a\rangle$ to $|d\rangle$ and $|e\rangle$ and $|b\rangle$ to $|f\rangle$ and $|g\rangle$. This allows the second step of the relaxation process but reduces it by a factor of $\frac{1}{8}(J_2/J_1)^2$ compared to the first step. Substituting these rates into the expression for the Orbach process (2.15) gave satisfactory agreement with experiment.

This prompted Harris (1969), in a later paper, to look for changes in the resonance signal from such triads when the single ion resonance was saturated by a pulse at a different frequency. This was done by using a cavity simultaneously resonant at 9.86 Ghz in the TE_{111} mode and at 33.1 Ghz in the TE_{104} mode. A suitable crystal orientation allowed a transition between the upper triad levels and the single ion resonance to occur at the same field. When pulses of power at 9.86 Ghz were used to saturate the single ion resonance weak pulses were detected at 33.1 Ghz which, at the end of the saturating pulse, decayed with a time constant closely equal to that of the single ions.

THE EXPERIMENTAL SYSTEM

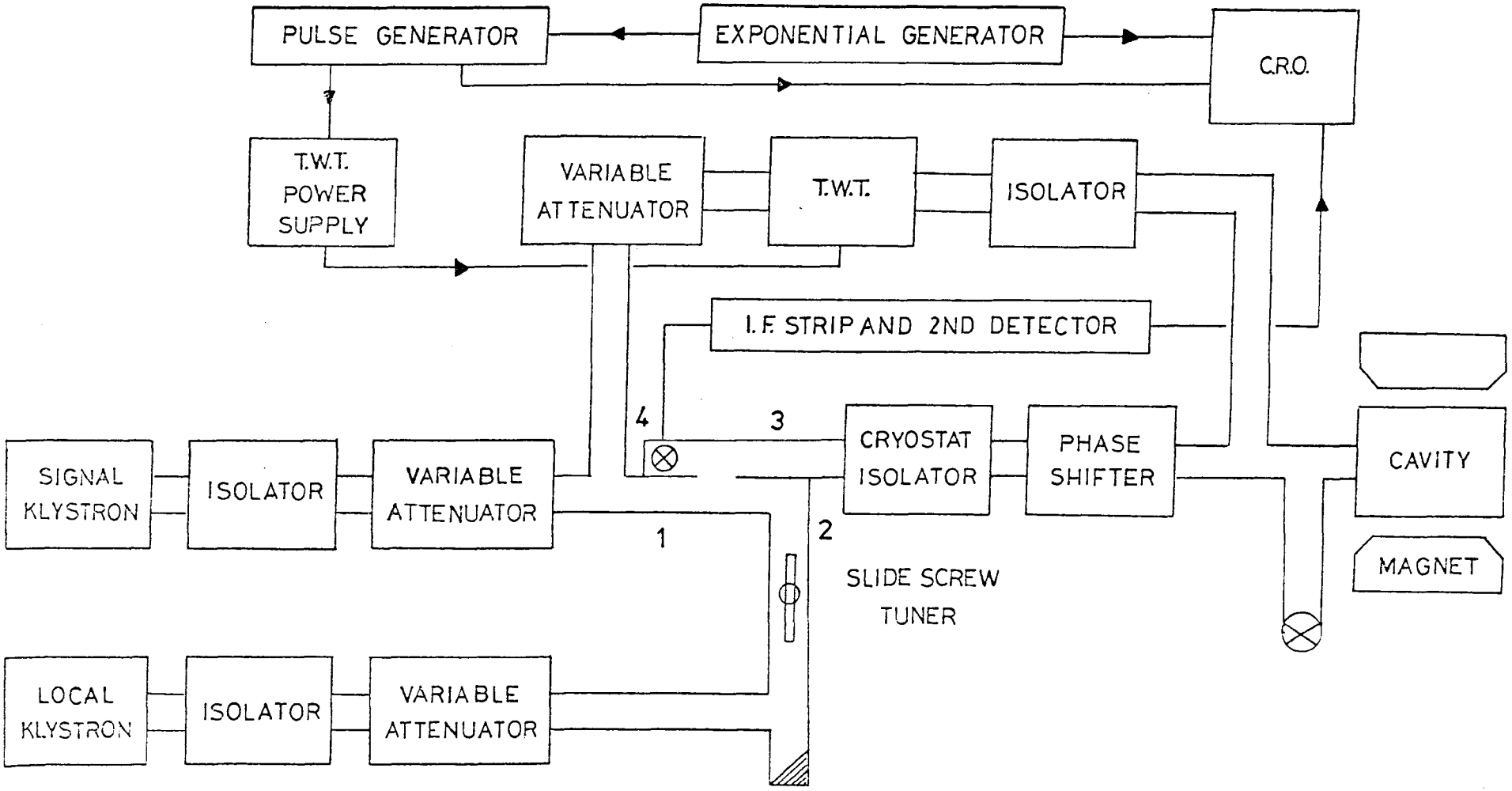

FIGURE 3.1

CHAPTER III

EXPERIMENTAL TECHNIQUES

The experimental results reported in this thesis were obtained using a Varian V-4502 spectrometer. The equipment has facilities for operating at X or Q band with either 100 kHz or audio frequency (a.f) modulation. The majority of the work was carried out at X band using superheterodyne detection and a.f modulation. Figure 3.1 shows the block diagram of the apparatus described in this chapter.

3.1 The Spectrometer

The X band signal klystron is manually tunable over the range 9 - 10 GHz and can be locked to the cavity frequency by means of a 10 kHz automatic frequency control system. A microwave bridge system, slightly unbalanced in amplitude, is used for detection of absorption signals. Klystron power from arm 1 is divided between arms 2 and 3. Power passing down arm 3 can be attenuated and phase shifted before reaching the reflection cavity. Part of the power returning from the cavity is detected at the crystal. Power entering arm 2 is reflected onto the detector crystal by a slide screw tuner which can be adjusted to change both the phase and the mean level of the reflected power. In this way the crystal is biased. During resonance the sample absorbs microwave power causing the bridge to be further unbalanced. This is detected as a power change at the crystal.

To allow a simple cavity to be employed external modulation coils were used to provide a.f. magnetic field modulation. For greater efficiency the coils were made part of a series resonant circuit fed by a Quad power amplifier. When detecting at low frequencies flicker noise due to the detector crystal is a serious sensitivity limitation. To overcome this superheterodyne detection is employed which involves

feeding power from a second klystron (the local oscillator) to the crystal detector. This klystron is tuned to oscillate 30 MHz away from the signal klystron. The two signals mix at the detector producing an audio modulated component at 30 MHz which is amplified before rectification at a second detector. This means that detection occurs at 30 MHz where noise considerations are at a minimum.

It was occasionally necessary to measure the microwave frequency of the signal klystron. A signal obtained from a waveguide to coaxial converter and mixed in a Hewlett Packard 5257A transfer oscillator allows the frequency to be found by the zero beats method.

3.2 The Pulsing Equipment

It has been shown that the amplitude of an absorption signal is directly proportional to the instantaneous population difference between the two levels concerned. To measure relaxation times the technique is to saturate the transition by a pulse of resonant microwave power and use continuous low power resonant microwaves to monitor the recovery of the transition after the pulse has passed. The signal amplitude at the second detector due to this low power radiation then measures the return of the population to their equilibrium values.

Saturating power was derived from a G.E.C. TWX8 travelling wave tube (T.W.T.). A T.W.T. is a broad band power amplifier giving, in this case, 30 db gain when on and 60 db when off. By feeding the T.W.T. with a few milliwatts of power from the signal klystron an output of about 1 watt at the same frequency could be obtained. Pulses of power are obtained by switching the T.W.T. power supply by a pulse generator. The pulse generator was designed and built with the aid of the electronics workshop to give pulse repetition frequencies continuously variable between 1 and 100 per second and variable pulse widths between 20 microsecs and 1.8 millisecs.

In order to analyse relaxation traces on an oscilloscope a double

exponential generator was built using pulse charged stable RC networks. Its output is the sum of two exponential functions each independently variable in amplitude and time constant. It was triggered from the pulse generator and its output fed to one channel of a dual beam oscilloscope, also triggered by the pulse generator. The output from the second detector was fed to the other channel and the generated exponential adjusted to match it. T_1 could then be read off.

3.3 The Magnet

The static magnetic field is obtained from a Varian V-3400 9" water cooled electromagnet which can be rotated through 360°. For work at X band 10 kilogauss can be obtained with an air gap of $2\frac{1}{2}$", while at Q band, with the addition of extra pole pieces, the maximum field is 15.25 kilogauss with an air gap of $1\frac{3}{4}$". The magnet is controlled by a 'Fieldial' magnetic field regulator allowing any value of field to be selected. This uses an error signal between the field controls, which are set to the desired field, and a Hall effect probe on one of the pole faces, to bring them to the same value.

The calibration accuracy of the field was good at g = 2 but rather poorer at high and low fields. The 'Fieldial' was therefore calibrated over its complete range using a proton resonance probe and the results least squares fitted to a linear function. Then, given any 'Fieldial' field, the true field can be calculated to within ±2 gauss.

3.4 The Cryostat and Cavity

A rectangular TE_{101} cavity was used for experiments at liquid helium temperatures. It was made from a length of copper waveguide which was sealed at the bottom with a copper plate and at the top by shimstock hard soldered into a cut through three of the waveguide walls. A 0.159" diameter iris was drilled through the shimstock. A 10 B.A. pin, threaded

through the broad face of the waveguide just before the iris, adjusted the cavity coupling. Experience soon taught the best setting for the coupling screw to give good coupling at helium temperatures. The cavity was broken at the quarter wavelength point to allow samples to be inserted on the narrow face. Samples were attached with a low temperature varnish. If required, a thin walled copper can could be screwed over the cavity to exclude even superfluid helium. An MD4 stainless steel cryostat manufactured by Oxford Instruments was used for the experiments. The cavity assembly was bolted to a length of stainless steel waveguide which passed to the top plate of the cryostat.

3.5 Low Temperature Techniques

Temperatures between 77°K and about 10°K were obtained by controlling the rate of flow of liquid helium into the cryostat from the storage dewar. Performed with care this could give good temperature stability for a few minutes although specific temperatures were difficult to obtain.

Temperatures below 4.2°K were obtained by pumping on liquid helium through a cartesian manostat which allowed the pressure above the helium to be kept constant. This allowed the sample to reach temperatures down to ~2.2°K in a controlled manner. Direct pumping on the helium would take the temperature down to ~1.6°K. The pressure was measured on a mercury manometer, a stainless steel tube let down into the cryostat being connected to one arm, while the other arm was evacuated.

Temperatures above 4.2°K could be obtained by a desorption method. The cavity was surrounded by granular activated charcoal held in a mesh can. When the liquid helium has boiled away the charcoal remains saturated with adsorbed gas. Gentle pumping causes the gas to desorb more quickly, therefore lowering the temperature of the system, as the heat of desorption used to release the molecules is extracted from the cavity. By adjusting the pumping speed, to balance refrigeration by desorption and heat leaks, the temperature

can be held constant. This helium desorption method, although satisfactory for taking e.p.r. spectra above 4.2°K by locking the klystron to the cavity, did not give a sufficiently stable cavity frequency to allow relaxation measurements, which preclude the use of the A.F.C. system.

In order to extend the temperature range over which relaxation measurements could be taken, a new temperature control system was devised, involving the use of an exchange gas. A P.T.F.E. can with a split in its wall was made up to surround the cavity. A thin walled stainless steel can, about 18" long, fitted over the P.T.F.E. can and was attached to the waveguide by flanges. The complete assembly fitted into the inner tail of the cryostat. The technique was to collect liquid helium in the cryostat with the stainless steel can serving to exclude liquid from direct contact with the cavity. Helium gas from a storage cylinder was then bled into the waveguide and allowed to escape via a small hole just above the cavity. By adjusting the flow of the helium gas any required temperature could be obtained. Relaxation measurements between 4.2°K and 11°K were made by using this technique.

Temperatures between 4.2°K and liquid nitrogen temperatures were measured by using a calibrated Allen Bradley $\frac{1}{8}$watt 100 ohm resistor supplied by Cryogenic Calibrations. The resistance was measured on a D.C. bridge using a Keithley 150 B microvolt ammeter as a null detector. This allowed resistances to be measured to 0.1% giving an accuracy of 0.1°K at 20°K. The reproducibility of the resistance characteristics between runs was good.

Some of the results reported in this thesis were obtained by employing a flow system. Nitrogen gas is passed through metal coils immersed in liquid nitrogen to cool it. The cold gas is then passed to a flow dewar mounted in the cavity. The temperature is monitored by a thermocouple positioned in the gas stream at the bottom of the flow dewar. The cavity is usually flushed with dry nitrogen gas to prevent water condensing in it. A goniometer screws over the top of the flow dewar allowing the sample to be mounted in the gas flow on a quartz rod. This technique gives temperatures in the range 77°K to about 200°K, depending on the flow rate.

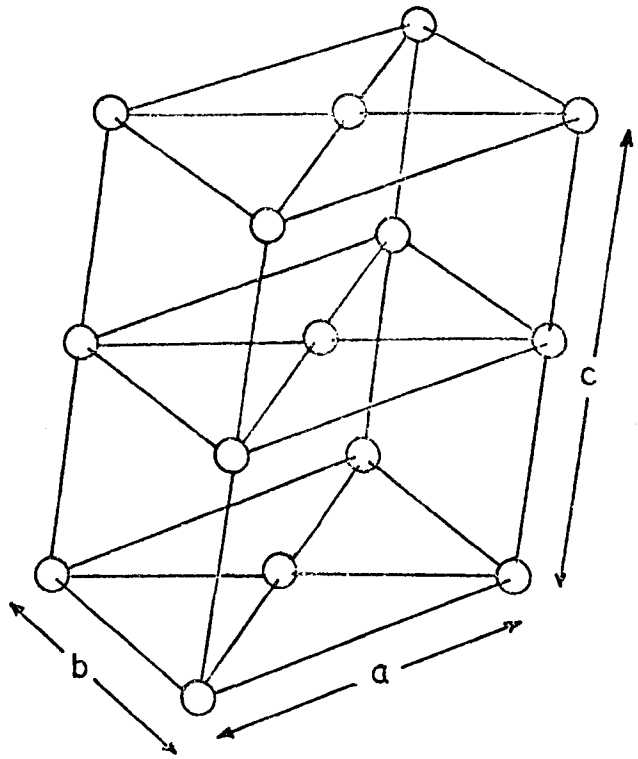

THE CRYSTAL STRUCTURE

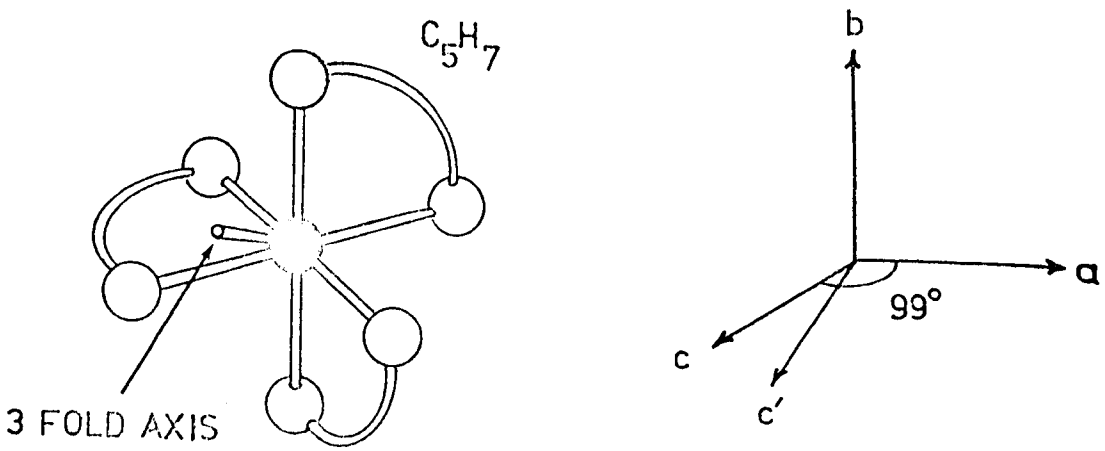

THE MOLECULAR STRUCTURE

FIGURE 4.1

CHAPTER IV

RUTHENIUM ACETYLACETONATE

4.1 Introduction

The first problem to be investigated was the possibility of studying the relaxation of pair lines in ruthenium doped aluminium acetylacetonate. The $4d^5$ ruthenium ion is similar to the $5d^5$ Ir^{4+} ion which has proved to form a very good system for the study of pair-type behaviour. Unfortunately, a phase change occurs in these crystals between 77°K and 4.2°K, giving rise to six ruthenium sites, which considerably complicates the pair spectra and reduces the intensity of each pair line. The single ion resonances were investigated as a first step in interpreting the pair lines prior to possible relaxation studies and to offer an introductory e.p.r. problem. Good single crystals doped with 2% ruthenium were obtained from Dr. D. E. Dugdale who had grown them by evaporation from solution in acetone (Dugdale 1967).

The crystal structure of the acetylacetonates has been determined as monoclinic (Astbury 1926, Roof 1956) with alternate stacking of right and left handed molecules. The symmetry axes of the molecules generally make angles of $\pm 31^\circ$ with the b axis, forming two magnetically inequivalent sites, but this has not been determined for ruthenium. The molecular structure consists of three acetylacetonate groups, $CH_3 - CO - CH - CO - CH_3$, surrounding the metal ion to form an octahedron of oxygen atoms. This chelate is shown in figure 4.1

4.2 Crystal Field Predictions

In this complex, ruthenium exists in its trivalent state, $4d^5$. The paramagnetic behaviour can be explained qualitatively by the strong crystal field approximation. The cubic component of the crystal field is diagonalised first, splitting the five orbital d states into a lower triplet, t_2, and an upper doublet, e. Crystal field energy is minimised by placing all of the d^5

electrons into t_2 thus breaking down Hund's rules. The large separation between t_2 and e allows t_2 to be considered as a completed subshell with one hole. This gives the lowest energy levels as for d' except that they are inverted. Applying spin-orbit coupling and the lower symmetry elements of V_c produces three Kramer's doublets. Paramagnetic resonance is observed from the lowest doublet with a highly anisotropic g tensor reflecting the presence of rhombic crystal field terms.

4.3 Preliminaries

Jarrett (1957) has investigated the e.p.r. spectrum in these crystals at liquid nitrogen temperatures. He found two magnetic sites with g values of:-

$g_z = 2.82 \pm 0.02$ $\quad g_x = 1.28 \pm 0.05$ $\quad g_y = 1.74 \pm 0.02$

He does not report the orientation of the tensor axes to the crystallographic axes. Atempts were made to reproduce this work but, curiously, no resonances were found at this temperature.

On cooling to liquid helium temperature six strong resonances were observed. In order to investigate their origin it was necessary to choose a convenient set of axes in the crystal to which to refer g value measurements. The reference axes were taken as the a and b crystallographic axes together with the direction perpendicular to both a and b, denoted c'. Angular variations were performed in the a, b and c' planes using DPPH as a g marker. Mounting the crystal for the angular variation in the c' plane required the use of a carefully machined stycast wedge.

4.4 The Treatment of Results

4.4.1 The Theoretical Situation

The results are treated by the method of Zeldes and Livingstone (1961). For a spin $\frac{1}{2}$ situation the spin Hamiltonian is

$$H_s = \underline{H}.g.\underline{S} \qquad (4.1)$$

TABLE 4.1

	2.861	0.196	1.075
SITE I	0.196	5.873	-2.033
	1.075	-2.033	1.916
	3.565	0.304	0.437
SITE II	0.304	5.729	-1.922
	0.437	-1.922	1.807
	3.118	0.520	0.904
SITE III	0.520	5.506	-2.051
	0.904	-2.051	2.553

TABLE 4.2

Principal g values and direction cosines with respect to a, b and c'.

g-value	a	b	c'	
2.60	0.0643	-0.9146	0.3992	
0.75	0.4220	-0.3376	-0.8414	I
1.83	-0.9043	-0.2225	-0.3643	
2.55	0.0396	0.9265	-0.3743	
0.96	0.1930	-0.3747	-0.9069	II
1.91	-0.9804	-0.0360	-0.1938	
2.56	0.0109	0.8910	-0.4539	
1.00	0.4372	-0.4136	-0.7986	III
1.905	-0.8979	-0.1868	-0.3987	

THE ANGULAR VARIATION IN THE 45° PLANE

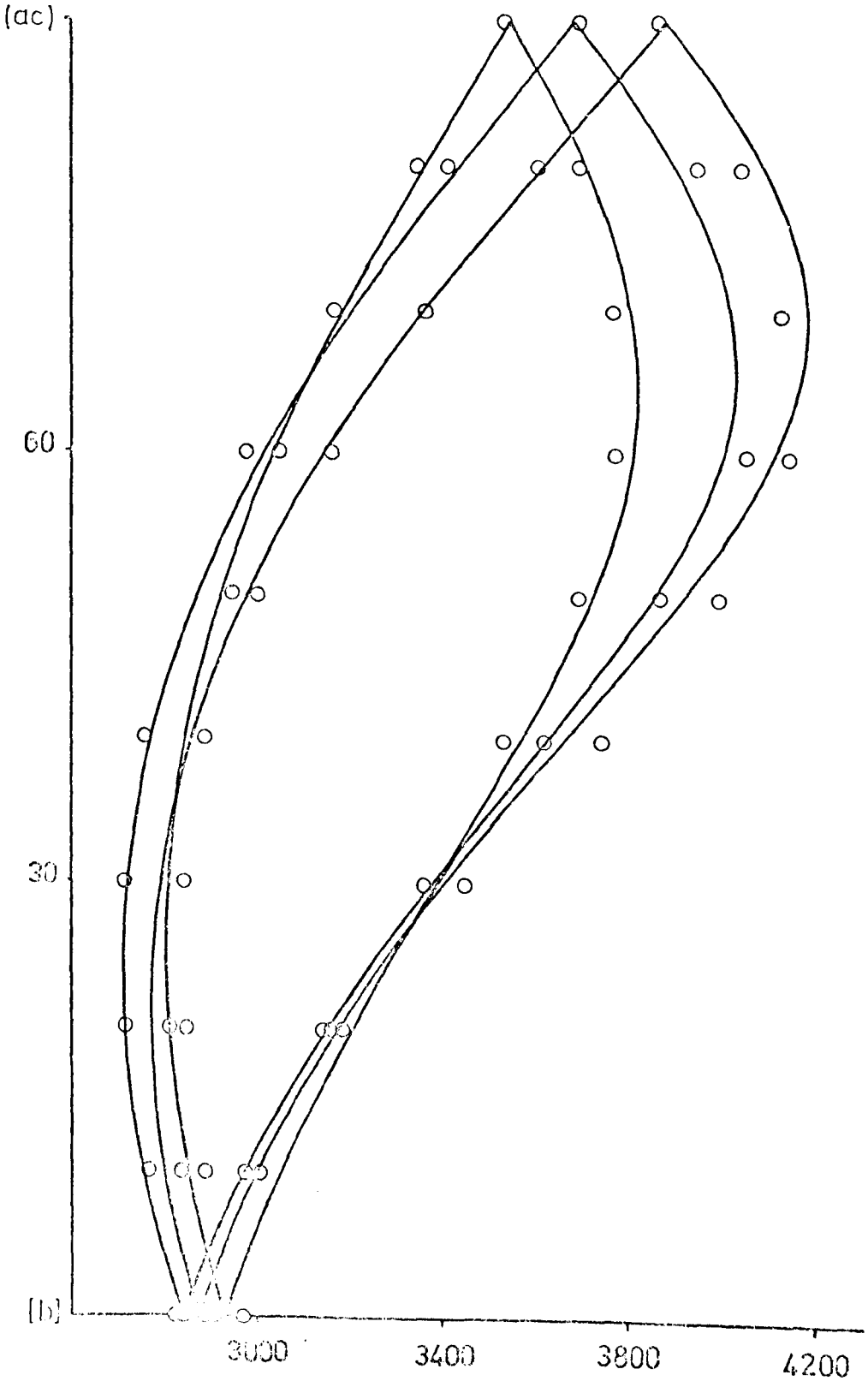

FIGURE 4.2

Squaring the resonance condition gives

$$(h\nu)^2 = \beta^2 (gH)^2 \qquad (4.2)$$

By writing $\underline{H}$ in direction cosines with respect to the crystallographic axes, for example $\underline{H} = H(l_a, l_b, l_{c'})$ an effective g value g' can be defined where

$$(g')^2 = (l_a, l_b, l_{c'}) \begin{bmatrix} (g^2)_{aa} & (g^2)_{ab} & (g^2)_{ac'} \\ (g^2)_{ba} & (g^2)_{bb} & (g^2)_{bc'} \\ (g^2)_{c'a} & (g^2)_{c'b} & (g^2)_{c'c'} \end{bmatrix} \begin{bmatrix} l_a \\ l_b \\ l_{c'} \end{bmatrix} \qquad (4.3)$$

In the c' plane, for example, where the direction cosines are $(\cos\vartheta, \sin\vartheta, 0)$ this can be written in the form

$$(g')^2 = G_{aa} \cos^2\vartheta + G_{ab} \sin\vartheta \cos\vartheta + G_{bb} \sin^2\vartheta \qquad (4.4)$$

Experimentally the g value of each line at a series of angles in this plane is found and its square least squares fitted to equation 4.4. Repeating this in the a and b planes determines the tensor with respect to a, b and c'. The problem now reduces to diagonalising $(g')^2$. The eigenvalues give the squares of the principal g values and the eigenvectors their orientation with respect to a, b and c'.

Since it was not possible to follow each line unambiguously from one plane to another, because of the pair equivalence, it was not possible to establish the relative signs of the cross products G_{ab} and $G_{bc'}$ of any one line with the results so far obtained. To resolve this problem, and as a final check on the g tensor, a crystal was mounted on a 45° stycast wedge and an angular variation performed in the plane including b and bisecting a and c'. The fit in this plane required G_{ab} and $G_{ac'}$ to take opposite signs. The angular variation in this plane is shown in figure 4.2. No attempt has been made to correct for mis-orientation although this angular variation is quite sensitive to changes in angle.

The tensors found for each pair from fitting the results to equation 4.3 are shown in table 4.1. Diagonalising the tensors which have G_{ab} as

THE G TENSORS OF THE Ru SITES

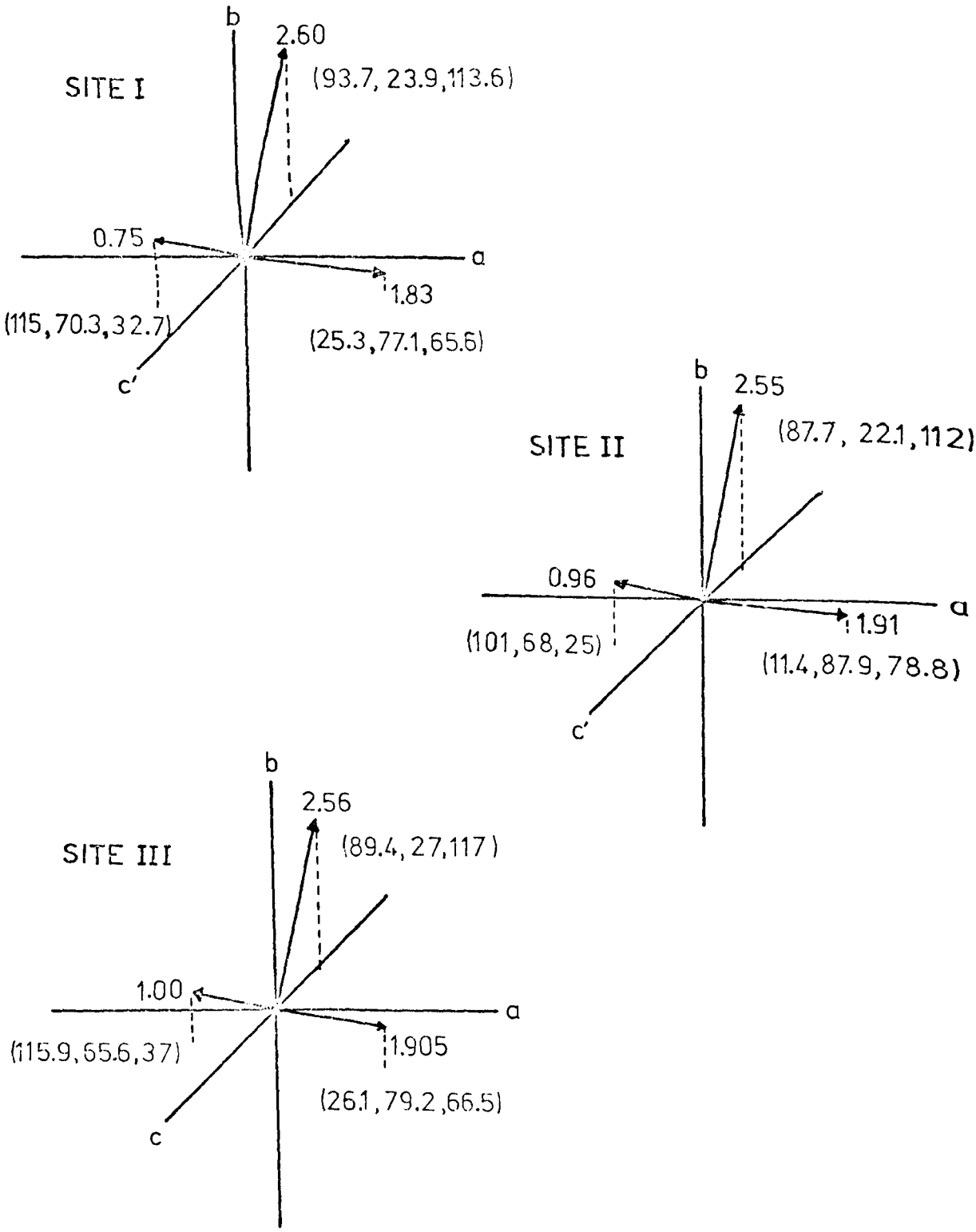

FIGURE 4.3

positive and $G_{bc'}$ as negative gives the principal g values and direction cosines of table 4.2. These are shown graphically in figure 4.3. The other member of each pair is obtained by rotating the tensor axes through 180° about b.

4.4.2 Errors

Misorientations were the major source of error in these experiments. They arose from actually mounting the crystal in the cavity and from the waveguide distorting on cooling. However, it was soon apparent from the angular variations that the six ruthenium sites were equivalent in pairs along the b axis and in the b plane. Then, by averaging the angular variations of each equivalent pair, it was possible to ignore misorientations as a first approximation.

Errors in principal g values and their direction cosines were calculated from the formulae given by Schonland (1959). Taking the error of each G_{ij} to be ±2% leads to the following errors from the third tensor of table 4.2.

g value	α°	β°	γ°
2.56 ± 0.01	89.5 ± 2	27.0 ± 2	117.0 ± 2
0.995 ± 0.015	116.0 ± 6	65.5 ± 3	37.0 ± 6
1.905 ± 0.01	26.0 ± 6	79.0 ± 3	66.5 ± 6

Errors in the other tensors will be similar.

4.5 Discussion of the Phase Change

The existence of a phase change is not unique to ruthenium doped into this particular complex. Similar behaviour has been reported for ruthenium doped into $Co(NH_3)_6Cl_3$ (Griffiths, Owen and Ward, 1953) where three different types of $(Ru(NH_3)_6)^{3-}$ complex were found, each with different rhombic distortions. As we have seen, ruthenium is particularly sensitive

A TYPICAL RUTHENIUM SPECTRUM

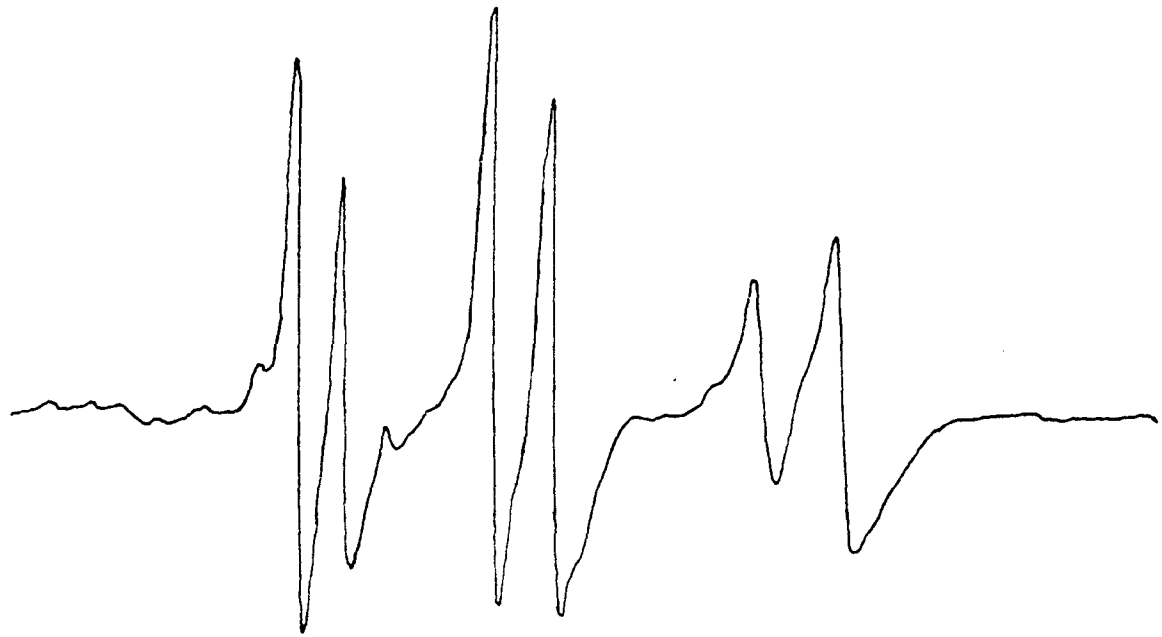

FIGURE 4.4

to rhombic terms.

McGarvey (1964) and Singer (1955) have investigated the paramagnetic behaviour of chromium in both the cobalt and aluminium isomorphs and have found a small E term. Their analyses took the rhombic z axis as parallel to the trigonal direction although no evidence exists for this assumption. However, since E is small ($\sim 0.009 cm^{-1}$), errors introduced in this way would not be very large. These measurements were taken at room temperature, indicating the presence of rhombic fields without introducing changes from the crystal structure of figure 4.1. The measurements of Jarrett at liquid nitrogen temperatures confirm this. Phase transitions have been noted in the chromium spectra at about $100^{\circ}K$ in the aluminium chelates and between $70^{\circ}K$ and $4.2^{\circ}K$ in the cobalt chelates.

Since the molecular structure does not indicate a rhombic component of crystal field, the origin of rhombic terms and the phase change will probably be found in the field due to neighbouring molecules. It does not seem possible to identify a detailed source for the phase change since no simple relationship exists between the principal g values and their directions at different sites, apart from their equivalence in pairs. This equivalence in pairs below the phase transition temperature suggests that no great change in crystal structure occurs.

4.6 The Pair Lines

Many small lines were observed in the spectrum which were attributed to pairs. At a general orientation the six ruthenium sites will give rise to twenty one different types of pair. Since the pair lines were not very intense and the situation was complicated by the number of pair types, these lines were not investigated, as it was felt that better systems for study could be found.

4.7 Orbital Reduction

Bleaney and O'Brien (1953) have shown, for a d^5 ion in a strong crystal field, that the principal g values are given by

$$g_z = 2\cos^2\theta\,(\sin^2\partial - (1 + k)\cos^2\partial) + 2\sin^2\theta\,(k - 1)$$

$$\tfrac{1}{2}(g_x + g_y) = -2\cos^2\theta\,(\sin\partial + \sqrt{2}k.\cos\partial\sin\partial) \qquad (4.5)$$

$$\tfrac{1}{2}(g_x - g_y) = 2\sin 2\theta\,(\cos\partial + (k/\sqrt{2})\sin\partial)$$

when g_x and g_y are given the same sign. The parameters θ and ∂ represent contributions from spin-orbit coupling and a crystal field with no symmetry restrictions and can be eliminated between the three equations. The parameter k is the orbital reduction parameter (taken as isotropic) first introduced by Stevens (1953). Orbital reduction arises when covalent bonds exist, since an electron in a d orbit then spends a fraction of its time at the ligands, as demonstrated in Chapter I.

Equation 4.5 gives two values for k depending on whether g_z takes a like or opposite sign to g_x and g_y. An orbital reduction parameter of 0.83 is sufficient to explain experimental results for the more covalent $Ir^{4+}(5d^5)$. Thus, for Ru^{3+}, k may be expected to satisfy $0.83 < k < 1$. A computer program was written to calculate k from equation 4.5. The following values were found for the three pairs of sites.

Site	1	2	3
k	0.857	0.910	0.894

4.8 The Hyperfine Interaction

Ruthenium has two isotopes possessing a nuclear spin of 5/2, Ru^{99} and Ru^{101} (Griffiths and Owen, 1952). Their abundances are 12.81% and 16.98% respectively and their magnetic moments 0.63 and -0.69. The strong resonances measured were due to the 70.21% abundant even isotopes but, under favourable conditions, two small resonances were detected on either side of the main line.

At most orientations, however, the width of the main transition obscured the hyperfine structure.

To a first approximation the hyperfine parameter A is given by the separation of adjacent hyperfine components. The hyperfine constant will represent an average for the two isotopes. Ru^{3+} in $Co(NH_3)_6Cl_3$, a somewhat analagous system, showed an isotropic hyperfine interaction of $50 \times 10^{-4} cm^{-1}$. The hyperfine structure of Ru^{3+} in these experiments also appeared to be isotropic with $A \sim 15 \times 10^{-4} cm^{-1}$.

A detailed analysis of hyperfine interactions is extremely complicated; suffice it to say that the isotropic component arises from the s-electron part of the molecular orbital close to the nucleus. Crudely speaking, the greater the degree of covalency the less unpaired spin remains at the metal ion to take part in the hyperfine interaction. This is confirmed by orbital reduction calculations, since fitting equation 4.5 to the results of Griffiths et al. gives an averaged orbital reduction parameter of 0.93, which is larger than the average value of 0.89 found from section 4.7.

THE MOLECULAR STRUCTURE OF CALCIUM CADMIUM ACETATE HEXAHYDRATE

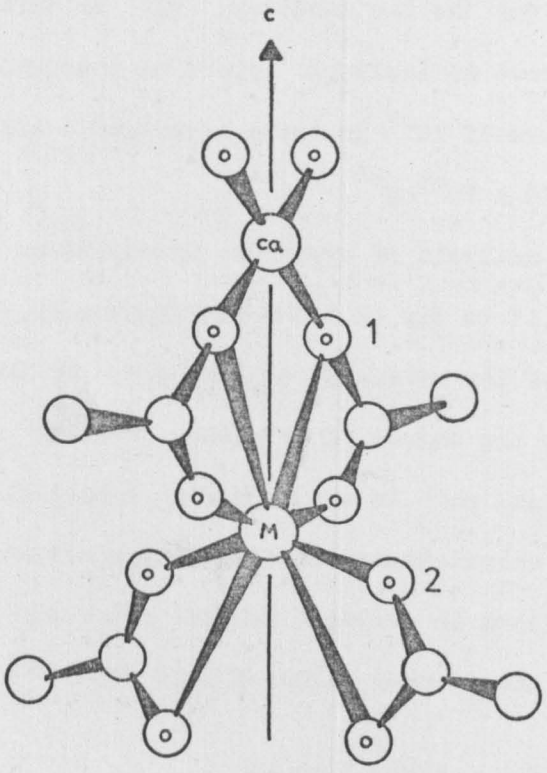

Atoms	M = Cu Dist.(Å)	M = Cd Dist.(Å)
M - O(1)	2.790(3)	2.677(8)
M - O(2)	1.973(2)	2.289(7)

FIGURE 5.1

CHAPTER V

RELAXATION STUDIES ON COPPER DOPED CALCIUM CADMIUM ACETATE

5.1 Introduction

Spin-lattice relaxation measurements were made on calcium cadmium acetate hexahydrate ($CaCd(Ac)_4.6H_2O$) crystals in which small percentages of the cadmium ions were replaced by copper ions. As we shall see in section 5.4, it had been suggested that exchange interactions of about $1cm^{-1}$ could exist between nearest neighbour copper ions. It was hoped that these antiferromagnetic exchange interactions would produce clusters which would be manifested in the relaxation behaviour.

5.2 Crystallographic Studies

Crystallographic studies have been carried out on $CaCd(Ac)_4.6H_2O$ and the isomorphous $CaCu(Ac)_4.6H_2O$ by Langs and Hare (1967). The molecular structure they give is shown in figure 5.1 together with some useful data. Tetragonal crystals are formed by both isomorphs. The crystal structure was found to consist of long chains of alternate calcium and cadmium atoms held together by acetate groups. The chains form parallel to the c axis of the crystal. The water molecules co-ordinate only to the calcium ions, filling the void of the lattice and binding polymeric chains together.

5.3 Crystal Field Calculations

Crystal field calculations have been carried out for the copper complex by Garner and Mabbs (1971). They considered the copper ion to be enclosed by two interpenetrating tetrahedra of oxygen atoms giving an eight co-ordinate complex within the group D_{2d}. The low symmetry of this arrangement requires the use of two crystal field parameters Dq and Cp. The g and A values of the spin Hamiltonian, together with the expected electronic transitions were obtained by solving the secular equations resulting from the perturbation

THE ENERGY LEVEL SCHEME

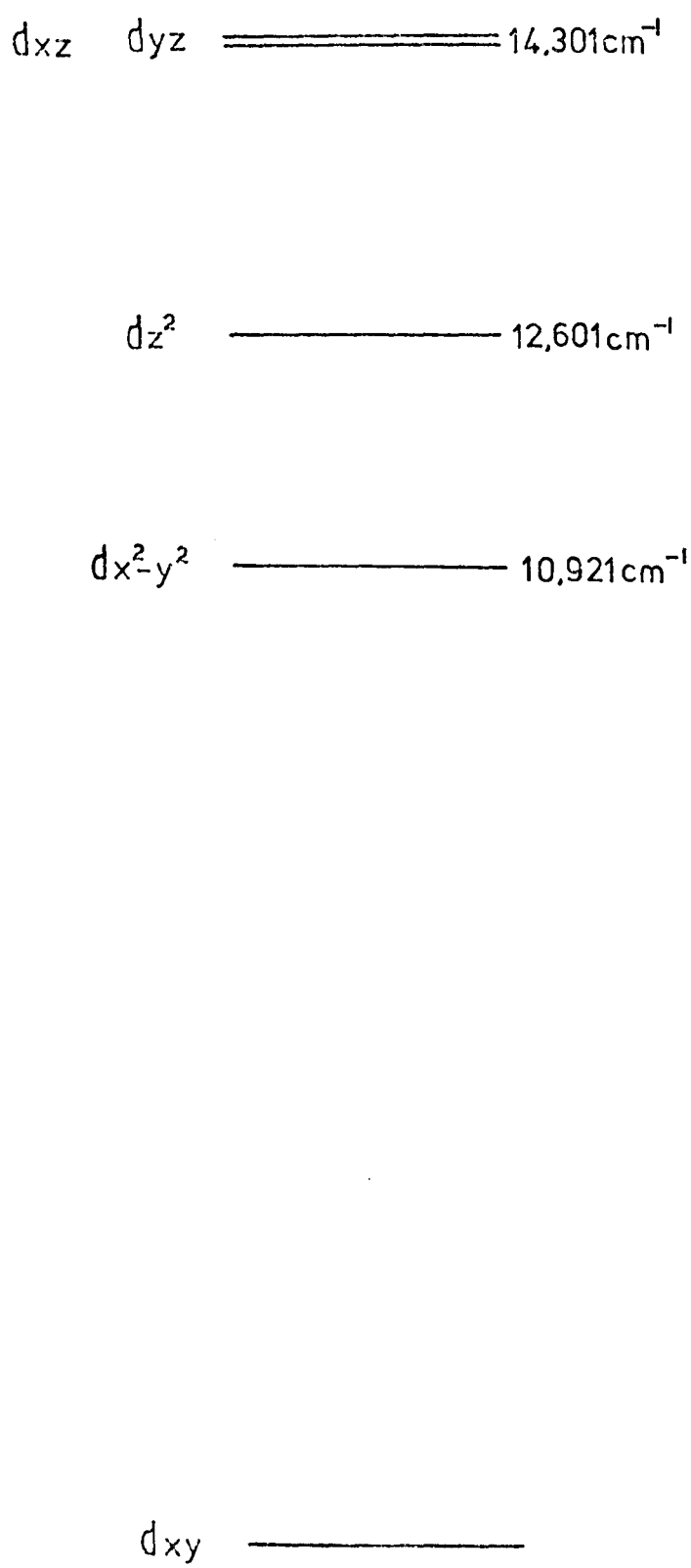

FIGURE 5.2

of the free ion ^2D term by the crystal field and spin-orbit interaction. An anisotropic orbital reduction parameter, k, was included in the calculations. The authors restricted the spin-orbit coupling constant to its free ion value of -828 cm^{-1} and varied Dq, Cp, $k_{\parallel}$, $k_{\perp}$ numerically to obtain the best fit to the experimental optical and e.p.r. data. They found, to a good approximation,

-Dq (cm^{-1})	-Cp (cm^{-1})	$k_{\parallel}$	$k_{\perp}$	(5.1)
1100	4000	0.79	0.82	

The energy level scheme is shown in figure 5.2.

5.4 Reported Magnetic Studies

Paramagnetic resonance has been performed on these crystals at room and liquid nitrogen temperatures by a number of authors (Mabbs and Smail (1970); Roy, Roy and Pal (1971); Gregson and Mitra (1969)). The first two papers are concerned with the pure copper salt but differ somewhat in the g values they report. Roy, Roy and Pal, however, also studied a magnetically dilute system and found no change in g values. Mabbs and Smail studied a crystal containing 0.5% copper and found parameters differing again from the other reported values. Satisfactory values appear to be,

$$g_z = 2.335 \qquad g_x = 2.065 \qquad (5.2)$$
$$A_{\parallel} = 0.0144\ cm^{-1} \qquad A_{\perp} = 0.0014\ cm^{-1}$$

At 140 ± 5°K a reversible phase change occurred in these crystals, giving rise to four magnetically inequivalent sites, each of which appeared to remain axial. The tensors of these sites were displaced by approximately 4° from the crystallographic c axis. This has been interpreted as the chains of calcium and cadmium/copper atoms adopting a zig-zag rather than a linear arrangement.

Roy, Roy and Pal undertook a line shape and width analysis on their results for the pure copper salt. They discovered that magnetic dipole-dipole interactions were insufficient to explain the angular dependence of the linewidth.

By including a term to represent anisotropic contributions from unresolved hyperfine structure and an exchange interaction of 0.02 cm^{-1} they were able to obtain good fits to their experimental data.

Gregson and Mitra also performed magnetic susceptibility and anisotropy experiments on the copper salt. By assuming a case of one dimensional antiferromagnetism along the polymeric chains they were able to fit their results to expressions derived by Fisher (1963) for this situation. By taking an isotropic orbital reduction parameter of 0.9 and an isotropic exchange interaction of 1 cm^{-1} their results fitted Fisher's expressions to within 2%.

5.5 The Experimental Procedure and Results

Good single crystals were grown following the method of Holden and Singer (1961). The calcium, cadmium and copper starting acetates were analar. A growth solution containing equal numbers of calcium and cadmium or calcium and copper atoms does not precipitate the double acetate compound. In order to grow the required crystals four calcium atoms are needed to each cadmium or copper atom. Calcium-cadmium mixtures were made up in these ratios but with a small percentage of the cadmium atoms replaced by copper. A range of copper concentrations was prepared. The mixtures were dissolved in warm distilled water and within a few days good single crystals grew by evaporation.

Spin-lattice relaxation times were measured by using the pulse saturation technique described in Chapter III. The majority of measurements were made at 4.2°K and below, these temperatures being attained by pumping on the liquid helium. In these crystals the presence of magnetically inequivalent sites at low temperatures presented something of a problem since, at a general orientation, the spectra from different sites overlapped each other. To avoid possible problems from cross relaxation and in order to saturate well defined resonances measurements were taken with the magnetic field along the c axis where the sites were all equivalent.

A number of crystals, containing different concentrations of copper,

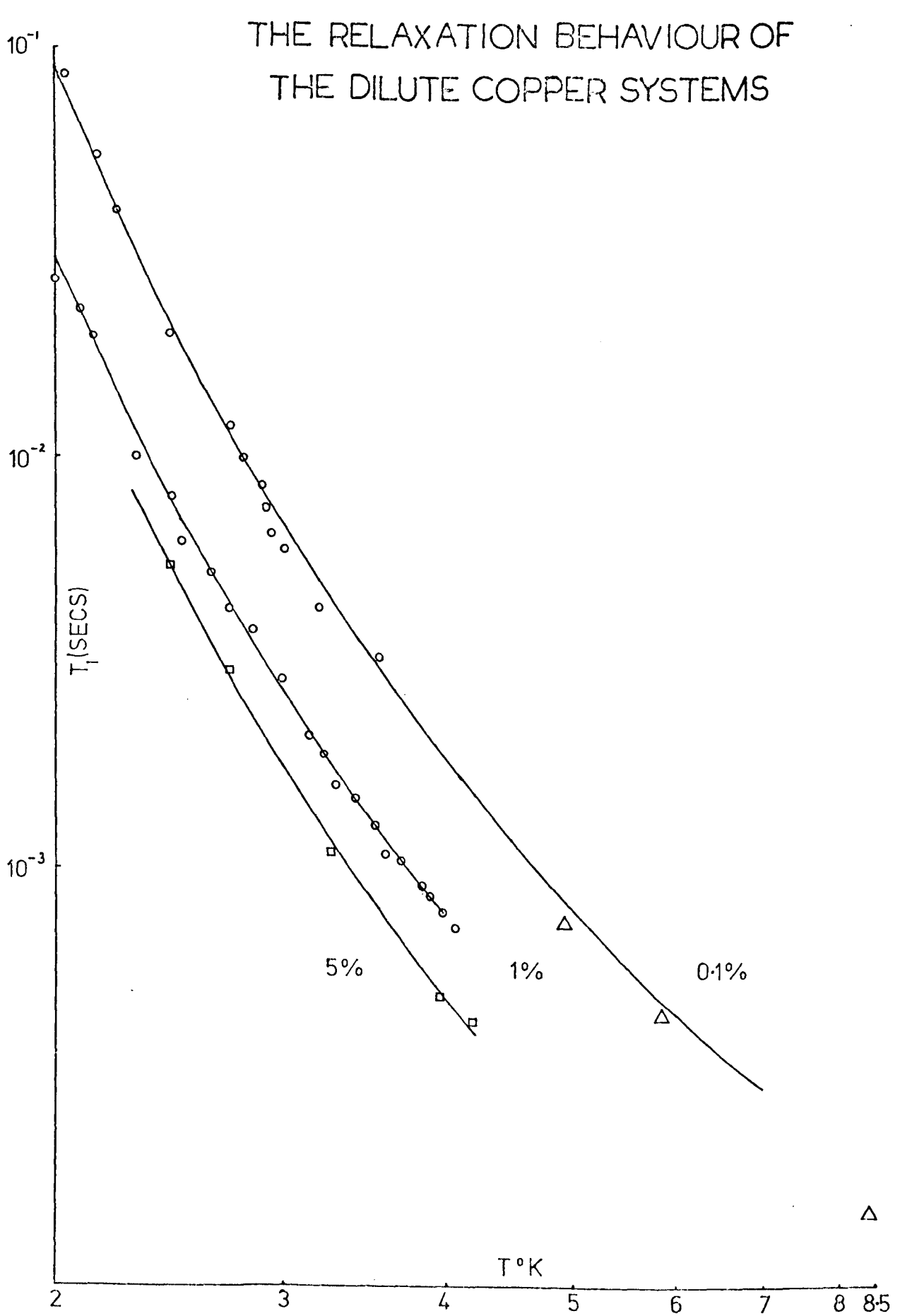
THE RELAXATION BEHAVIOUR OF
THE DILUTE COPPER SYSTEMS
10^{-1}
10^{-2}
10^{-3}
T_1(SECS)
5%
1%
0·1%
T°K
2
3
4
5
6
7
8
8·5

FIGURE 5.3

were investigated. This was done to show up any concentration dependence in the relaxation behaviour. Some experimental results are shown in figure 5.3. Since these results do not show the usual direct or Raman behaviour they were least squares fitted to an expression of the form

$$T_1 = A \exp\left\{\frac{\Delta}{T}\right\} \qquad (5.3)$$

This gave the following parameters

Concentration	A x 10^{-6} (secs)	$\Delta(^{\circ}K)$
0.1 %	42.8	15.26
1 %	21.0	14.53
5 %	11.45	15.1

where the concentration is the percentage of copper replacing cadmium in solution. The percentage of copper in the crystals is not necessarily as great.

Since the hyperfine interaction parameter along c is large ($A_{\parallel} = 0.0144$ cm^{-1}) and since the nuclear spin of two of the copper isotopes is 3/2, four resonances some 150 gauss apart are seen (see figure 5.5). The 69.09 % abundant Cu^{63} and the 12.09 % abundant Cu^{65} isotopes have slightly different nuclear magnetic moments. This causes the outer hyperfine transitions to be composed of two partially resolved lines. Then, in order to work with a symmetrical line shape, relaxation measurements were usually taken on the hyperfine component second lowest in field.

Relaxation measurements were also made on each of the hyperfine components in turn, usually only at $4.2^{\circ}K$. However, since each hyperfine component showed a different relaxation time, a series of readings were taken on two of the lines in the temperature range $2^{\circ}K$ to $4.2^{\circ}K$. This experiment showed that the relaxation time of each hyperfine component had the same functional dependence on temperature and only differed in magnitude.

To check whether the relaxation process changed above $4.2^{\circ}K$ the exchange gas temperature control system of Chapter III was devised to extend

the range over which measurements could be taken. Measurements were extended on the 0.1 % system up to 9°K. These measurements, taken in a separate experiment, are shown by the triangles in figure 5.3.

5.6 Discussion of the Relaxation Process

Chapter II introduced two relaxation mechanisms which are able to give rise to relaxation times which are exponentially dependent on temperature. The first of these, the Orbach process (section 2.2.5), requires the presence of an excited electronic state at an energy Δ above the ground state, where Δ is less than $k\theta_D$ and appears in the exponent. However, since figure 5.2 shows that the first excited electronic state is some 11,000 cm^{-1} above the ground state, this is clearly not the required mechanism.

The second way in which such behaviour may occur requires the presence of exchange coupled clusters. Single ions may then cross relax to the clusters which may relax the Zeeman energy by two phonon processes. However, no paramagnetic evidence has been found for such clusters during these investigations and, furthermore, the magnitude of the exchange interactions between copper ions suggested in section 5.4 is small compared with that required to give the form of the observed behaviour. The work of Harris and Yngvesson on exchange coupled clusters of spin $\frac{1}{2}$ ions indicates higher order clusters than pairs are needed to effect this mechanism. Since exponential behaviour is observed even with very low copper concentrations, further mechanisms must be sought to explain the observed behaviour.

5.7 Modifications to the Relaxation Theories

An examination of the nature of the crystals under study shows that they have some important properties that have not been accounted for in the derivations of single ion relaxation processes. There is a striking difference in the atomic weights of copper and cadmium. The atomic weight of copper is 63.54 whereas the atomic weight of cadmium, the atom which copper replaces, is 112.4. Furthermore, the crystallographic data shows that the copper-oxygen

and cadmium-oxygen distances, d, differ between the isomorphs. The electrostatic forces between the metal ions and the oxygen ligands are proportional to $1/d^2$, making the forces binding the copper ions to the nearest oxygen ions about 1.35 times stronger than similar forces for the cadmium ions.

The large mass difference between the copper and cadmium ions can be expected to cause the paramagnetic ion to behave as a mass defect in the lattice. Furthermore, the change in binding forces may reinforce this behaviour. Montroll and Potts (1955) have analysed the effect of lattice defects on the vibrational modes of a one dimensional crystal lattice. They show that a mass defect in the crystal lattice can lead to one of two effects. When the mass of a substituting ion exceeds that of the substituted ion the characteristic vibrational frequency, ω_i, associated with the defect is less than the Debye limiting frequency, ω_D, of the perfect lattice. The defect then undergoes forced oscillations under the influence of lattice waves. When the mass of the substituting ion is less than that of the substituted ion, ω_i is greater than ω_D, and a new lattice mode, localised at the defect, is formed.

The situation which concerns us here is the formation of a local mode at the copper site. The effect of such a local mode diminishes with distance r as

$$r^{-1} \exp(-Ar) \qquad (54)$$

Because of this localisation, the strain at the defect associated with the local mode is larger than that in any of the band modes. The enhancement of strain increases with increasing localisation. In addition the strain at the defect atom due to each band mode is reduced from that associated with a normal atom.

We have already seen in Chapter II that the mechanism producing spin-lattice relaxation depends on the phonon modulation of the crystalline field in the vicinity of the paramagnetic ion. When the paramagnetic ion is clearly acting as a mass defect we might expect considerable modification

to the relaxation behaviour, since the nature of the local phonon spectrum has altered.

5.8 Relaxation in the Presence of a Local Mode

Theoretical treatments for the relaxation of paramagnetic ions in the presence of local modes have been given by several authors, including Kochelaev (1960), Klemens (1961, 1962) and Maradudin (1966). The analysis of Maradudin followed the general formalism of Mattuck and Strandberg (1960). He found, in the harmonic approximation, the usual expressions for the direct and Raman processes. He further showed that, in the absence of anharmonicities in the lattice vibrations (terms higher than quadratic in the interatomic displacements), the local modes can make no contribution to the relaxation. On introducing cubic anharmonicities he was able to derive, for the contribution of local modes to Raman-type relaxation,

$$\frac{1}{T_R} \propto \left\{ \exp\left(\frac{h\nu}{kT}\right) + 1 \right\} p(\omega_o)[p(\omega_o) + 1] \frac{\gamma_o}{\nu^2 + 4\gamma_o^2} \qquad (5.5)$$

where ω_o is the frequency of the local mode, γ_o its width and ν the spin resonant frequency. By taking $\exp(h\nu/kT)$ as constant, and defining a local mode temperature θ_o as $\theta_o = \hbar\omega_o/k$, equation 5.5 can be approximated (by use of 2.9 and for $T \lesssim \theta_o/4$) to,

$$\frac{1}{T_R} \propto \left[\exp\left(\frac{-\theta_o}{T}\right) \right] \frac{\gamma_o}{\nu^2 + 4\gamma_o^2} \qquad (5.6)$$

Klemens was able to derive a similar result by considering one of the possible relaxation mechanisms involving a local mode. His first paper (Klemens 1961) showed that cubic anharmonicities broaden the local mode by about 1 %. This relaxes energy conservation sufficiently to allow relaxation processes involving local modes. His second paper (Klemens 1962) considered the following relaxation process. The initial state was taken as the local mode, excited with a phonon, and the ion in a given spin state. In the

intermediate state the same local phonon is found but, since this is broad, the spin can be inverted without violating energy conservation. In the final state the spin remains inverted while the local phonon has decayed to two band phonons to remove the spin flip energy. This is not the only possible process involving a local mode but they all lead to the same temperature dependence (Feldman, Castle and Murphy, 1965).

Feldman et al (1965) have found experimental evidence of relaxation processes involving local modes. They studied the relaxation of interstitial atomic hydrogen and deuterium in CaF_2. These rather gross lattice defects showed relaxation times which required expressions of the form exp (Δ/T) at high temperatures. Experimentally Δ was found to be 850°K for hydrogen and 640°K for deuterium.

5.9 Discussion of the Results

We have found that over a range of concentrations the copper relaxation times are proportional to exp (15/T). The results taken on the 0.1 % crystals above 4.2°K and shown in figure 5.3 are in fact fitted to the more general expression of equation 5.5, which improves the fit in this region. The agreement between the predictions of the local mode relaxation model and the experimental results is good.

The discussion of section 5.8 indicates that the local mode frequency in these crystals is expected to lie above the Debye limiting frequency. This implies, however, that the temperature of the lattice is only about 12 or 13°K which is rather low. Physically, it would seem more likely that the local mode frequency lies in a well defined frequency gap in the phonon spectrum, probably between the acoustic and optical bands.

A weak dependence of the relaxation time on the paramagnetic concentration is found. Fitting the relaxation times at 4.2°K for a range of concentrations, c, to the relationship

$$T_1 = Ac^n$$

THE ANGULAR VARIATION OF T_1 FOR THE LOW FIELD LINE

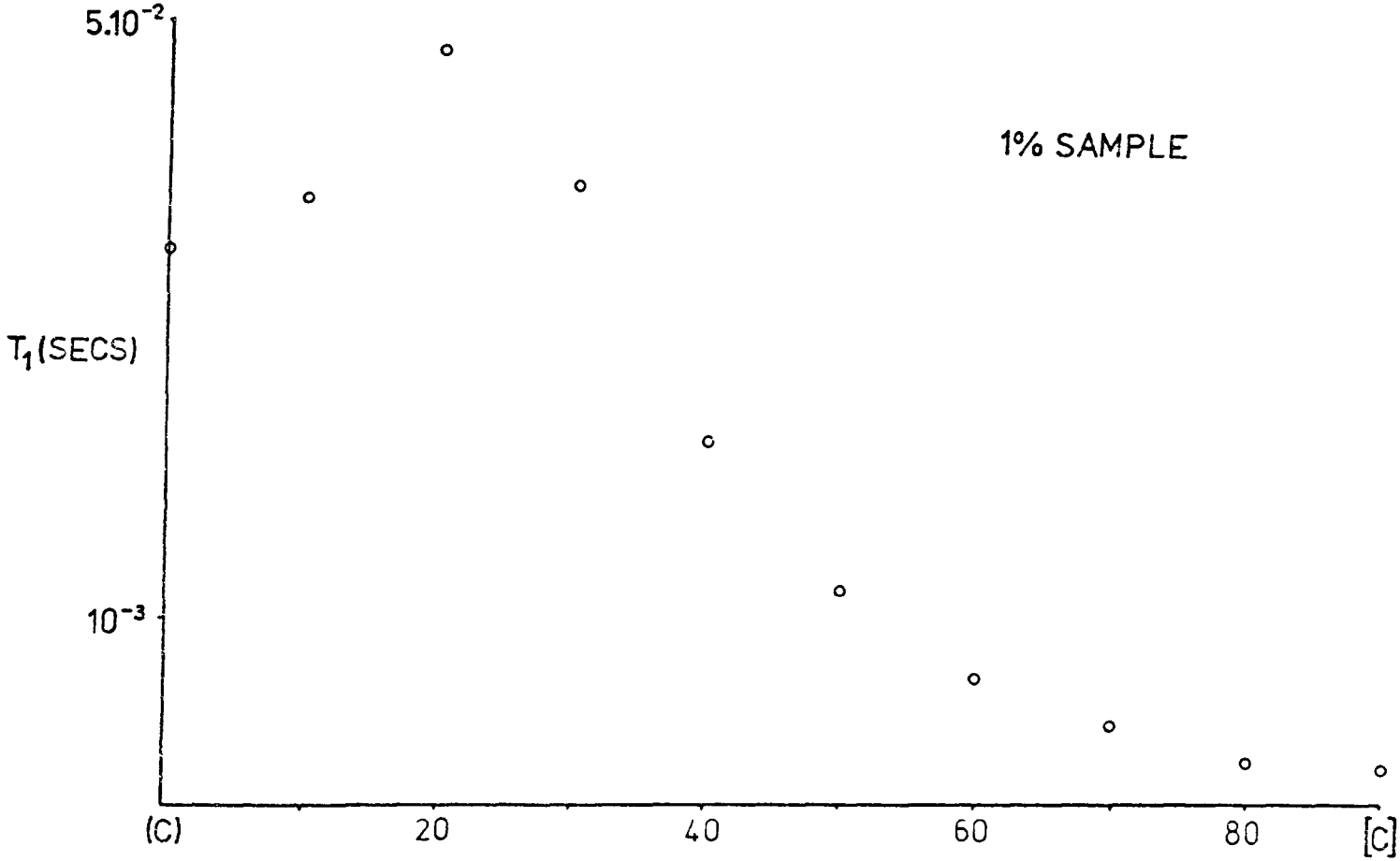

FIGURE 5.4

gives n as approximately $-\frac{1}{4}$. This is a much weaker dependence than that expected for relaxation involving exchange coupled clusters.

The work of Montroll and Potts indicates indirectly a possible source of concentration dependent relaxation. They show that it is energetically favourable for the lattice defects giving rise to localised modes to be found close to each other. The local modes may then interact, albeit weakly since adjacent copper sites are some 8Å apart, to produce further broadening of the local mode frequency. Even without this clustering of defects, a statistical enhancement of local mode interactions will occur with increasing concentration. Such interactions will be equivalent to increasing γ_o in equation 5.5 and lead to an increase in the predicted relaxation rate.

Since the details of the broadening mechanisms between local modes are unknown it is not possible to derive an explicit expression for the concentration dependence. However, it is interesting to speculate on the consequences of equation 5.5. Differentiating $\gamma_o/(\nu^2 + 4\gamma_o^2)$ with respect to γ_o shows that T_1 takes a minimum value when $\gamma_o = \frac{1}{2}\nu$. Thus, if a local mode can be broadened beyond the point when $\gamma_o = \frac{1}{2}\nu$ the relaxation time will begin to increase.

The relaxation times show an angular dependence which is expected to arise from changes in the matrix elements connecting the paramagnetic states. Particularly since the copper ion is a Kramer's system these matrix elements will vary with angle in a complex manner. The angular dependence of the relaxation time of the resonance line lowest in field is shown in figure 5.4. As we shall see in the next section the measured relaxation times should be corrected for the anisotropy in the hyperfine interaction.

5.10 The Relaxation over the Hyperfine Structure

The difference in relaxation time measured at each hyperfine component offers further evidence for relaxation involving a local mode. Because the four resonance lines are separated by only a few line widths, cross relaxation

TABLE 5.1

	$\frac{1}{2}, \frac{3}{2}$	$\frac{1}{2}, \frac{1}{2}$	$-\frac{1}{2}, \frac{3}{2}$	$\frac{1}{2}, -\frac{1}{2}$	$-\frac{1}{2}, \frac{1}{2}$	$\frac{1}{2}, -\frac{3}{2}$	$-\frac{1}{2}, -\frac{1}{2}$	$-\frac{1}{2}, -\frac{3}{2}$
$\frac{1}{2}, \frac{3}{2}$	$\frac{1}{2}G_{\parallel}+\frac{3}{4}A$		$\frac{1}{2}G_{\perp}$		$\frac{\sqrt{3}}{2}B$			
$\frac{1}{2}, \frac{1}{2}$		$\frac{1}{2}G_{\parallel}+\frac{A}{4}$	$\frac{\sqrt{3}}{2}B$		$\frac{1}{2}G_{\perp}$		B	
$-\frac{1}{2}, \frac{3}{2}$	$\frac{1}{2}G_{\perp}$	$\frac{\sqrt{3}}{2}B$	$-\frac{1}{2}G_{\parallel}-\frac{3}{4}A$					
$\frac{1}{2}, -\frac{1}{2}$				$\frac{1}{2}G_{\parallel}-\frac{A}{4}$	B		$\frac{1}{2}G_{\perp}$	$\frac{\sqrt{3}}{2}B$
$-\frac{1}{2}, \frac{1}{2}$	$\frac{\sqrt{3}}{2}B$	$\frac{1}{2}G_{\perp}$		B	$-\frac{1}{2}G_{\parallel}-\frac{A}{4}$			
$\frac{1}{2}, -\frac{3}{2}$						$\frac{1}{2}G_{\parallel}-\frac{3}{4}A$	$\frac{\sqrt{3}}{2}B$	$\frac{1}{2}G_{\perp}$
$-\frac{1}{2}, -\frac{1}{2}$		B		$\frac{1}{2}G_{\perp}$		$\frac{\sqrt{3}}{2}B$	$-\frac{1}{2}G_{\parallel}+\frac{A}{4}$	
$-\frac{1}{2}, -\frac{3}{2}$				$\frac{\sqrt{3}}{2}B$		$\frac{1}{2}G_{\perp}$		$-\frac{1}{2}G_{\parallel}+\frac{3}{4}A$

$A = A_{\parallel} = 0.0144\ (cm^{-1})$ $\quad B = A_{\perp} = 0.0014\ (cm^{-1})$

Along $\underline{c}$ $\quad G_{\parallel} = 0.33\ (cm^{-1})$ $\quad G_{\perp} = 0.03\ (cm^{-1})$

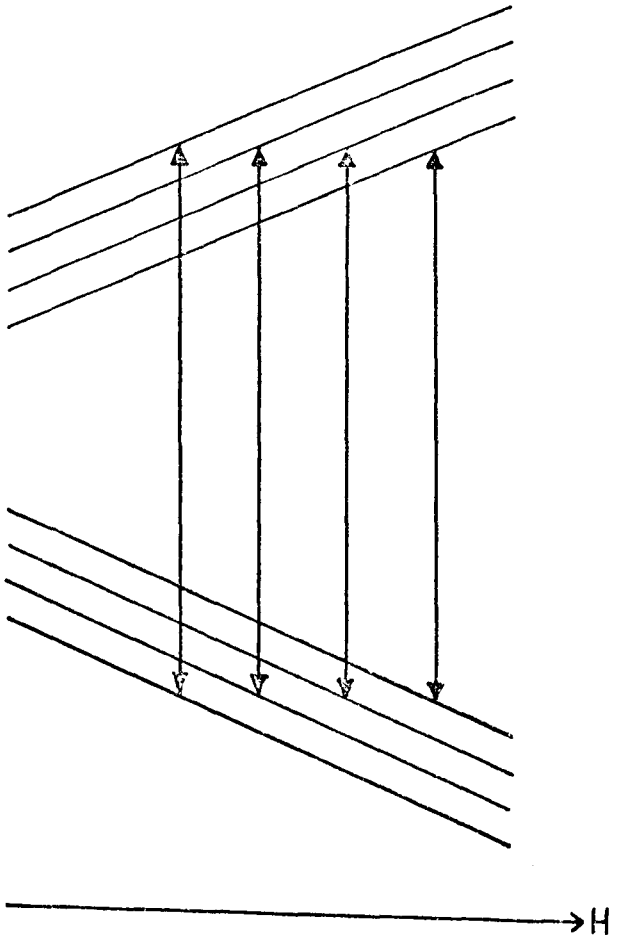

FIGURE 5.5

TABLE 5.2

Measured T_1	0.79	0.93	1.1	1.3
Predicted T_1	0.87	0.98	1.08	1.19
Measured T_1	0.41	0.51	0.65	0.66
Predicted T_1	0.47	0.52	0.58	0.64
Measured T_1	0.375	0.44	0.57	0.64
Predicted T_1	0.43	0.48	0.53	0.58
Measured T_1	0.43	0.50	0.68	
Predicted T_1	0.48	0.53	0.59	

The values of T_1 are in arbitrary units.

processes may be expected to bring the hyperfine components to the same spin temperature. The off diagonal elements found in the energy matrix of the copper ion (table 5.1) will further aid the establishment of a common spin temperature. Assuming, as is often the case, that the spins attain internal thermal equilibrium at a rate which is fast compared with the processes bringing about equilibrium between the spins and the lattice, the only difference in measuring T_1 at each hyperfine component will be the magnitude of the magnetic field at which measurements are taken.

The relaxation theories of Chapter II, for processes in which T_1 depends on the magnetic field, predict that the measured value of T_1 will decrease with increasing field. Such behaviour is contrary to that found in this series of experiments. Now, it is known from equation 5.5 that

$$T_1 \propto \nu^2 + 4\gamma_o^2 \qquad (5.7)$$

In order to predict the observed relaxation behaviour over the hyperfine components it is necessary to assume that $\nu^2 \gg 4\gamma_o^2$. We have seen above that the measured relaxation time at any of the hyperfine components is a measure of the relaxation of all four components. When the hyperfine transition lowest in magnetic field is at resonance (see figure 5.5) the contributions to the measured relaxation are

$$T_1 \propto (h\nu)^2 + (h\nu - A)^2 + (h\nu - 2A)^2 + (h\nu - 3A)^2$$

$$\text{ie.} \quad T_1 \propto (4(h\nu^2 - 12h\nu A + 14A^2) \qquad (5.8)$$

When the other components are at resonance the contributions to the measured relaxation times are

$$T_1\,(2\text{nd}) \propto (4(h\nu)^2 - 4h\nu A + 6A^2) \simeq 3.8(h\nu)^2$$

$$T_1\,(3\text{rd}) \propto (4(h\nu)^2 + 4h\nu A + 6A^2) \simeq 4.2(h\nu)^2 \qquad (5.9)$$

$$T_1\,(4\text{th}) \propto (4(h\nu)^2 + 12h\nu A + 14A^2) \simeq 4.6(h\nu)^2$$

where ν is the microwave frequency and, since $A \simeq 0.05h\nu$, terms in A^2 are

THE RELAXATION BEHAVIOUR OF $CaCu[OAc]_4 6H_2O$

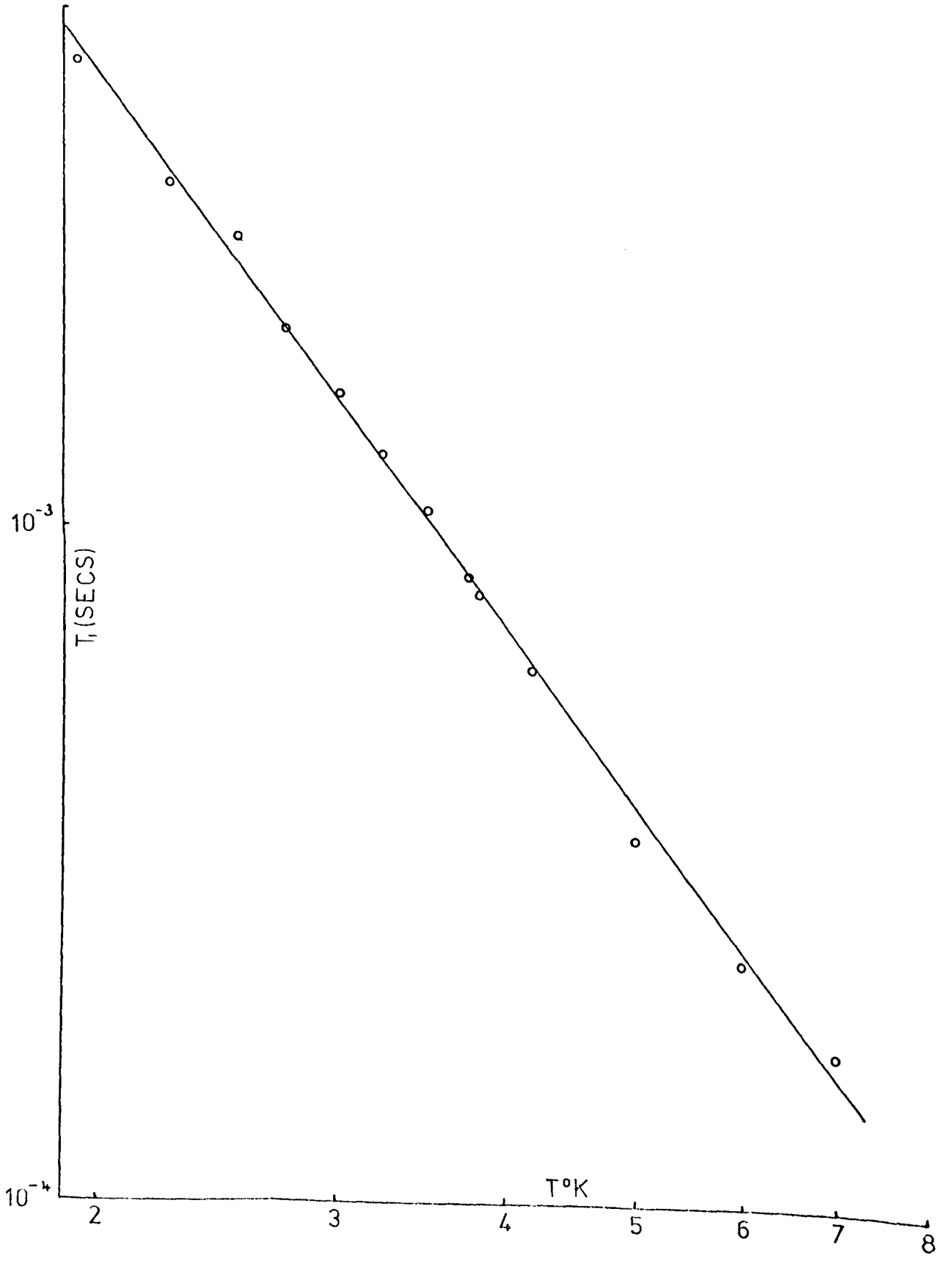

FIGURE 5.6

ignored. Using the experimental data the unknowns can be removed from these equations and the predicted relaxation times found. The results are shown in table 5.2 where observed and predicted relaxation times are listed.

Although this interpretation successfully predicts the form of the relaxation behaviour over the hyperfine components it consistently underestimates the magnitude of the effect.

5.11 The Relaxation Behaviour of $CaCu(Ac)_4.6H_2O$

A good test of the theory of defect mode relaxation should be found at high copper concentrations. In the pure copper salt the copper ions are no longer acting as substitutional mass defects in the lattice and consequently possess no defect nature. The relaxation theories of Chapter II might then be expected to hold. Relaxation studies were carried out on a small crystal of $CaCu(Ac)_4.6H_2O$ and gave the results shown in figure 5.6. It is immediately obvious from this figure that the exponential behaviour found at low copper concentrations has been lost. Fitting the relaxation times to a power law gives the dependence

$$T_1 \propto T^{-2.73} \qquad (5.10)$$

which is shown by the full line in the figure. This behaviour cannot be attributed to the copper ions acting independently of each other and relaxing by conventional mechanisms. The discussion of the results found at low copper concentrations shows that the single ion direct and Raman processes will cause slower relaxation than that shown in figure 5.6 and consequently slower relaxation than that found in the concentrated crystals.

The reported results of section 5.4 suggest that each copper ion is exchange coupled to its neighbours along the polymeric chains. Such interactions may be expected to influence the relaxation processes occurring in these magnetically concentrated crystals. The relaxation behaviour of an exchange coupled assembly of paramagnetic ions has been considered by Richards (1965). Richards takes a three bath model comprising an exchange system, a

Zeeman system and the lattice and assumes, at low temperatures, that the fastest means of relaxing the Zeeman energy to the lattice is via the exchange system. The coupling between the exchange system and the lattice is considered to give rise to the observed relaxation time. Spin correlation effects are included by a density matrix approach. Using this approach Richards shows that Raman relaxation in a linear chain is a special case which goes as T^9 instead of T^7 when $T \ll \theta_D$. When T is of the order of θ_D the Raman contribution goes as T^2. Nearest neighbour interactions do not give rise to a direct relaxation process in the linear chain. Next nearest neighbour interactions are required to give direct relaxation with a rate proportional to T.

If the copper ions are relaxing by a direct process it would not be surprising to find that a phonon bottleneck is being detected since the spin concentration is very high. One-phonon relaxation will cause an enormous number of additional phonons to be introduced into a narrow phonon band in the lattice, which could well lead to a severe bottleneck. The experimental behaviour found could then be due to a complex form of phonon bottleneck. If this is a correct explanation it implies that the defect Raman process is no longer operative, since such relaxation occurs by using densely populated regions of the phonon spectrum and many phonon pairs.

5.12 The Possibility Of Additional Investigations

Attempts were made to grow the mixed acetate of calcium and zinc with a small percentage of the zinc replaced by copper. Since the atomic weight of zinc is 65.37 and that of copper 63.54 such crystals would no longer cause the copper ions to act as mass defects. A study of the copper relaxation would have been of immense value in confirming the defect mode relaxation in the acetate containing cadmium. Unfortunately it proved impossible to grow these crystals and indeed no reference to successful growths can be found in the literature.

Several methods of investigation are available for detecting local modes, most of which are reviewed by Klein (1968). The results obtained from

applying an independent technique would be instructive. The usual technique is direct infrared lattice absorption but, since the local mode frequency is expected to be approximately 300 Ghz (~ 1mm), some difficulty may be expected in using this apprcach. Raman scattering from the local mode could be a more practical possibility, but the incident radiation would probably have to lie in the infrared, since the crystals absorb strongly in the visible region. Measurements on the lattice heat capacity may indicate the presence of the local modes by showing anomalous behaviour about 15°K. Local modes have also been detected by neutron scattering.

CHAPTER VI

PARAMAGNETIC INVESTIGATIONS OF SOME DIMERIC COMPLEXES

6.1 Introduction

As we have seen in Chapter II, exchange coupled clusters are held to be a possible origin for concentration dependent relaxation processes. In view of the central role played by clusters in these thoeries it was our wish to study the spin-lattice relaxation mechanisms occurring in exchange coupled pairs of ions. Reported results of such mechanisms have always occurred in systems where diamagnetic host lattices have been relatively heavily doped with isomorphous paramagnetic impurities. Investigating relaxation in such crystals is complicated by the number of different pairs and higher order clusters that may arise. Further complications may be caused by cross relaxation processes and the necessary presence of intense single ion resonances. In view of this, investigations into a system which avoids many of these problems could be of value.

Such a system can arise when paramagnetic pairs form a natural part of the crystal structure. To be of use this dimeric system must satisfy certain conditions. The magnitude of the exchange interaction within a single pair or dimer must be small enough to allow the paramagnetic states to remain well populated at temperatures where relaxation measurements are possible. This requires the exchange energy to be no greater than a few degrees Kelvin. The dimers must be sufficiently well separated to eliminate interactions between neighbouring pairs. Of course,a ferromagnetic interaction within the dimers would be ideal as this leaves a paramagnetic ground state. However, such conditions are not easily met!

6.2 Cobalt Diethyldithiophosphinate

The first attempt at obtaining such a system was the growth of a dimeric cobalt complex. Kuchen, Metten and Judat (1964,1965) have reported

dimeric complexes of zinc and cobalt diethyldithiophosphinate which have the structure shown below.

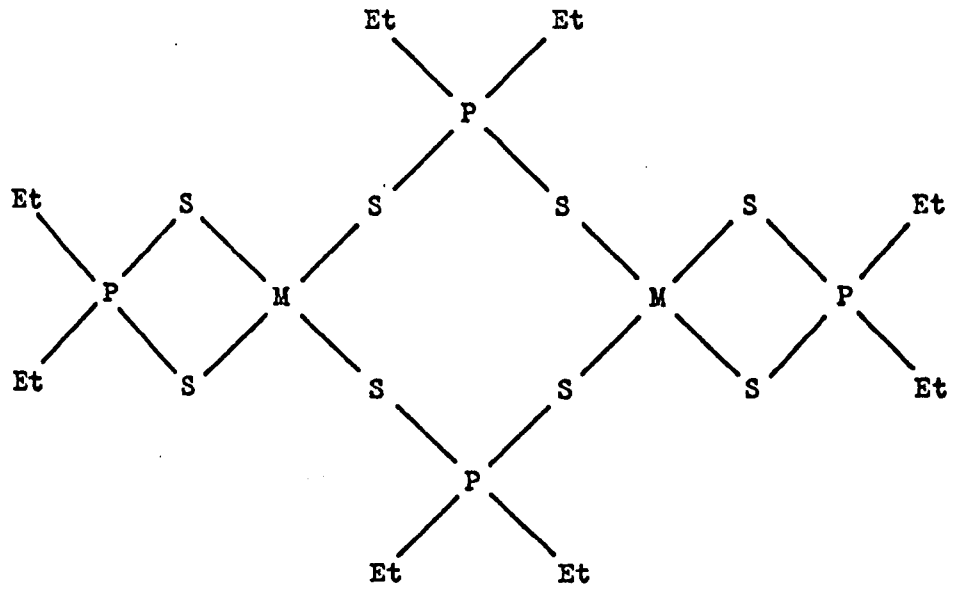

where M = Zn or Co.

Attempts were made to grow single crystals of $\left[Zn(Et_2PS_2)_2\right]_2$ containing small amounts of the paramagnetic cobalt dimers $\left[Co(Et_2PS_2)_2\right]_2$. Dark green single crystals were grown from solution in isopropyl alcohol. These crystals were investigated at liquid helium temperatures but the spectra found were rather complex. Calligaris, Ciana and Ripamonti (1966) have shown that the dimeric and monomeric species are in equilibrium in solution which means that the mixed complex may be formed in the association processes occurring during crystallisation. Thus single ion spectra may be contributing to the observed resonances. Because of the lack of obvious pair spectra this investigation was pursued no further.

6.3 Dimeric Complexes of the Form $Cs_3M_2Cl_9$

6.3.1 Crystallographic Studies

The next crystals to be studied were of the form $Cs_3M_2Cl_9$ where M = Cr, V or Ti. The crystal of $Cs_3Cr_2Cl_9$ has been determined by X-ray analysis by Wessel and Ijdo (1957). The crystal structure is shown in figure

THE CRYSTAL STRUCTURE OF $Cs_3Cr_2Cl_9$

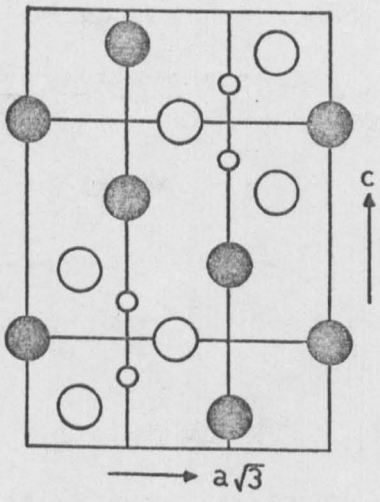

THE $11\bar{2}0$ MIRROR PLANE

Cr ○

Cs ●

Cl ○

a=7·22±0·01Å c=17·93±0·02

THE $Cr_2Cl_9^{3-}$ ANION

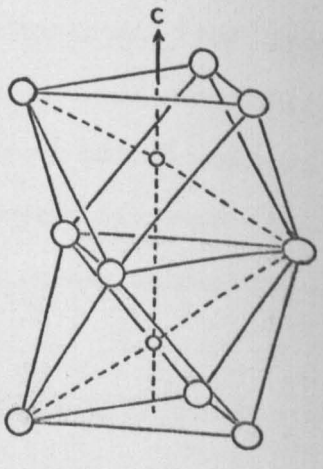

FIGURE 6.1

6.1. The chlorine ions describe two octahedra sharing a common face. The cesium and chlorine ions form a close packing with six layers of four atoms each. The chromium ions are not central with respect to their respective octahedra but rather are displaced away from each other along the trigonal axis. $Cs_3V_2Cl_9$ and $Cs_3Ti_2Cl_9$ were found to be isomorphous with $Cs_3Cr_2Cl_9$.

6.3.2 Susceptibility Studies

Susceptibility studies have been carried cut on these compounds in the temperature range 80°K - 300°K by Saillant and Wentworth (1968). Since the samples are dimeric the evenly coupled Curie-Weiss model for susceptibility should not be applicable. An expression for the susceptibility of an assembly of isolated paramagnetic dimers has been derived by Kambe (1950). The susceptibility of an assembly of N_A ions of spin S is defined by

$$X = \frac{N_A g^2 \beta^2}{3kT} S(S + 1) \qquad (6.1)$$

For an exchange coupled pair of ions

$$N_s = \frac{(2S + 1) \exp(-E_s/kT)}{\sum (2S + 1) \exp(-E_i/kT)} \qquad (6.2)$$

The atomic susceptibility of an assembly of dimers with spins (3/2,3/2) becomes, for example,

$$X = \frac{N_A g^2 \beta^2}{3kT} \left(\frac{3 \exp(5J/T) + 15 \exp(3J/T) + 42}{7 + 5 \exp(3J/T) + 3 \exp(5J/T) + \exp(6J/T)} \right) \qquad (6.3)$$

Such behaviour should be easily identifiable since the susceptibility will pass through a maximum value as the temperature is reduced. Saillant and Wentworth, however, found that their results fitted a Curie-Weiss expression.

$Cs_3Cr_2Cl_9$ was characterised by a Curie-Weiss constant θ of 38°K. The samples of $Cs_3V_2Cl_9$ followed Curie-Weiss behaviour only as far as 90°K with θ = 116°K. A distinct curvature was found below 90°K which was thought to be possibly associated with a phase transition. Such a curvature is

predicted by the (1,1) analogue of equation 6.3 but the tabulated results were insufficient to determine a value for J.

The samples of $Cs_3Ti_2Cl_9$ did not give totally reproducible results, but did show large changes in magnetic moment over the temperature range considered. The effective magnetic moment varied between 1.2 and 1.4 β at 300°K and 0.8 to 0.5 β at 80°K. The authors suspected the presence of an unknown contaminant in their crystals.

The discrepancy between the observed and predicted susceptibility behaviour in these dimeric crystals is, at first sight, difficult to explain. However, some doubt must exist over the way in which the crystals were grown. The temperatures to which starting mixtures were heated to allow crystal growth are consistently low when compared with the published phase diagrams. The temperatures used by Saillant and Wentworth were, $Cs_3Cr_2Cl_9$ 650°C, $Cs_3V_2Cl_9$ 650°C, $Cs_3Ti_2Cl_9$ 695°C. As we shall see in section 6.3.3 these temperatures will not guarantee the formation of the required phase.

6.3.3 Crystal Growth

Crystals of the form $Cs_3M_2Cl_9$ were grown from the melt. The chromium, vanadium and titanium chlorides were obtained from Alpha Inorganics, the cesium chloride from the Chemistry Department at Keele. Stoichiometric quantities of these materials (40% MCl_3, 60% CsCl) were heated in a quartz tube to above 100°C while the tube was being evacuated. Once the mixture was water-free the vacuum was sealed and the tube slowly passed through a two-chamber furnace. The first chamber was held at 50°C above the temperature of the required dystectic and the second chamber at 50°C below it. The port connecting the two chambers then had a thermal gradient across it centred at about the dystectic temperature.

Phase diagrams for all three systems have been published. The $CrCl_3$ - CsCl system has been described by Efimov and Pitirimov (1963), the VCl_3 - CsCl system by Shchukarev and Perfilova (1963) and the $TiCl_3$ - CsCl system by Markov and Chernov (1959). The temperature required to grow

PHASE DIAGRAM FOR THE $CrCl_3$–$CsCl$ SYSTEM

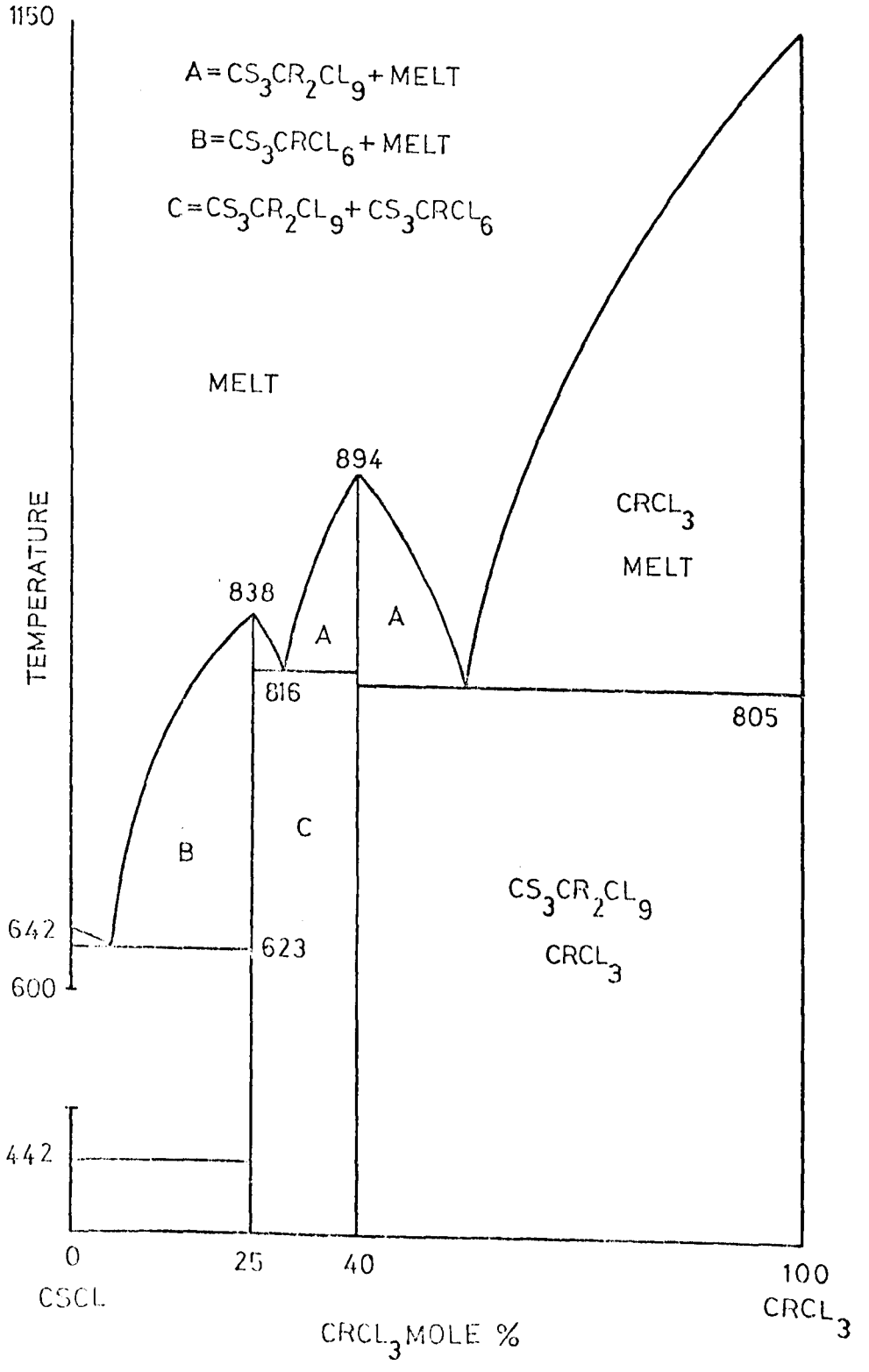

FIGURE 6.2

$Cs_3Cr_2Cl_9$ is 894°C, $Cs_3V_2Cl_9$ 700°C and $Cs_3Ti_2Cl_9$ 781°C.

Reference to the phase diagram of figure 6.2, for mixtures of CsCl and $CrCl_3$, shows that between 894°C and about 810°C only crystals of $Cs_3Cr_2Cl_9$ will be formed. Below 810°C Cs_3CrCl_6 or $CrCl_3$ may also appear depending on any non-stoichiometry. A slow passage of the tube through the furnace will cause any unwanted phases to appear at the top of the tube from where they may be discarded. Zone refining the $Cs_3Cr_2Cl_9$ afterwards produced no significant change in its behaviour.

6.3.4 The Single Ions in Trigonal Sites

Before considering the paramagnetic behaviour of the dimers, it will be useful to study the predictions of the ionic model for the single paramagnetic ions in trigonal sites.

Titanium^{3+}

Ti^{3+} ($3d^1$) has the free ion ground state ^2D. A cubic crystal field splits this into a triplet, T_2, 10 Dq below a doublet, E. The trigonal component of the crystal field and the spin-orbit coupling can be applied simultaneously as a perturbation on the triplet. Spin-orbit coupling between T_2 and E is neglected. The perturbation leaves three Kramer's doublets whose energy order depends on the sign of the trigonal field parameter, δ. The net result of these interactions can be either a highly anisotropic or a nearly isotropic g tensor depending on the sign and magnitude of δ. The interpretation of experimental results has required the inclusion of covalent bonding with the ligands to reduce the orbital moment. The presence of low lying excited orbital states makes relaxation very rapid.

Vanadium^{3+}

V^{3+} ($3d^2$) has the free ion ground state ^3F which is split by a cubic crystal field to leave an orbital triplet lowest. The trigonal component of the crystal field leaves an orbital singlet ground state at energy δ below the doublet. The three fold spin degeneracy is removed when spin-orbit coupling mixes the ground state into the first doublet. This leaves a spin 1

system with a rather large zero field splitting of λ^2/δ and a somewhat anisotropic g factor. D values in the range 7 - 8.3 cm^{-1} have been reported with $g_{\parallel} \simeq 1.9$ and $g_{\perp} \simeq 1.7$.

Chromium^{3+}

Cr^{3+} ($3d^3$) has the free ion ground state ^4F. A cubic crystal field leaves an orbital singlet as the ground state well separated from excited orbital states. A trigonal distortion splits the first excited triplet which is mixed into the ground state by spin-orbit coupling. This causes a slight anisotropy in g and a small zero field splitting. Usually $g_{\parallel} \simeq g_{\perp} = 1.97 - 1.99$.

6.3.5 Preliminary Results

The dark purple rods of $Cs_3Cr_2Cl_9$ grown from the melt were found to cleave both parallel and perpendicular to the growth direction. X-ray studies showed six-fold symmetry was present along the perpendicular direction showing this to be the c axis. Once cleaved, crystals were kept over silica gel in an evacuated dessicator since they were unstable in air over long periods.

The first growths of these crystals showed the following paramagnetic behaviour. At room and liquid nitrogen temperatures an intense resonance was found at $g = 1.99$ that fitted well to a Lorentzian line shape. Its peak to peak width at 77°K was several hundred gauss. At 4.2°K the broad resonance had been replaced by four resonances with line widths of 150 gauss. One of these resonances was approximately isotropic at $g \simeq 1.9$ with an intensity, which when compared to the other resonances, varied from growth to growth. This strongly suggests that it is a defect or possibly an impurity. The angular dependence of the remaining three lines at 4.2°K indicated a spin 1 system. Below 4.2°K the intensity of the spin 1 resonances dropped rapidly. Furthermore, a spin 3/2 system appeared, made visible by rapid narrowing. This spin 3/2 system was not distinguishable at 4.2°K.

Apart from the features previously described, the various crystal

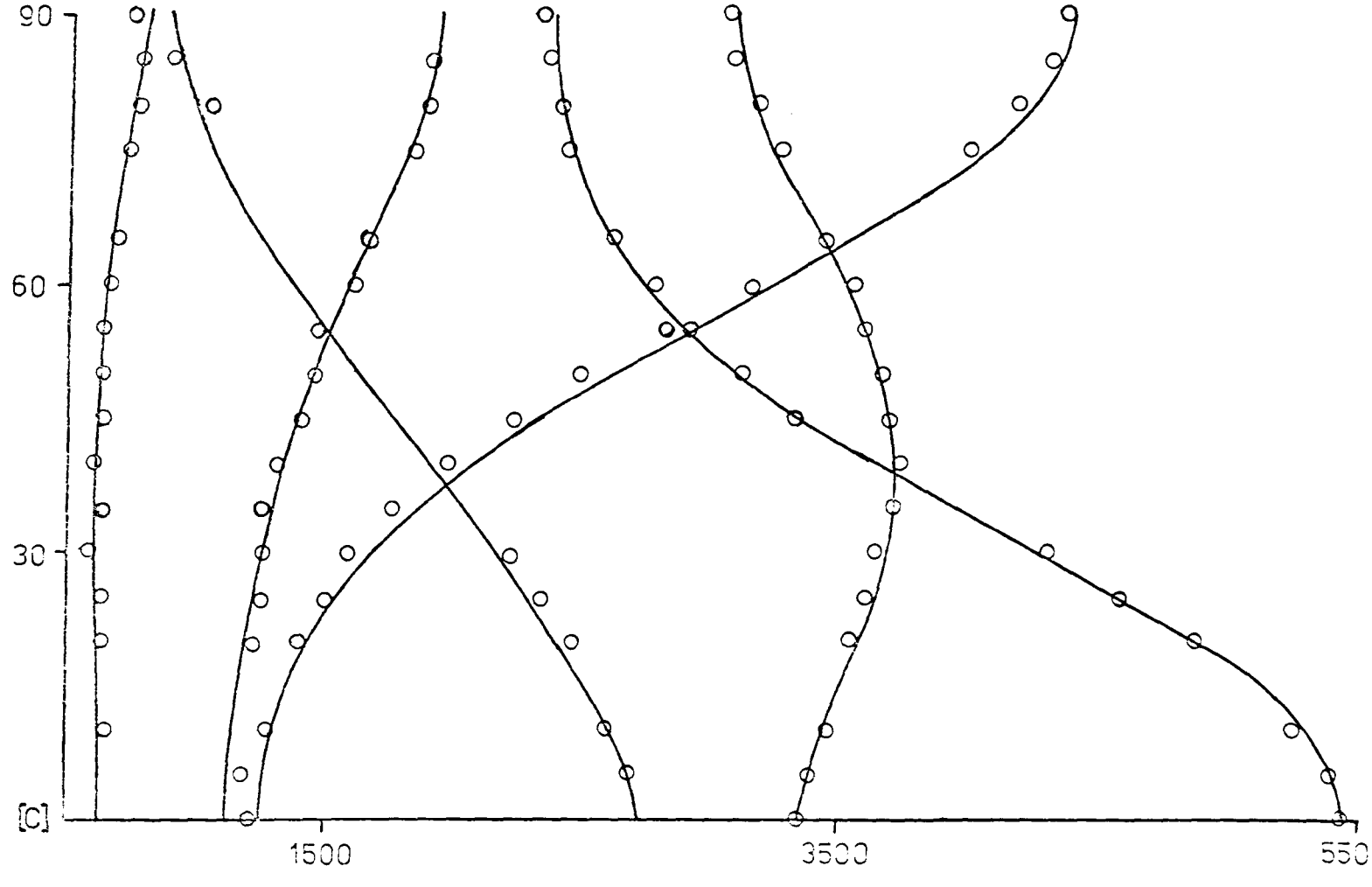
THE ANGULAR VARIATION OF THE S=3/2 SPECTRUM
90
60
30
[C]
1500
3500
5500

FIGURE 6.3

growths showed a narrow g = 2 resonance superimposed on the broad resonance at high temperatures. This line broadened considerably when the temperature was lowered below 77°K. This behaviour is consistent with that reported for polycrystalline $CrCl_3$ where line widths of 54 gauss and 990 gauss have been found at temperatures of 90°K and 13°K respectively.

6.3.6 The Spin 3/2 System

Angular variations were performed at about 1.6°K in planes perpendicular and parallel to the growth direction. The angular variation in the latter plane was isotropic, indicating an axial site. The spectrum in the former plane was fitted to a spin Hamiltonian of the form;

$$\mathcal{H}_s = g_{\parallel}\beta H_z S_z + g_{\perp}\beta H_x S_x + D(S_z^2 - \tfrac{1}{3}S(S+1)) \qquad (6.4)$$

where the z axis of the Hamiltonian corresponded to the c axis of the crystal.

Measurements along c, where the energy matrix can be solved immediately, show that D is of the same order as the Zeeman energy. This makes off diagonal elements in the energy matrix large and the results of perturbation theory invalid. Consequently, to predict transitions off axis the energy matrix has to be diagonalised directly. This was done on the University computer. The programs used in these calculations were developed by Dowsing (private communication). The first program predicted resonance fields at any angle given values of $g_{\parallel}$, $g_{\perp}$ and D. By measuring $g_{\parallel}$ and D along c, angular variations could be predicted using different $g_{\perp}$ values to obtain a good fit. Slight changes could then be made to $g_{\parallel}$ and D to improve the fit. A more sophisticated program was later obtained from Dr. Dowsing which read in resonant fields and the angles at which they occurred and then varied $g_{\parallel}$, $g_{\perp}$ and D by an iterative process to obtain fits to all of the experimental points. Using these programs the angular variation of figure 6.3 was fitted to a spin 3/2 system with

$$\begin{aligned} g_{\parallel} &= 1.981 \\ g_{\perp} &= 1.988 \\ D &= 0.097\ \text{cm}^{-1} \end{aligned} \qquad (6.5)$$

This is shown by the continuous lines in the figure.

The ordering of the energy levels depends upon the sign of D. On axis the high field and low field $M_s = \pm 1$ resonances have the same transition probability, and, by taking $D > 0$ the transitions are $|3/2\rangle \leftrightarrow |1/2\rangle$ and $|-1/2\rangle \leftrightarrow |-3/2\rangle$ respectively. If $E_s - E_r = h\nu$, the intensity of the transition $E_r \rightarrow E_s$ is:

$$I_{rs} \propto \frac{1 - \exp(-h\nu/kT)}{\sum_i \exp((E_r - E_i)/kT)} \qquad \frac{I_{H.F.}}{I_{L.F.}} = \frac{Z_{L.F.}}{Z_{H.F.}} \qquad (6.6)$$

The intensities of the high field and low field transitions from equation 6.6 will differ since the partition function, Z, is evaluated at different fields. For the spin 3/2 described at $\sim 1.6^{\circ}K$ the intensity ratio is calculated to be ~ 1.6. Experimentally, the high field transition is found to be the most intense on axis so D is positive.

6.3.7 The Origin of the Impurity Spectra

It seems reasonable to associate the spin 3/2 resonances with a single chromium ion. The phase diagram of figure 6.2 shows that, apart from $Cs_3Cr_2Cl_9$, there may be $CrCl_3$ or Cs_3CrCl_6 present. The line at liquid nitrogen temperatures which has already been attributed to $CrCl_3$ may well derive from local aggregations of the starting material. This could occur if the growth mixture was not held in the molten state for long enough before cooling.

It was possible to grow crystals without the spin 3/2 spectrum and the isotropic resonance (c.f. 6.3.8). This suggests that these spectra are associated with non-stoichiometries. In isolation, Cs_3CrCl_6 should give an isotropic resonance. However, since the axial spin 3/2 system was more intense than the isotropic line, it seems more reasonable to associate it with the remaining compound we might expect to find in the crystal. The axial nature of the site could arise by considering the Cs_3CrCl_6 to appear as a $Cs_3Cr_2Cl_9$ complex which has lost a chromium and three chlorines from

one end and yet is surrounded by the $Cs_3Cr_2Cl_9$ phase. The $CrCl_3$ vacancy would then produce an axial distortion at the remaining chromium directed along the c axis.

6.3.8 Discussion of the Crystals so far

Clearly better crystals were required to study phenomena due to exchange interactions. The spin 1 system seen at 4.2°K indicated the presence of such interactions. Intensity studies were attempted on the spin 1 lines in these crystals but the presence of the S = 3/2 lines with their rapidly changing line widths made this extremely difficult. A further difficulty was the choice of a suitable intensity reference with a g value well removed from 2 so as not to overlap other lines.

The phase diagram of $Cs_3Cr_2Cl_9$ shows that a starting mixture slightly rich in $CrCl_3$ will have more opportunity to form $Cs_3Cr_2Cl_9$ since the relevant eutectic is further removed in temperature and composition. Furthermore, local aggregations of $CrCl_3$ will have broadened out at 4.2°K. Consequently, a stoichiometric starting mixture was made up to which was added 10% excess additional $CrCl_3$. This produced good crystals in which the S = 3/2 and isotropic resonance were not present. In view of this, $Cs_3V_2Cl_9$ and $Cs_3Ti_2Cl_9$ were grown in the same manner.

6.3.9 The Spin 1 System

The new crystal growths allowed the three line spectrum at 4.2°K to be fitted to spin Hamiltonian of the form

$$H_s = g_z \beta H \cos\theta \, S_z + g_x \beta H \sin\theta \, S_x + D(S_z^2 - \tfrac{1}{3}S(S+1)) \qquad (6.7)$$

The large splitting found on axis, where the energy matrix can be solved exactly, indicated a strong D term making the results of perturbation theory invalid. The angular variation was fitted by computer using the programs described in section 6.3.6. The following parameters were found to give

THE ANGULAR VARIATION OF THE S=1 SPECTRUM

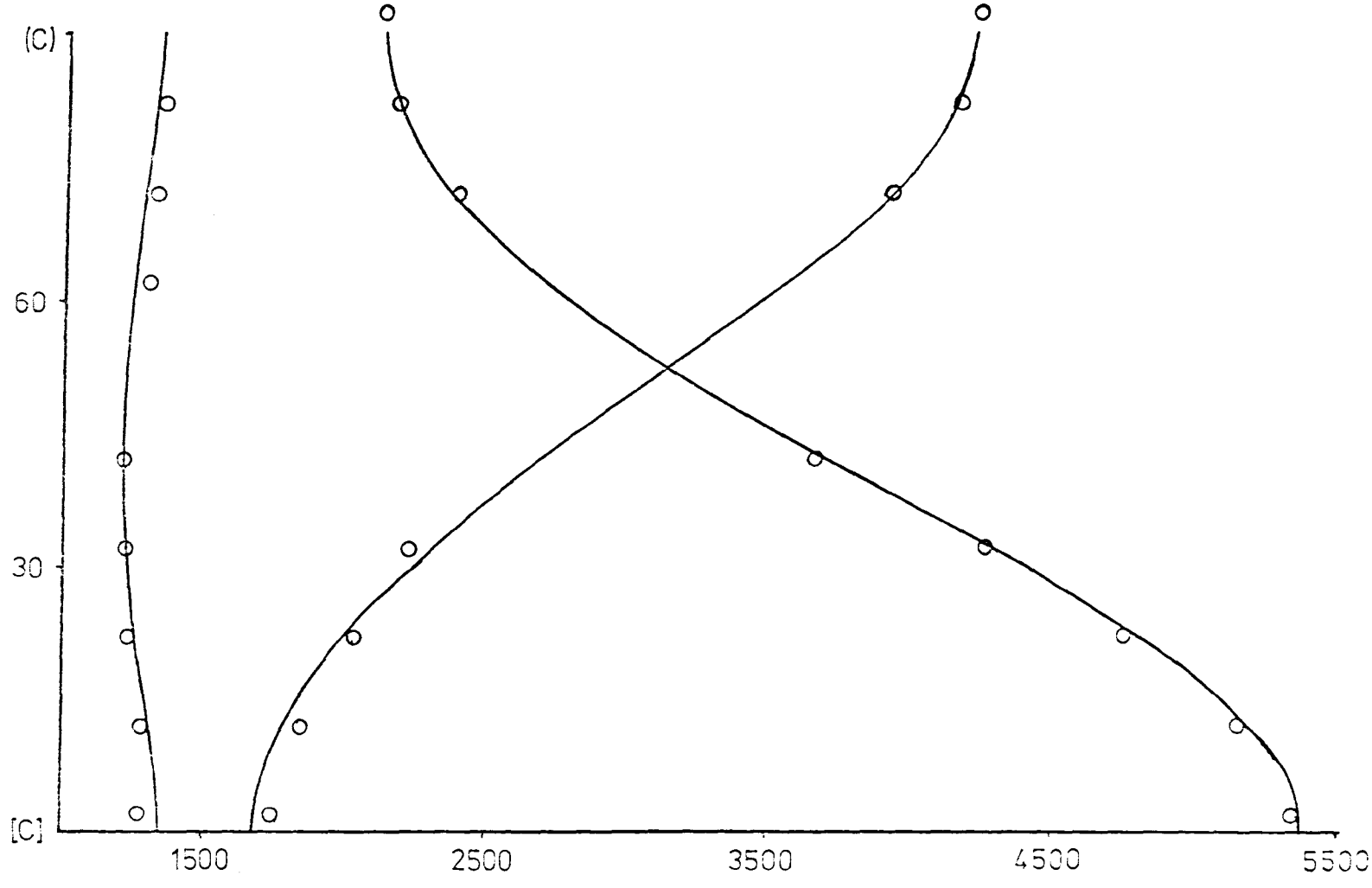

FIGURE 6.4

the best fit at 4.2°K.

$$g_z = 1.974 \pm 0.005$$
$$g_x = 2.001 \pm 0.005 \qquad (6.8)$$
$$D = 0.1848 \pm 0.0005 \text{ cm}^{-1}$$

This fit is shown in figure 6.4.

The large D term produced strong mixing of spin states off axis making three transitions observable. Intensity measurements described in section 6.3.11 showed, on axis, that the high field resonance gained in intensity relative to the low field resonance. By the treatment of section 6.3.6 this implies that D is positive.

6.3.10 The Exchange Situation

It was shown in Chapter I that an exchange interaction between paramagnetic ions can be represented by a vector coupling of the spins ($J\underline{S}_i \cdot \underline{S}_j$). Thus the two spin 3/2 chromium ions in each $Cr_2Cl_9^{3-}$ dimer may couple to form total spin states of 3, 2, 1 and 0. The spin 1 system just described is such a total spin state.

Owen (1961) has shown that when the exchange energy gives the dominant term in equation 1.23 the Hamiltonian may be written as,

$$\begin{aligned} H = {} & (J/2)[S(S+1) - S_i(S_i+1) - S_j(S_j+1)] + g\beta \underline{H}.\underline{S} \\ & + (A/2)S(I_i + I_j) + (3a_s D_e + \beta_s D_c)\left[S_z^2 - \tfrac{1}{3}S(S+1)\right] \\ & + (a_s E_e + \beta_s E_c)\left[S_x^2 - S_y^2\right] \end{aligned} \qquad (6.9)$$

where

$$a_s = \frac{1}{2}\left\{\frac{S(S+1) + 4S_i(S_i+1)}{(2S-1)(2S+3)}\right\}, \quad \beta_s = \frac{3S(S+1) - 3 - 4S_i(S_i+1)}{(2S-1)(2S+3)} \qquad (6.10)$$

These coefficients take the values shown in the following table.

$S_i = S_j = 3/2$			$S_i = S_j = 1$			$S_i = S_j = 1/2$			
S	$3a_s$	β_s	S	$3a_s$	β_s	S	$3a_s$	β_s	
1	51/10	-12/5	1	3	-1	1	3/2	0	(6.11)
2	3/2	0	2	1	1/3				
3	9/10	2/5							

Thus, for example, the D term of the spin 1 system is comprised of $(5.1D_e - 2.4D_o)$. The thermal population of a level in a total spin state S is determined by Maxwell-Boltzmann statistics and takes the form

$$\frac{\exp(-E_s/kT)}{\sum_s (2S+1)\exp(-E_s/kT)} \qquad (6.12)$$

6.3.11 The Intensity Variation of the Spin 1 Lines

The spin 1 resonances show large changes in intensity with temperature. These changes were measured against the copper resonance in a small crystal of calcium copper acetate hexahydrate (see Chapter V). This gave a line comparable in width and amplitude to the spin 1 lines at $4.2^{\circ}K$ and showed no change in linewidth with temperature. The reference crystal was orientated to give its resonance near $g = 2$ while the $Cs_3Cr_2Cl_9$ crystal was fixed with the magnetic field along the c axis.

Apart from gain, all three lines were recorded under the same conditions at a series of temperatures below $4.2^{\circ}K$. Since temperatures could be stabilised in this region, the lines were recorded several times at each temperature. There was no change in line shape with temperature, allowing the quantity (peak to peak width)^2 x height to be taken as a measure of intensity. Because of the population changes occurring within the spin 1 levels at low temperatures due to its large D term (see section 6.3.9), the intensities of the two spin 1 resonances were summed at each temperature before being compared to the reference. Separate recordings were averaged at each temperature.

The intensity of a $\Delta M_s = \pm 1$ transition within a total spin state S

INTENSITY DEPENDENCE OF THE S=1 TRANSITIONS IN $CS_3CR_2CL_9$

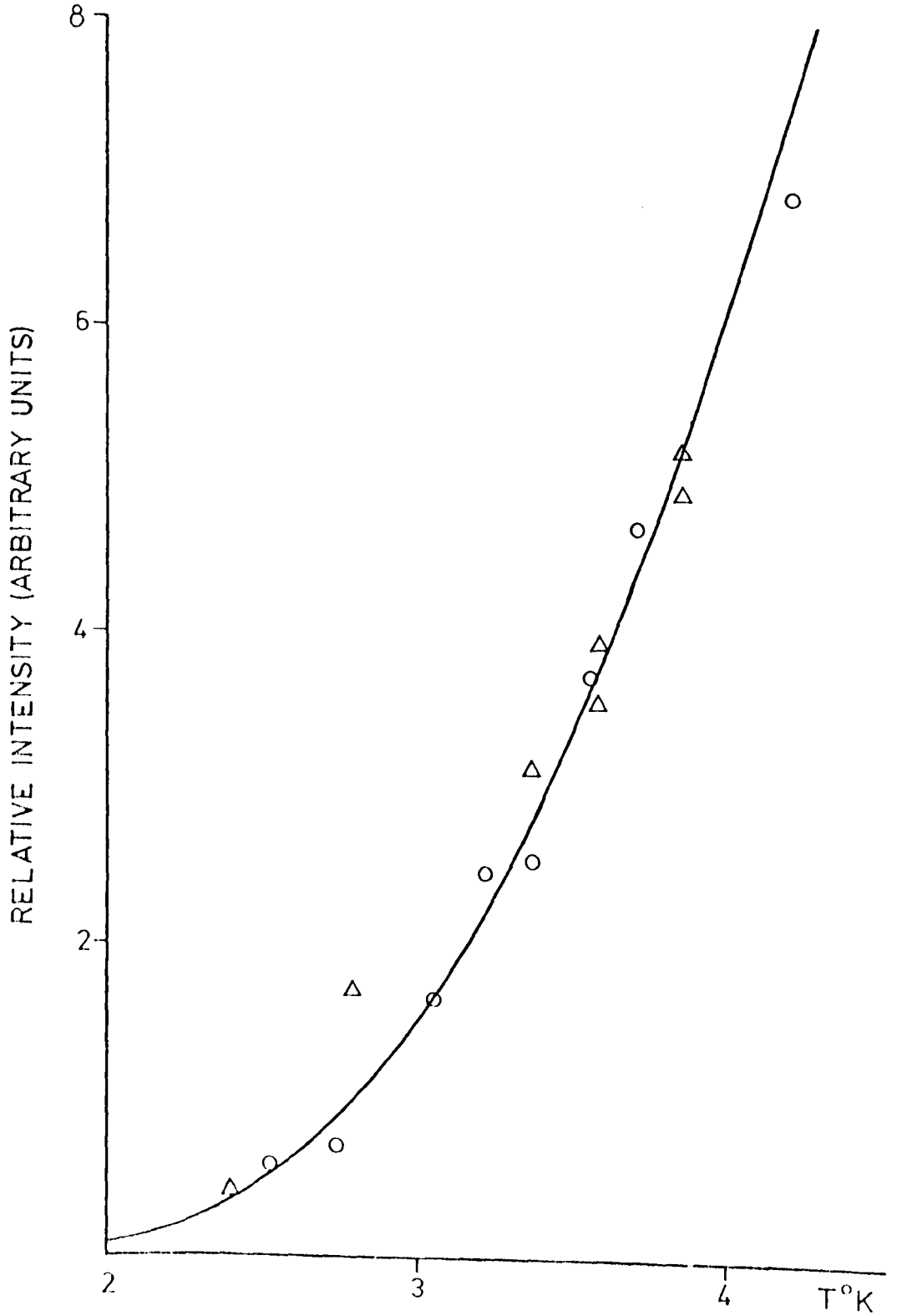

FIGURE 6.5

at energy E_s is proportional to

$$\frac{\exp(-E_s/kT)(1 - \exp(-h\nu/kT))}{\sum_S (2S + 1)\exp(-E_s/kT)} \qquad (6.13)$$

The intensity of the copper line is proportional to

$$1 - \exp(-h\nu/kT) \qquad (6.14)$$

Thus the intensity of the spin 1 lines, relative to the copper is proportional to

$$\frac{\exp(-J/T)}{1 + 3\exp(-J/T) + 5\exp(-3J/T) + 7\exp(-6J/T)} \qquad (6.15)$$

This expression was programmed and J iterated to give the best fit to the experimental data. The value of J giving the best fit was found to be 17°K. The results of two separate experiments are shown in figure 6.5, where one set of data is represented by circles and the other by triangles.

The main source of error in determining the value of J arises from measuring the intensity of the lines, since the temperature measurements are certainly better than 0.1°K. The internal consistency of the results indicates that the error in J is not greater than ±1°K.

6.3.12 The Temperature Dependent D Term

While taking intensity measurements along the c direction it was observed that the separation between the spin 1 lines changed with temperature. In order to study this phenomenon further, measurements were taken in the temperature range 77°K to 4.2°K. These temperatures were achieved by the helium flow and desorption techniques of Chapter III. On cooling between 77°K and 20°K, the high temperature Lorentzian resonance continuously narrowed. Just below 20°K the line width reached a minimum then broadened rapidly and took on an asymmetric shape. By about 8°K the line had resolved into two separate resonances. Below 8°K these lines narrowed and moved rapidly apart. Their separation is shown in figure 6.6 as a function of temperature.

THE VARIATION OF THE D TERM

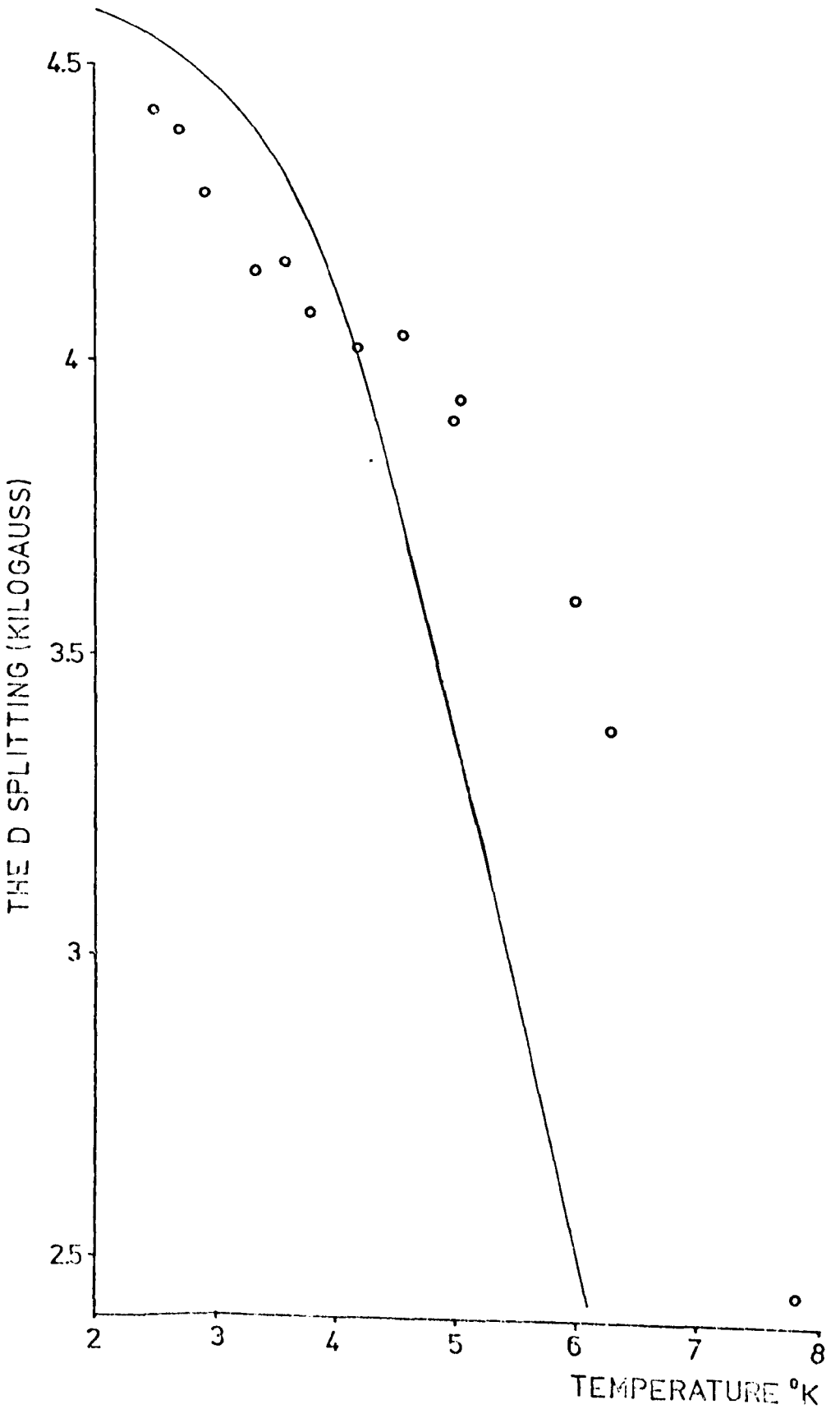

FIGURE 6.6

Clearly, to explain such behaviour, a mechanism must be found to make the effective D value a function of temperature. We believe that exchange interactions between dimers provide such a mechanism, but before continuing to discuss the model, we will consider some of the work that has been reported in this area.

It has been known for many years that magnetic dipolar interactions alone will not predict the observed line widths in some crystals. Van Vleck (1948) was able to explain this by introducing exchange interactions into the calculations. He considered an assembly of similar paramagnetic ions and took the Hamiltonian of this system as a sum of Zeeman, dipolar and exchange terms. The analysis treated the effect of exchange on the second and fourth moments of the observed resonance line. The second moment, for example, is defined as the mean square resonance frequency, $\omega_{nn'}^2$, weighted by the appropriate transition probability,

$$\langle \omega^2 \rangle_{av} = \frac{\sum_{nn'} \omega_{nn'}^2 |\langle n|S_x|n'\rangle|^2}{\sum_{nn'} |\langle n|S_x|n'\rangle|^2} \qquad (6.16)$$

where n and n' are eigenstates of the complete Hamiltonian.

The dipolar interactions do not commute completely with the Zeeman interactions and, as a consequence, give rise to weak resonances at 0, $2g\beta H/h$, $3g\beta H/h$, ... If the part of the Hamiltonian giving rise to these resonances is not removed, the moments calculation will include large contributions from the subsidiary lines. Despite the matrix elements for these transitions being very small, their mean square frequency deviation from the main line is large.

On calculating the second and fourth moments, Van Vleck showed that exchange interactions make no contribution to the second moment but do increase the fourth moment. This requires the absorption to taper off less sharply in the wings and to peak more sharply at the centre. This reduces the half width of the resonance and is referred to as exchange narrowing.

Anderson and Weiss (1953) have investigated the problem of exchange narrowing by considering the spin system to absorb a single frequency which varies in a random way over a range determined by the local dipolar field. Exchange interactions are considered to determine the rate at which the frequency varies randomly. By comparison with Van Vleck's work they derived the following expression for line width

$$\frac{\langle(\Delta\omega^2)\rangle_{AV}\ \text{dipole-dipole}}{J/\hbar} \qquad (6.17)$$

When the exchange frequency $J/\hbar$ exceeds the resonant frequency, the off diagonal elements of the dipolar interaction are included which makes the line broader, in agreement with experimental measurements.

The ability of a spin to sample the spread of resonant frequencies available to it at a rate determined by the exchange energy, offers a physical picture of exchange narrowing. When the sampling rate is large the spin only has time to respond to an average value of the dipolar field and consequently the line width is reduced.

Bagguley and Griffiths (1948) performed e.s.r. on single crystals of copper sulphate at 3.04 cm, 1.23 cm and 0.85 cm. Copper sulphate contains two magnetically inequivalent sites which requires the Zeeman term for the assembly of spins to be of the form $\Sigma g_1\beta HS_{1Z} + \Sigma g_2\beta HS_{2Z}$. Such a Zeeman term no longer commutes with the exchange term, allowing the exchange to influence it. Experimental evidence of this was found. At 0.85 cm, along certain crystallographic directions, two lines from different sites were just resolved. At the lower frequencies, where the separation between these lines will be less, only one line was found. A knowledge of the expected line widths showed that the appearance of only one line was not due to a lack of resolution.

This behaviour was interpreted in terms of an exchange frequency linking the two sites. When the two lines took their greatest experimental separation, at 0.85 cm, the exchange frequency was insufficient to average

the lines. At 1.23 cm, where the two lines were not quite distinguishable, the frequency difference of the lines was of the same order as the exchange frequency and hence gave it a numerical estimate of about 0.15 cm^{-1}. As expected, at the lowest frequency (3.04 cm), a single narrowed line was found.

A similar mechanism is proposed to explain the results found in $Cs_3Cr_2Cl_9$. However, before continuing, the feasibility of such interdimeric exchange paths will be considered. The chemist's electronegativity parameter measures the ability of an atom to attract an electron to itself. It sums, in one parameter, the general chemical behaviour of an atom. A difference in electronegativities of greater than about 2 between two atoms favours ion formation. For $Cs_3Cr_2Cl_9$ the relevant values are

Cl	Cs	Cr
2.85	0.85	1.55

From these figures the Cs - Cl bond is expected to be ionic, in fact cesium chloride is often used as a model of an ionic crystal. The degree of covalency predicted for the Cr - Cl bond leads to the intra dimeric exchange interactions of 17°K. These considerations, in conjunction with the crystal structure of figure 6.1, suggest that inter dimeric exchange paths are feasible, proceeding via two intermediate chlorine atoms. These inter dimeric exchange paths are expected to be considerably weaker than the intra dimeric paths.

The model we now adopt is to consider each dimer to consist of two ions, a and b, surrounded by z nearest neighbour dimers. This may be pictured as

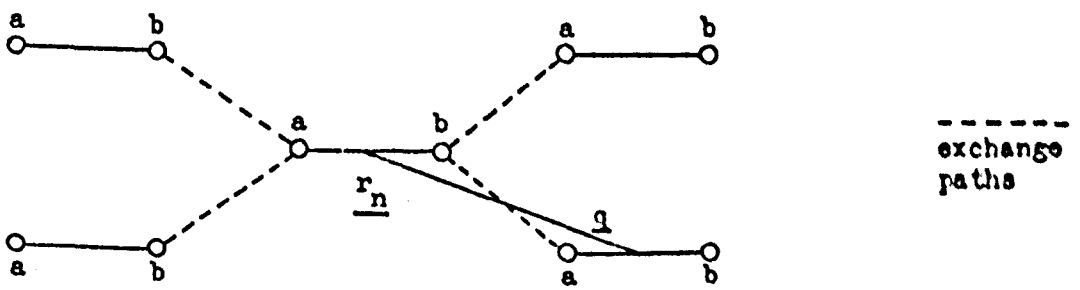

The central dimer is labelled by the vector $\underline{r}_n$ and its neighbours generally by $\underline{r}_n + \underline{q}$. The assumption is made, from a consideration of the crystal

structure, that exchange between dimers only occurs between neighbouring ions with different alphabetical labels, namely a_n with b_{n+q} and b_n with a_{n+q} etc. Before writing the Hamiltonian for the complete assembly of dimers some new operators are defined to simplify the calculations,

$$\underline{J}_n = \underline{S}_{na} + \underline{S}_{nb} \qquad \underline{K}_n = \underline{S}_{na} - \underline{S}_{nb} \tag{6.18}$$

together with the projection operator $P_J = |J\rangle\langle J|$

The Hamiltonian along the z direction is then,

$$H = \sum \omega_o \underline{J}_{nz} + \sum D_J P_J J_{nz}^2 + \sum \frac{\Delta}{2}(J(J+1))P_J + \sum_{\substack{\text{pairs} \\ n+q\ n}} 4j(\underline{S}_{na} \cdot \underline{S}_{n+q\ b}) \tag{6.19}$$

where ω_o is the detecting quantum, Δ the intra dimeric exchange energy and $4j$ the inter dimeric exchange energy.

By use of equations 6.18 the contribution of inter dimeric exchange to the Hamiltonian may be written

$$H = \sum_n j\left[\underline{J}_n \cdot \underline{J}_{n+q} - \underline{K}_n \cdot \underline{J}_{n+q} + \underline{J}_n \cdot \underline{K}_{n+q} - \underline{K}_n \cdot \underline{K}_{n+q}\right] \tag{6.20}$$

The Hamiltonian is now truncated to remove the high frequency transitions which we do not detect. The zero field splitting terms are already in a satisfactory form since each D term is evaluated only within its own spin manifold. Terms between spin manifolds are not represented. The cross terms in equation 6.20 can be omitted since they only produce transitions between manifolds with $\Delta J = \pm 1$. Care must be exercised with the last term of equation 6.20 since, in part, it causes simultaneous up and down transitions between different spin manifolds which do not cause a large energy change. This means a term of the form

$$\sum_{\substack{n,q \\ \text{pairs}}} j \sum_{J,J'} (P_J \underline{K}_n P_{J\pm1}) \cdot (P_{J\pm1} \underline{K}_{n+q} P_J) \tag{6.21}$$

must be retained. The total Hamiltonian can now be written as the sum of three terms.

$$H = H_o + H_1 + H_2 \qquad (6.22)$$

where

$$H_o = \sum_n \left[\omega_o J_{nz} + \frac{1}{2} J(J+1) P_J \right]$$

$$H_1 = \sum_n \left[\sum_J D_J P_J J^2_{nz} \right]$$

$$H_2 = \sum_{\substack{n,q \\ \text{pairs}}} j \left[\underline{J}_n \cdot \underline{J}_{n+q} - \sum_J (P_J \underline{K}_n P_{J\pm1}) \cdot (P_{J\pm1} \underline{K}_{n+q} P_J) \right]$$

Dr D. E. Dugdale has applied the analysis of Kubo and Tomita (1954) to the problem of predicting the observed spectrum from this Hamiltonian. Since, at high temperatures, no fine structure is observed H_1 is treated as a perturbation on H_o and H_2. Using this approach Dr Dugdale was able to derive, for the observed line width of the high temperature resonance, Ω,

$$\Omega = \frac{\sigma^2}{\zeta_e} \sqrt{\frac{2\pi}{3}} \qquad (6.23)$$

where

$$\sigma^2 = \frac{4D_1^2 \langle B_1 \rangle + 84 D_2^2 \langle B_2 \rangle + 504 D_3^2 \langle B_3 \rangle}{4 \langle B_1 \rangle + 20 \langle B_2 \rangle + 56 \langle B_3 \rangle} \qquad (6.24)$$

$$\zeta_e^2 = \frac{4D_1^* D_1 \langle B_1 \rangle + 84 D_2^* D_2 \langle B_2 \rangle + 504 D_3^* D_3 \langle B_3 \rangle}{4D_1^2 \langle B_1 \rangle + 84 D_2^2 \langle B_2 \rangle + 504 D_3^2 \langle B_3 \rangle} \qquad (6.25)$$

when $\langle B_1 \rangle = \frac{\exp(-\Delta/T)}{Z}$, $\langle B_2 \rangle = \frac{\exp(-3\Delta/T)}{Z}$, $\langle B_3 \rangle = \frac{\exp(-6\Delta/T)}{Z}$

and $Z = 1 + 3\exp(-\Delta/T) + 5\exp(-3\Delta/T) + 7\exp(-6\Delta/T)$

$$D_1^* = zJ^2 \left[\frac{3D_1}{2} (8 \langle B_1 \rangle + 40 \langle B_2 \rangle + 112 \langle B_3 \rangle) + D_1 \cdot \frac{32 \times 99}{25} \langle B_2 \rangle - D_2 \cdot \frac{16 \times 378}{25} \langle B_2 \rangle \right]$$

$$D_2^* = zJ^2 \left[\frac{3D_2}{2} (8 \langle B_1 \rangle + 40 \langle B_2 \rangle + 112 \langle B_3 \rangle) + D_2 \left(\frac{26 \times 48}{25} \langle B_1 \rangle + \frac{14 \times 102}{25} \langle B_3 \rangle \right) \right.$$

$$\left. - D_1 \cdot \frac{16 \times 18}{25} \langle B_1 \rangle - D_3 \cdot \frac{14 \times 162}{25} \langle B_3 \rangle \right]$$

$$D_3^* = zJ^2\left[\frac{3D_3}{2}(8\langle B_1\rangle + 40\langle B_2\rangle + 112\langle B_3\rangle) + D_3\cdot\frac{14\times 57}{25}\langle B_2\rangle - D_2\cdot\frac{14\times 27}{25}\langle B_2\rangle\right]$$

Once this result is found, the angular dependence of the line width is fairly readily obtainable. With the magnetic field at an angle θ to z, the term DJ_z^2 becomes

$$D(S_{x'}^2\sin^2\theta + S_{z'}^2\cos^2\theta - \sin\theta\cos\theta(S_{z'}S_{x'} + S_{x'}S_{z'})) \qquad (6.26)$$

which can be written as

$$DJ_z^2\left(\frac{3\cos\theta - 1}{2}\right) + \frac{D\sin^2\theta}{4}(J_+^2 + J_-^2) - \frac{D\sin\theta\cos\theta}{2}[(J_+J_z + J_zJ_+) + (J_-J_z + J_zJ_-)] \qquad (6.27)$$

Using this expression in H_1 gives, for the linewidth at θ,

$$\frac{\sigma^2}{\zeta_e}\sqrt{\frac{2\pi}{3}}\left[\left(\frac{3\cos^2\theta - 1}{2}\right)^2 + \frac{5}{2}\cos^2\theta\sin^2\theta\exp\left(-\tfrac{1}{2}\left(\frac{\omega_o}{\zeta_e}\right)^2\right) + \frac{1}{4}\sin^4\theta\exp\left(-\tfrac{1}{2}\left(\frac{2\omega_o}{\zeta_e}\right)^2\right)\right] \qquad (6.28)$$

The above considerations apply when there is strong exchange narrowing of the spectrum, namely when $\zeta_e^2 \gg \sigma^2$. Once the spectrum is resolved into distinct resonances the exchange interactions between dimers should be treated as a perturbation on H_0 and H_1. A consideration of this situation shows that the measured D term should be of the general form

$$D = D_{max}(1 - A\exp(-J/T)) \qquad (6.29)$$

where A is a constant and D_{max} is the value of D_1 at $0^\circ K$, the temperature at which all the averaging mechanisms are 'switched off'. The exponential function predicts much faster changes in D with temperature than we in fact observe. This is illustrated in figure 6.6 where a function of this form is shown by the continuous line.

As we shall shortly see, the strong averaging predictions start to break down when $\zeta_e^2 \sim 10\sigma^2$. If we assume that the perturbation approach to the weak averaging situation requires $\sigma^2 \sim 10\zeta_e^2$ before it is valid, we find

that this condition will not be met until the temperature is below $3^{\circ}K$. This is just the temperature region where useful results are becoming unavailable because of the depopulation of the spin 1 levels into the diamagnetic ground state.

6.3.13 The Treatment of the High Temperature Results

In order to compare the strong averaging results with the experimental behaviour, the D terms associated with the paramagnetic spin manifolds are required. The low temperature results of figure 6.6 allow the spin 1 D term to be extrapolated to a value of 0.225 cm^{-1} at $0^{\circ}K$. Some uncertainty must exist over this value since the D term appears to be approximately linear in temperature below $5^{\circ}K$, an unexpected result which we cannot predict.

The spin 2 D term has no crystal field contributions (c.f. 6.11). It consists of dipolar, D_d, and anisotropic exchange, D_E, terms only. The anisotropic exchange contribution is of the order $(g - 2)^2 J$ which takes a maximum value of 0.008 cm^{-1}. However, when the contribution of anisotropic exchange is calculated in detail (see, for example, Smith (1966) for V^{2+}), it is often found to be much reduced from the estimate of $(g - 2)^2 J$. In view of this D_2 will be regarded as being wholly dipolar in origin.

The dipolar term is given by,

$$D_d = -\frac{g^2 \beta^2}{r_{ij}^3} \qquad (6.30)$$

where r_{ij} is the separation between the two paramagnetic ions. D_d takes a value of -0.056 cm^{-1} in the present case. However, in the presence of covalency, a fraction, f, of the total spin of each paramagnetic ion will be transferred to each ligand leaving a fraction $(1 - 6f)$ of spin at each metal ion. The dipolar interaction must then be calculated by considering the interaction between two sets of distributed dipole moments. This problem has been investigated by Smith (1966) and the following results are obtained by applying his treatment to the more complex geometry of our situation.

The Hamiltonian for the dipolar interaction is taken to have the form

$$H_d = -F\frac{g^2\beta^2}{R^3}(3S_{AZ}S_{BZ} - \underline{S}_A\cdot\underline{S}_B) \qquad (6.31)$$

where F is a reduction factor. The contributions to F arise from metal ion-metal ion, metal ion-ligand and ligand-ligand interactions. The ligand-ligand interactions include the situation when both metal ions transfer spin to the same ligand. This situation makes complex contributions to F and is neglected at present. For the $Cr_2Cl_6^{3-}$ anion the other contributions to F give

$$F = 1 - 9.93f + 29f^2 \qquad (6.32)$$

It is difficult to predict the contribution to F from spin transfer to a common ligand from both chromium ions because the geometry of the pair is not simple. For example, the $Cr^{3+} - Cl^- - Cr^{3+}$ angle is approximately 72°. The contribution to F will be in f^2 and is not necessarily positive. Since the spin transfer fraction f is expected to be small, ~1%, it is unlikely that the latter contributions will change the prediction that F is less than 1, leading to a value for D_2 of less than $-0.084\ cm^{-1}$.

In section 6.4 some results are presented on dilute dimeric materials, which it was hoped would contain the same anion. We will see that these chromium dimers give a spin 2 D value of $-0.0434\ cm^{-1}$. Such a value seems very small when compared to the predictions of the dipole model, but may set a lower limit on the possible value of D_2.

We now have evidence to suppose that D_1 lies between $0.185\ cm^{-1}$ and $0.223\ cm^{-1}$ and D_2 between $-0.084\ cm^{-1}$ and $-0.043\ cm^{-1}$. Furthermore, we suspect that D_1 and D_2 have values near, but not equal to, the largest available values in the above ranges. When D_1 and D_2 are known, D_3 can be predicted from equation 6.9. Since a fairly comprehensive set of linewidth measurements were obtained with the magnetic field along the x direction, a computer program was written to calculate the value of J by rearranging equation 6.28 and dividing by the observed linewidth. This calculation was performed for each temperature above $12^\circ K$ at which experimental results had

THE ANGULAR DEPENDENCE OF THE LINEWIDTH

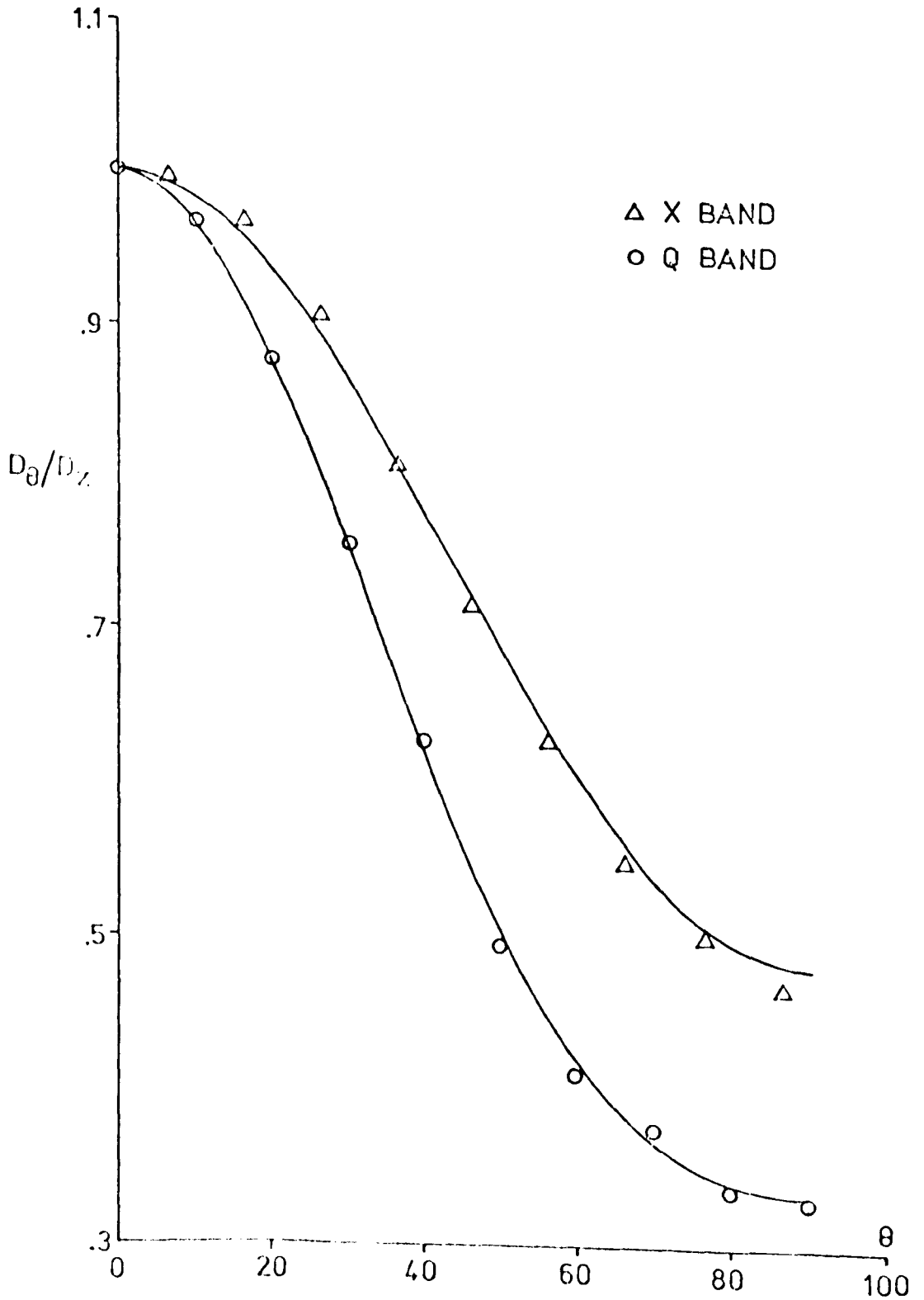

FIGURE 6.7

been taken. D_1 and D_2 were iterated over the values described above. The standard deviation in the j values was calculated for each pair of D values, D_1 and D_2, and the smallest deviation found for each value of D_1. This gave

D_1	D_2	D_3	ζ_e^2 (290°K)
0.19	-0.066	-0.109	1.85
0.20	-0.068	-0.115	2.18
0.21	-0.072	-0.119	2.66
0.22	-0.076	-0.125	3.26
cm^{-1}	cm^{-1}	cm^{-1}	cm^{-2}

The expression for the angular dependence of the linewidth offers a way of choosing between these values. If we concern ourselves with the anisotropy predicted by equation 6.28 the only unknown in the expression is ζ_e. The observed anisotropy depends markedly on the ratio ω_o/ζ_e. When this ratio is small, the anisotropy is least pronounced. In view of this, measurements were initially taken at Q band frequencies, giving the results shown in figure 6.7. The value of ζ_e^2 predicted by the linewidth at each angle was calculated and an average value of 2.5 cm^{-2} found. This compares with the room temperature value of 2.66 cm^{-2} predicted by the data with $D_1 = 0.21\ cm^{-1}$.

As a further check on the effect of the microwave quantum on the linewidth, a further experiment was carried out at X band. As predicted, the linewidth along the z direction was the same as that measured along this direction at Q band. Using the value of ζ_e found from the Q band measurements, the predicted angular dependence of the linewidth is shown in figure 6.7, together with the measured anisotropy. The experimental agreement with the anisotropy predictions is seen to be good.

We now adopt the values

$$D_1 = 0.21\ cm^{-1}\quad D_2 = -0.072\ cm^{-1}\quad D_3 = -0.119\ cm^{-1}\quad J = 0.161\ cm^{-1}$$

in order to consider the absolute temperature dependence of the linewidth. This value of J gives $\zeta_e^2 = 2.45\ cm^{-2}$ and improves the fit slightly in the region of minimum linewidth. Evaluating equation 6.28 by use of these

THE TEMPERATURE DEPENDENCE OF THE LINEWIDTH

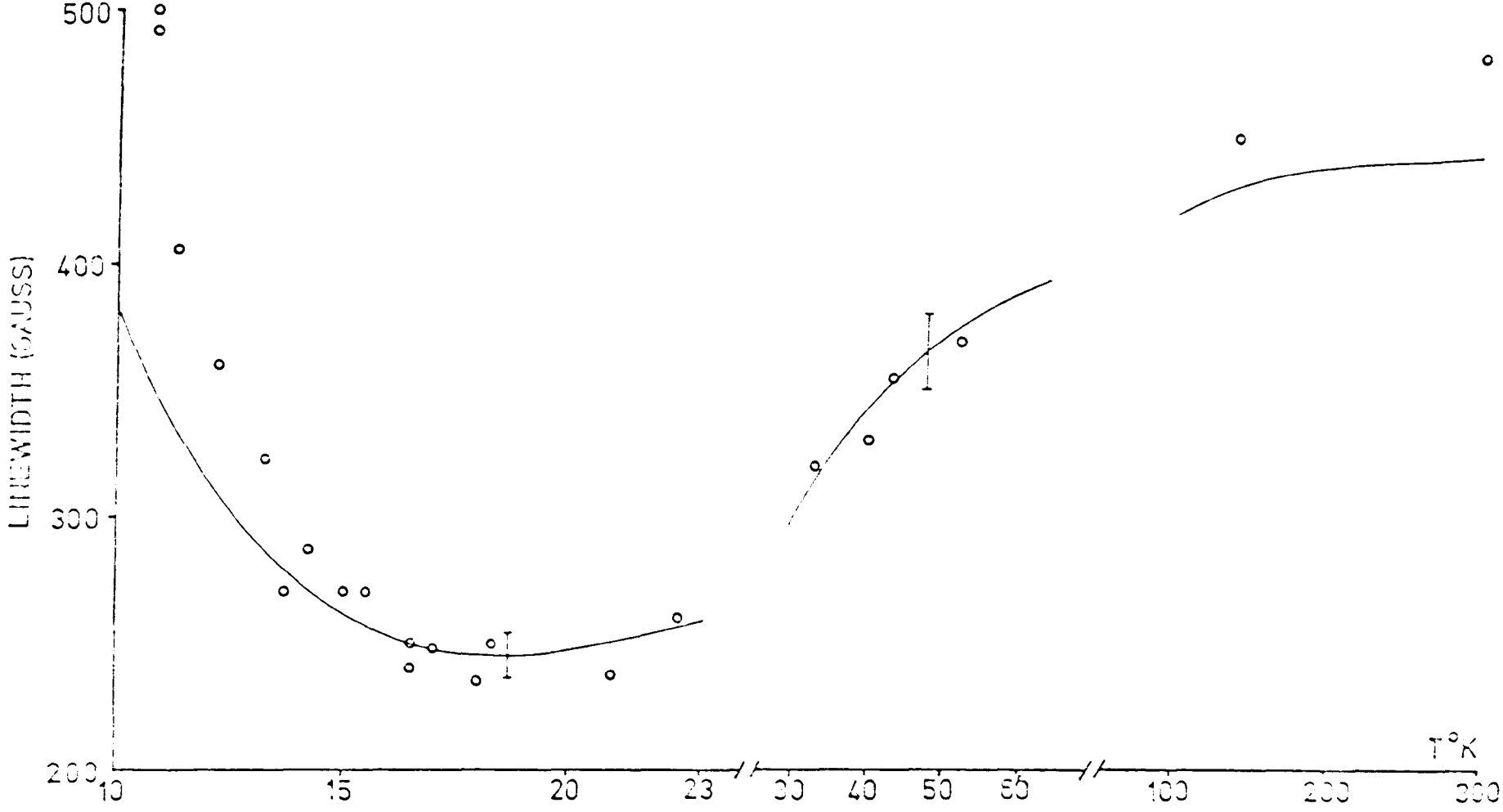

FIGURE 6.8

parameters gives the fit shown in figure 6.8. The fit is seen to be less good at the very low temperatures because the perturbation condition is breaking down. In this region, the detected linewidth is becoming the sum of two broad resonances centred at different fields, making the measured linewidth less meaningful. At high temperatures, the linewidth is somewhat underestimated, possible because dipolar interactions between neighbouring dimers have been neglected and also because the relative magnitudes of σ^2 and ζ_e^2 do not differ as much as they do at intermediate temperatures. Overall the fit is considered to be good for a one parameter theory. The error bars in figure 6.8 allow for a measuring error of ±5% in the linewidth since, particularly at the lower temperatures, it was not always possible to maintain the temperature for long enough to take several measurements.

6.3.14 The Vanadium and Titanium Dimers

$Cs_3V_2Cl_9$ and $Cs_3Ti_2Cl_9$ were grown by similar methods to $Cs_3Cr_2Cl_9$. Since these crystals are isomorphous, a simple picture predicts the exchange interactions within the different dimers will be of the same order. However, table 6.1 shows that the orbital radii differ for these ions, leading to overlap with the ligand ions, S, going as $S(Ti^{3+}) > S(V^{3+}) > S(Cr^{3+})$.

TABLE 6.1

Ion	Spin	Z	$\langle r^{-3} \rangle$	$\langle r^2 \rangle$
Ti^{3+}	1/2	22	2.552	1.893
V^{3+}	1	23	3.217	1.643
Cr^{3+}	3/2	24	3.959	1.447
			a.u.	a.u.

The susceptibility results bear this out. These crystals were investigated down to helium temperatures.

$Cs_3V_2Cl_9$

No resonances were observed in the vanadium crystals. The large

D term of a single vanadium ion in an axial site immediately suggests the reason for this. For two exchange coupled spin 1 ions;

S	$3a_s$	β_s
1	3	-1
2	1	6/7

Thus the D term for both the spin 1 and spin 2 manifolds includes large crystal field contributions. These D terms are presumably too large to be averaged out. The strong D term defines the axis of quantisation and, since $g\beta H \ll D$, mixing off axis is small. The $|1\rangle \leftrightarrow |-1\rangle$ transition of V^{3+} in $\alpha - Al_2O_3$ has been observed on axis, with the r.f. field parallel to H, because of an E term attributed to strains in the crystal. This was attempted with the vanadium dimers but no resonances were detected. Even if such weak resonances were present they would probably be extremely difficult to detect because of the broadening mechanisms present in these crystals.

$\underline{Cs_3Ti_2Cl_9}$

At all temperatures the titanium crystals showed four resonances around g = 2. Since these lines showed no changes in intensity with temperature they were pursued no further. These lines may have been due to the unknown contaminant which dominated the susceptibility results of Saillant and Wentworth.

On cooling the crystals below nitrogen temperatures, a very broad resonance was found at about 13 kilogauss when the magnetic field was considered to be perpendicular to c. This line was not found until the temperature was below about 60°K, presumably because of fast relaxation. By approximately 20°K the line could no longer be detected. This behaviour suggests that the line belongs to the spin 1 manifold of exchange coupled titanium pairs. The exchange interaction is antiferromagnetic with a J value probably lying in the range 150 - 250°K.

We saw in section 6.3.4 that titanium^{3+} ions can have either an isotropic or a highly anisotropic g tensor. If we assume each ion has an

isotropic g tensor with a g value around 2 the dimers should give rise to a spin 1 system with g approximately equal to 2. Taking the paramagnetic sites as axial, with c as the axis of distortion, the transitions in such a system, with the magnetic field along x, occur when

$$h\nu = ((g\beta H)^2 + \frac{D^2}{4})^{\frac{1}{2}} \pm \frac{D}{2} \qquad (6.33)$$

Taking $h\nu = 0.33$ cm^{-1} and $g\beta H = 1.3$ cm^{-1} ($H = 13$ kg), gives D as 4.75 cm^{-1}. The spin 1 D term arising from two spin $\frac{1}{2}$ ions will be the sum of dipolar and anisotropic exchange terms only. However, since the exchange interaction is large, such a D value arising through anisotropic exchange is feasible. Lack of time precluded further investigations on those crystals but measurements at Q band are planned for the future to test the above speculations.

6.4 Dilute Dimeric Complexes

The susceptibility results of Saillant and Wentworth and of Earnshaw and Lewis (1961) included measurements on systems in which the cesium atoms of the $Cs_3M_2Cl_9$ compounds were replaced by alkylammonium cations. They found that the Curie-Weiss constants depended upon the nature of the cation and concluded that magnetic dilution was more nearly approached in these crystals. In fact, Earnshaw and Lewis were able to fit their results for $(Et_4N)_3Cr_2Cl_9$ ($Et = C_2H_5$) to Kambe's expression and found $J = 2.5^{\circ}K$. In view of this, and despite there being no X ray data, crystals of $(Et_4N)_3M_2Cl_9$ ($M = Cr, V$) and $[(n\text{-}C_4H_9)_4N]_3Cr_2Cl_9$ were grown in the hope that the $M_2Cl_9^{3-}$ anion would be preserved from the cesium crystals.

The tetraethylammonium salts were grown from thionyl chloride. Stoichiometric quantities of chromium chloride and tetraethylammonium chloride were weighed and a small excess of the latter chloride added. This mixture was added to thionyl chloride and boiled to increase solubility. It was then cooled very slowly in an electrothermal bath. Crystals containing vanadium were grown similarly except that the mixture was not boiled. Good single

THE PHASE CHANGE IN $(Et_4N)_3Cr_2Cl_9$

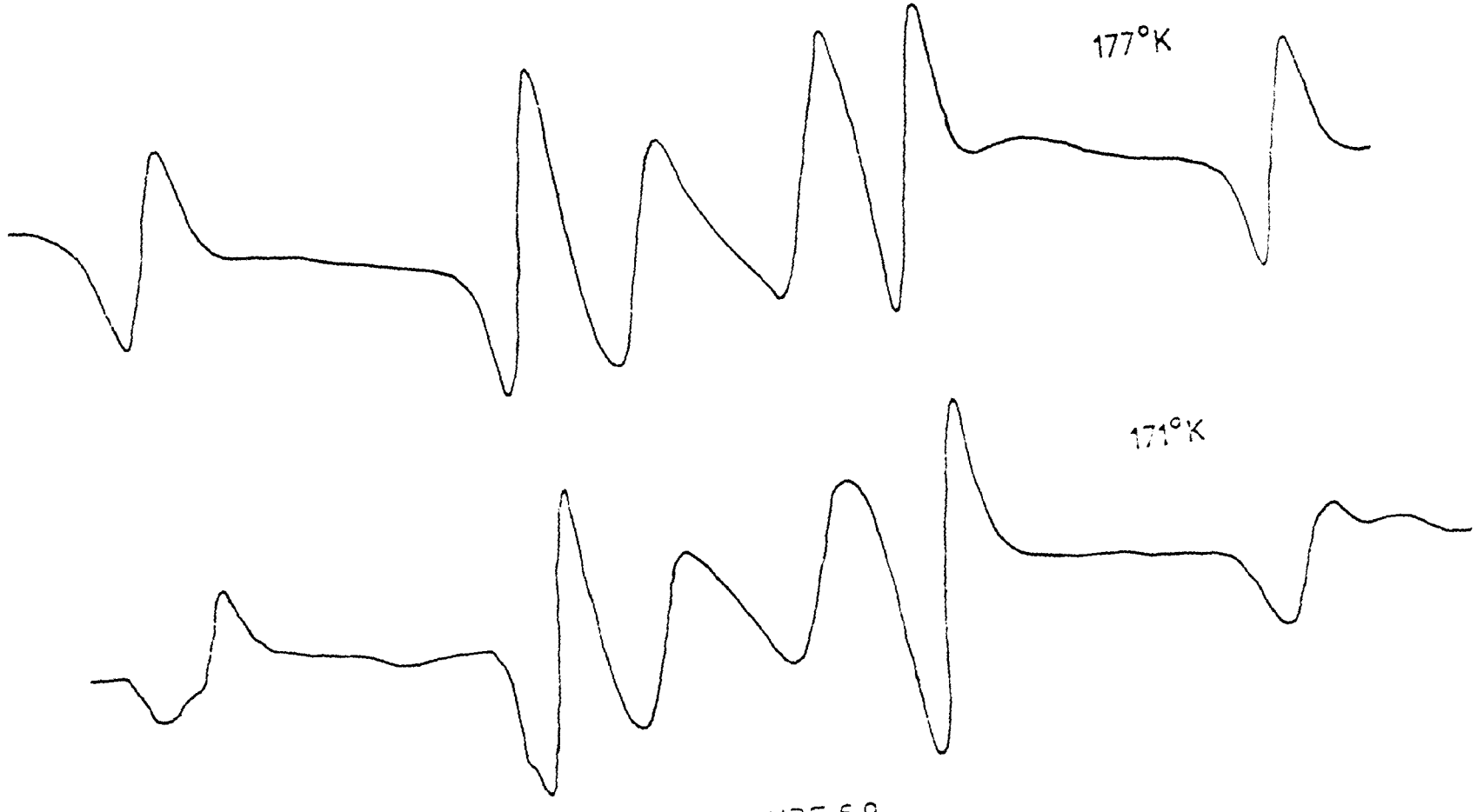

FIGURE 6.9

crystals of both samples were obtained. Attempts to grow the tetrabutyl salts following the general method given by Saillant and Wentworth failed to produce good single crystals.

The crystals of $(Et_4N)_3Cr_2Cl_9$ grew as small blue needles. They were fragile and highly deliquescent. The most satisfactory way of handling them was to transfer them to liquid paraffin from the thionyl chloride just prior to use. The liquid paraffin served to exclude water while the crystals were being cooled below 273°K.

The e.p.r. spectrum was initially investigated at X band and liquid nitrogen temperatures. On axis six strong resonances were observed, four of which could be attributed to a spin 2 system. The intensity of the remaining two resonances varied from growth to growth suggesting an impurity centre. Off axis the spin 2 lines appeared to split. Initially an attempt was made to include a spin 3 system with the same D value as the spin 2 system. The inner four transitions of such a spin 3 system would be coincident with the spin 2 lines along the c axis, and show splittings off axis of the right magnitude. However, no evidence was found for the outer transitions $(|\pm 3\rangle \leftrightarrow |\pm 2\rangle)$ which should have been observed.

To ensure that the splittings were not due to strains from mounting the sample on the cavity wall with vacuum grease, a crystal was placed in a thin quartz tube which was then attached to the cavity; the splittings persisted. Since the spectrum was found to show no splitting near room temperature, a nitrogen flow experiment was carried out to allow investigations over a range of temperatures. This experiment showed that the splitting appeared reversibly between 177°K and 171°K. Spectra taken off axis, either side of this transition temperature, are shown in figure 6.9. The intensity of each split component is half that of the unsplit line, showing there are two equally populated magnetically inequivalent sites. Since the splittings are not detectable along the c direction or in the c plane, the site inequivalence would seem to be due to a small tilting of the magnetic axes with respect to

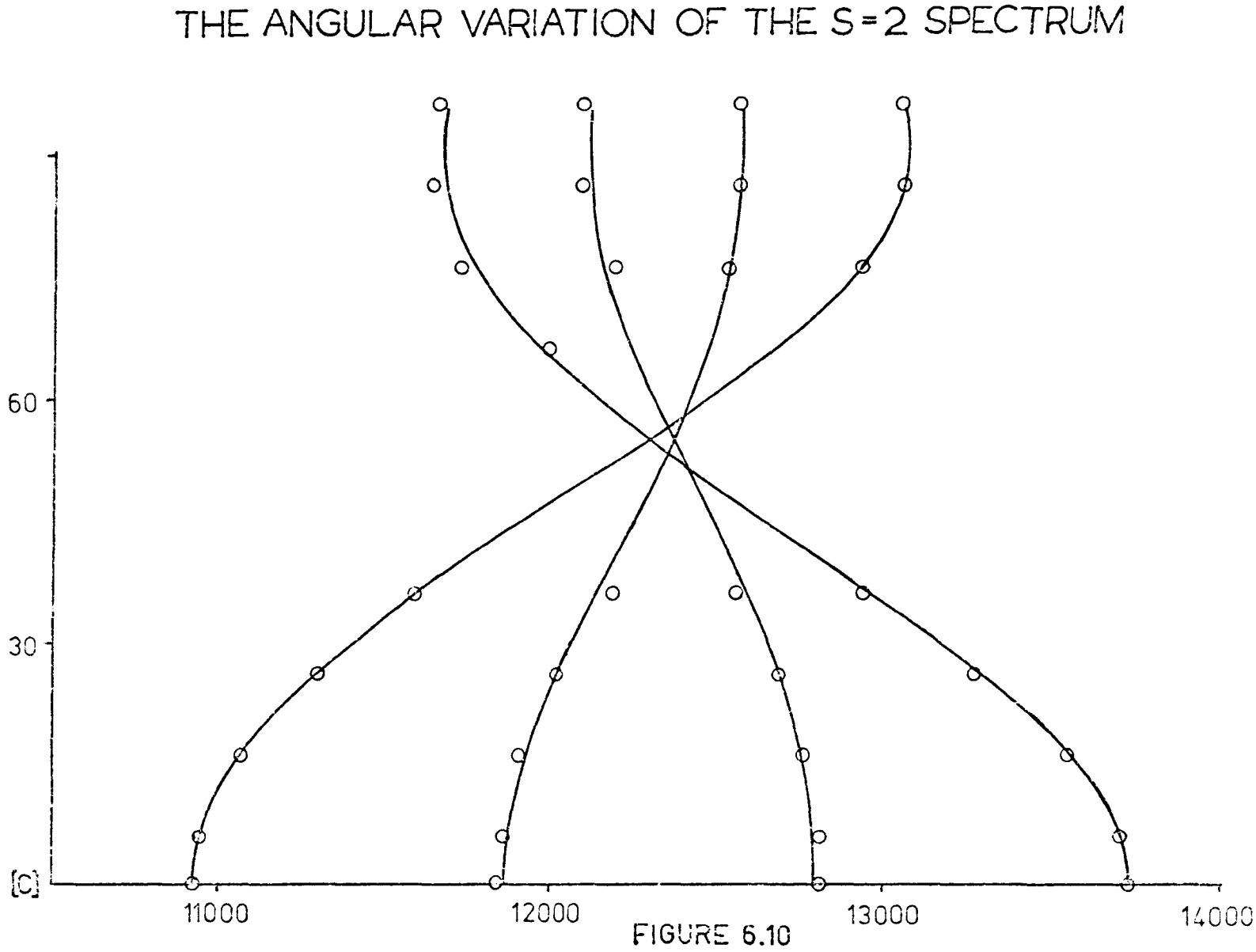
THE ANGULAR VARIATION OF THE S=2 SPECTRUM
60
30
0
11000
12000
13000
14000

FIGURE 6.10

the crystallographic c axis.

An angular variation was performed at Q band with the cavity in a cold stream of nitrogen gas to preserve the crystal. The field positions of the lines were fitted by the spin Hamiltonian

$$H_s = g_{\parallel}\beta H \cos\theta S_z + g_{\perp}\beta H \sin\theta S_x + D(S_x^2 - \tfrac{1}{3}S(S+1))$$

where the z direction corresponds to the crystallographic c axis. It was found that

$$g_{\parallel} = 1.984 \qquad g_{\perp} = 1.980 \qquad D = 0.0434 \text{ cm}^{-1}$$

These parameters give the fit shown in figure 6.10. Once again the parameter D is not truly representative since the line separations appear to change, albeit slightly, with temperature.

Intensity measurements were made as a function of temperature with the magnetic field along the c axis. The procedure used was the same as that described in section 6.3.11. A single ion chromium resonance in ruby was used as a reference. The relative intensity of a $\Delta M_s = \pm 1$ transition within a spin 2 manifold is proportional to

$$\frac{\exp(-3J/T)}{1 + 3\exp(-J/T) + 5\exp(-3J/T) + 7\exp(-6J/T)} \qquad (6.34)$$

This expression is shown fitted to the experimental data in figure 6.11 with the best fit corresponding to $J = 20^{\circ}K$. It was often not possible to record the spectrum several times at each temperature, but since four spin 2 resonances were present, some averaging of the results was possible. The measurements give a value for J that is accurate to $\pm 2^{\circ}K$.

The absence of S = 1 and S = 3 transitions is unfortunate yet interesting. A mechanism to broaden them beyond resolution must be found. Broadening by fast relaxation will not explain this. Equation 6.11 shows that, for the spin 2 manifold, $\beta_s = 0$, implying that there is no crystal field contribution to the D term. This is not the case for the spin 1 and spin 3 manifolds. There seems to be a possible source of broadening arising from

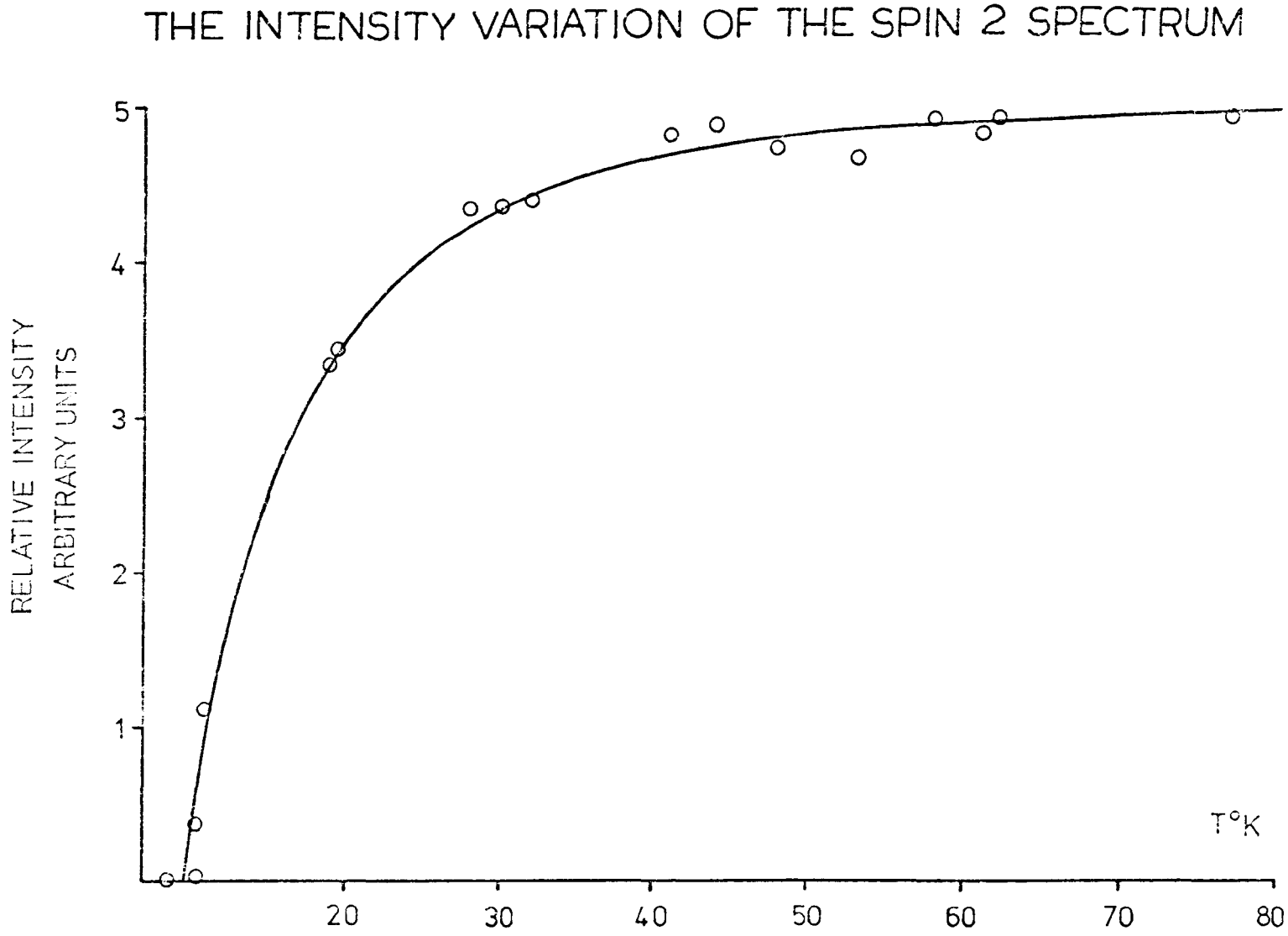
THE INTENSITY VARIATION OF THE SPIN 2 SPECTRUM
RELATIVE INTENSITY
ARBITRARY UNITS
5
4
3
2
1
T°K
20
30
40
50
60
70
80

FIGURE 6.11

the crystal field. Local variations in the crystal field are a possibility and certainly the phase change occurring in these crystals suggests strong crystal field effects are present.

Since the spin 2 D term in $(Et_4N)_3Cr_2Cl_9$ is somewhat smaller than we had hoped, and since transitions in the spin 1 and spin 3 manifolds were not resolved, crystals of $(Pr_4N)_3Cr_2Cl_9$ (Pr = C_3H_7) were prepared. The crystals were grown by the same method used for $(Et_4N)_3Cr_2Cl_9$. Large, dark blue, plate-like crystals were quickly formed. Preliminary investigations using a nitrogen flow system indicated a spin 2 spectrum with a D term of about 0.04 cm^{-1}. Once again the resonance lines appeared split, suggesting a phase change. Additional resonances were found in these crystals which, although not appearing to belong to spin 1 or spin 3, will be interesting to follow up at a later date.

The behaviour of $(Et_4N)_3V_2Cl_9$

No paramagnetic behaviour attributable to pairs was found in these crystals. The arguments of section 6.3.4 concerning the size of the D terms again hold. Furthermore, the crystal field can contribute to the D term of each spin state of the pair, allowing the broadening mechanisms found in $(Et_4N)_3Cr_2Cl_9$ to be operative on all resonances.

REFERENCES

Abragam and Price (1951) Proc. Phys. Soc. A65 209

Advances in Quantum Electronics (1960) Columbia Press

Advances in Quantum Electronics (1961) Columbia Press

Anderson and Weiss (1953) Rev. Mod. Phys. 25 269

Astbury (1926) Proc. Roy. Soc. (London) 112 448

Bagguley and Griffiths (1948) Nature 162 538

Bleaney and O'Brien (1953) Proc. Phys. Soc. B69 1216

Bloembergen, Shapiro, Pershan and Artman (1959) Phys. Rev. 114 445

Calligaris, Ciana and Ripamonti (1966) Ric. Sci. 36 1358

Dugdale (1967) Ph.D. Thesis, Durham

Earnshaw and Lewis (1961) J. Chem. Soc. 396

Efimov and Pitirimov (1963) Russ. J. Inorg. Chem. 8 1042

Feldman, Castle and Murphy (1965) Phys. Rev. 138 A1208

Fisher (1963) J. Math. Phys. 4 124

Garner and Mabbs (1970) J. Chem. Soc. A71 1711

Gill (1962) Proc. Phys. Soc. 79 58

Gregson and Mitra (1969) J. Chem. Phys. 50 2021

Griffiths and Owen (1952) Proc. Phys. Soc. A65 951

Griffiths, Owen and Ward (1953) Proc. Roy. Soc. A219 526

Harris (1969) J. Phys. C. 2 1413

Harris and Yngvesson (1968) J. Phys. C. 1 990

Holden and Singer (1961) "Crystals and Crystal Growing" Heinemann

Jarrett (1957) J. Chem. Phys. 27 1298

Kambe (1950) J. Phys. Soc. Japan 5 48

Klein (1968) "Physics of Colour Centres" Academic Press N. Y. (ed Fowler)

Klemens (1961) Phys. Rev. 122 443

Klemens (1962) Phys. Rev. 125 1795

Kochelaev (1960) Sov. Phys. Doklady 5 349

Kubo and Tomita (1954) J. Phys. Soc. Japan 9 888

Kuchen, Metten and Judat (1964) Chem. Ber. 97 2306

Kuchen, Metten and Judat (1965) Chem. Ber. 98 3981

Langs and Hare (1967) Chem. Comm. 890

Mabbs and Smail (1970) J. Chem. Soc. A71 1716

Markov and Chernov (1959) "Phase Diagrams for Ceramists" American Ceramic Society (1964)

Maradudin (1966) Solid State Physics 18 274

Mattuck and Strandberg (1960) Phys. Rev. 119 1204

McGarvey (1964) J. Chem. Phys. 40 809

Mims and McGee (1960) Phys. Rev. 119 1233

Montroll and Potts (1955) Phys. Rev. 100 525

Orbach (1961) Proc. Roy. Soc. (London) A264 458

Orton (1968) "Electron Paramagnetic Resonance" Iliffe

Owen (1961) J. App. Phys. 32 213S

Owen and Thornley (1966) Rep. Prog. Phys. 29 675

Richards (1965) Phys. Rev. 137 A1327

Roof (1956) Acta. Cryst. 9 781

Roy, Roy and Pal (1971) Phys. Rev. (B) 3 3597

Saillant and Wentworth (1968) In. Chem. 7 1606

Schonland (1959) Proc. Phys. Soc. 73 788

Scott and Jeffries (1962) Phys. Rev. 127 51

Shchukarev and Perfilova (1963) Russ. J. Inorg. Chem. 8 1100

Singer (1955) J. Chem. Phys. 23 379

Smith (1966) Ph.D. Thesis, Oxford

Stevens (1952) Proc. Phys. Soc. A65 209

Stevens (1953) Proc. Roy. Soc. A219 542

Stoneham (1965) Proc. Phys. Soc. 86 1163

Van Vleck (1940) Phys. Rev. 57 426

Van Vleck (1948) Phys. Rev. 74 1168

Wessel and Ijdo (1957) Acta. Cryst. 10 466

Zeldes and Livingstone (1961) J. Chem. Phys. 34 247